LONG-TERM PERFORMANCE EVALUATION OF NUDECK IN KEARNEY EAST BYPASS

Nebraska Department of Transportation (NDOT)

Project No. SPR-P1(15) M026

December 2019

LONG-TERM PERFORMANCE EVALUATION OF NUDECK IN KEARNEY EAST BYPASS

Nebraska Department of Transportation (NDOT)

Project No. SPR-P1(15) M026

FINAL REPORT

Investigators
George Morcous, Ph.D., P.E.
University of Nebraska – Lincoln

Marc Maguire, Ph.D., P.E.
Utah State University

December 2019

Technical Report Documentation Page

Report No.	Government Accession No.	Recipient's Catalog No.

Title and Subtitle LONG-TERM PERFORMANCE EVALUATION OF NUDECK IN KEARNEY EAST BYPASS	1. Report Date December 2019
	2. Performing Organization Code
3. Author(s) George Morcous, Marc Maguire, and Raed Tawadrous	4. Performing Organization Report No.
5. Performing Organization Name and Address University of Nebraska-Lincoln 1110 South 67th St. Omaha, Nebraska 68182-0178	6. Work Unit No.
	7. Contract or Grant No.
8. Sponsoring Agency Name and Address Nebraska Department of Transportation Bridge Division P. O. Box 94759 Lincoln, NE 68509-4759	9. Type of Report and Period Covered Final Report
	10. Sponsoring Agency Code

11. Supplementary Notes

12. Abstract

The Kearney East Bypass bridge is the first project that implements the newly developed precast concrete deck system (known as 2nd generation NUDECK). The new system consists of full-depth full-width precast prestressed concrete deck panels that are 12 ft (3.66 m) long each. The panels have covered shear pockets at 4 ft (1.22 m) spacing on each girder line to host clustered shear connectors that are adjustable in height. Narrow unreinforced transverse joints are used to eliminate the need for deck overlay. Also, deck panels are post-tensioned in the longitudinal direction using a new post-tensioning system that eliminates the need for post-tensioning ducts, strand threading, and grouting operations.

The project has twin bridges: a southbound bridge with cast-in-place (CIP) concrete deck, and northbound bridge with the new precast concrete (PC) deck system. The two bridges were completed in the fall of 2015 and opened to traffic in the fall of 2016. Due to the unique features of the new PC deck system, this research project was initiated to monitor short-term performance using live load test and long-term performance under traffic loads to evaluate the system performance. Both CIP concrete deck and PC deck bridges were instrumented and tested during the summer of 2016 to compare the performance of their superstructures. Also, finite element analysis (FEA) was conducted to predict the performance of the new PC deck system. The results of both analytical and experimental investigations indicated that the PC deck system performs as predicted and very comparable to the conventional CIP concrete deck.

1. Keywords: Precast Concrete, Deck Panels, Accelerated Bridge Construction, load test, strain measurements, deflections	

2. Security Classification (of this report) Unclassified	3. Security Classification (of this page) Unclassified	4. No. of Pages: 101	22. Price

Form DOT F1700.7 (8-72)

DISCLAIMER

The contents of this report reflect the views of the authors who are responsible for the facts and the accuracy of the data presented herein. The contents do not necessarily reflect the official views or policies of the Nebraska Department of Transportation, nor of the University of Nebraska-Lincoln. This report does not constitute a standard, specification, or regulation. Trade or manufacturers' names, which may appear in this report, are cited only because they are considered essential to the objectives of the report. The United States (U.S.) government and the State of Nebraska do not endorse products or manufacturers.

ACKNOWLEDGEMENTS

This project was sponsored by Nebraska Department of Transportation (NDOT), University of Nebraska-Lincoln (UNL), and Utah State University (USU). The efforts of faculty/staff and graduate/undergraduate students at UNL and USU are acknowledged. Special thanks to the district engineers for providing necessary support to conduct bridge instrumentation and testing.

TABLE OF CONTENTS

1 INTRODUCTION 8

1.1 Background 8

1.2 Project Description 10

1.3 Objectives 18

2 DECK VISUAL INSPECTIONS 19

2.1 October 7, 2015 Visit 19

2.2 June 6, 2016 Visit 23

2.3 June 22, 2017 Visit 26

2.4 October 16, 2018 Visit 31

2.5 July 24, 2019 Visit 34

3 LOAD TESTING 37

3.1 Bridge Instrumentation 37

3.2 Live Load Test 42

3.3 Finite Element Analysis (FEA) 45

3.4 Testing and Analysis Results 48

4 LONG-TERM MONITORING 58

4.1 November 21, 2016 59

4.2 October 16, 2018 61

4.3 July 24, 2019 63

5 CONCLUSIONS 69

5. REFERENCES 70

6. APPENDICES 72

APPENDIX A: Bridge Fabrication and Construction 72

APPENDIX B: Bridge Inspections 94

APPENDIX C: Prestress Loss Calculations 98

ABSTRACT

The Kearney East Bypass Bridge is the first project that implements the newly developed precast concrete deck system (known as 2nd generation NUDECK). The new system consists of full-depth full-width precast prestressed concrete deck panels that are 12 ft (3.66 m) long each. The panels have covered shear pockets at 4 ft (1.22 m) spacing on each girder line to host clustered shear connectors that are adjustable in height. Narrow unreinforced transverse joints are used to eliminate the need for deck overlay. Also, deck panels are post-tensioned in the longitudinal direction using a new post-tensioning system that eliminates the need for post-tensioning ducts, strand threading, and grouting operations.

The project has twin bridges: a southbound bridge with cast-in-place (CIP) concrete deck, and northbound bridge with the new precast concrete (PC) deck system. The two bridges were completed in the fall of 2015 and opened to traffic in the fall of 2016. Due to the unique features of the new PC deck system, this research project was initiated to monitor short-term performance using live load test and long-term performance under traffic loads to evaluate the system performance. Both CIP concrete deck and PC deck bridges were instrumented and tested during the summer of 2016 to compare the performance of their superstructures. Also, finite element analysis (FEA) was conducted to predict the performance of the new PC deck system. The results of both analytical and experimental investigations indicated that the PC deck system performs as predicted and very comparable to the conventional CIP concrete deck.

1 INTRODUCTION

1.1 Background

The use of prefabricated bridge elements and systems (PBESs) has been identified by the Federal Highway Administration (FHWA) as one of the main strategies to achieve the goals of Accelerated Bridge Construction (ABC), which are reducing onsite construction time and impact on traveling public. Full depth precast concrete (PC) deck systems are highly needed PBESs because cast-in-place (CIP) concrete bridge decks are time-consuming to construct in addition to being one of the most deterioration bridge components. Full-depth PC deck systems have several advantages over conventional CIP concrete decks commonly used in highway bridge construction. The quality and durability of PC decks are superior to those of CIP concrete decks as production occurs in a controlled environment eliminating the variability in environmental conditions, casting crews, and curing procedures. Moreover, shrinkage cracking of PC decks is minimized due to the relatively small panel size and delayed restraining caused by supporting girders, which is a primary contributor to early age cracking of CIP concrete decks.

Full-depth PC deck systems can be designed as either composite or non-composite with the supporting girders (mostly steel or concrete). While non-composite concrete deck panels are more economical and simpler to produce and erect, composite systems are commonly used to enhance the structural capacity of the superstructure and attain shallower and lighter girder sections, which improves the efficiency and economy of bridge construction. Existing composite deck systems use either continuously open channels (troughs) or closely spaced (usually at 2 ft (0.6 m)) discrete openings (pockets) over girder lines to accommodate the girder shear connectors (usually studs or bars). These troughs or pockets are often grouted in the field after deck erection, then, the deck surface is covered by an overlay to protect these connections from water and chloride ingress and improve the surface appearance and riding ability. Deck overlays often extend construction/maintenance duration and increase bridge life-cycle cost as bridge deck needs to be overlaid several times during the bridge service life.

Transverse joints between adjacent PC deck panels are usually reinforced using hooked or headed bars projecting from the shear keys of the panels. These joints have to be wide enough to develop the overlapping bars, then filled with grout or flowable concrete, which make the joints susceptible to cracking, penetration, and eventually corrosion of reinforcing bars. Another solution is the use of longitudinal post-tensioning strands along the entire bridge length to pre-compress adjacent panels and transverse joints. This solution requires embedding post-tensioning ducts in each panel, splicing these ducts after panel erection, threading prestressing strands into each duct, post-tensioning strands after grouting transverse joints, and then grouting these ducts. These operations complicate panel fabrication and erection processes and, consequently, reduce the attractiveness of precast concrete deck systems as an accelerated, economical, and durable alternative to CIP concrete decks.

A new precast concrete deck system (known as 2nd generation NUDECK) was recently developed jointly by Nebraska Department of Transportation and University of Nebraska-Lincoln to address the shortfalls of existing systems. The new PC deck system has the following features:

1. Shear connectors are spaced at the largest spacing allowed by AASHTO LRFD bridge design specifications (4 ft) to simplify panel and girder fabrication and erection.
2. The largest precast concrete deck panels are designed (full-width 12 ft long panels) to reduce the number of panels to be produced, transported, and erected; as well as the number of transverse joints.
3. No reinforcing bars and/or post-tensioning ducts are projecting at the transverse joints to simplify panel forming and avoid conflicts/misalignments between adjacent panels during erection.
4. Covered shear pockets are used to minimize penetrations to panel surface, which eliminates the need for deck overlay.
5. Panels are transversely pre-tensioned and longitudinally post-tensioned to control panel cracking during construction and in service.
6. Post-tensioning (PT) strands are located underneath the deck soffit and above the girder top flange (i.e. haunch area) to eliminate the need for placing post-tensioning ducts inside

the panels, threading strands through embedded ducts and across the joints, and grouting the ducts after post-tensioning, which are tedious and laborious operations.

7. Live load continuity reinforcement are located at the haunch area below the deck panels and over each girder line to enhance deck durability.

The new precast concrete deck system was first implemented in the construction of the Kearney East Bypass project located in Kearney, NE in the summer of 2015 after conducting several analytical and experimental investigations to evaluate the structural performance and constructability of the new system. For more information about these investigations, refer to Morcous, et al. (2013), Morcous and Khayat (2014), and Morcous, et al. (2015). The next section summarizes the implementation of these features in this project and Appendix A shows more photos about the construction sequence of the new system.

1.2 Project Description

The project is a relocation of Highway 10 in Buffalo County, Kearney, NE, where the bridge connects 11th street to the 56th street over the US-30 and six Union Pacific Railroad tracks. This project has twin bridges: southbound bridge with CIP concrete deck; and northbound bridge with the new PC deck system. Figure 1.1 shows the plan view of the two bridges and cross section view of the northbound bridge. Each bridge is a two-span continuous bridge that is 41 ft 8 in. (12.7 m) wide and 332 ft (101.2 m) long. Each span is 166 ft (50.6 m) long and consists of five precast/prestressed concrete girders (NU1800) at 8 ft 6 in. (2.59 m) spacing supporting 8 in. (200 mm) thick concrete deck that has a 14^{o} skew and 2% cross slope in one direction. The northbound bridge has a total of 28 precast concrete deck panels: 26 typical panels and 2 end panels. Each typical panel is 12 ft (3.66 m) long and has discrete covered rectangular shear pockets at 4 ft (1.22 m) spacing to connect to the supporting girders as shown in Figure 1.2. End panels are slightly different to accommodate post-tensioning anchorage blocks, which are designed specifically for the new post-tensioning system. Panels are lifted and placed on the deck support system attached to the girder top flange after laying down the post-tensioning strands and adjusting the height of shear connectors by cranking them up to achieve adequate embedment in the shear pockets of the panels and compensate for girder camber. Figure 1.3

shows the deck support system, shear connector, and post-tensioning strands and deviators at the girder top flange before deck panel installation. Data on the girder profiles is shown in Appendix A. Figure 1.4 presents the erection of the first panel at the intermediate pier showing the unreinforced transverse joint and continuity reinforcement (i.e. epoxy coated bars). It also shows end panels post-tensioning anchorage blocks, which are some of the unique features of the new deck system and will be evaluated in this study. Figure 1.5 shows the bridge deck during and after grouting transverse joints, while Figure 1.6 shows the longitudinal post-tensioning of the precast deck panels using the new ductless post-tensioning system. More information about strand elongation and measured surface strains are in Appendix A. Figure 1.7 shows the technique used to grout the shear pockets and haunches after post-tensioning using self-consolidating concrete (SCC). Figure 1.8 shows the deck surface after grinding and casting the rail. Deck was left intentionally without overlay to allow visual inspections and long-term monitoring for few years. Data on the compressive strength of precast and cast-in-place concrete is listed in Appendix A.

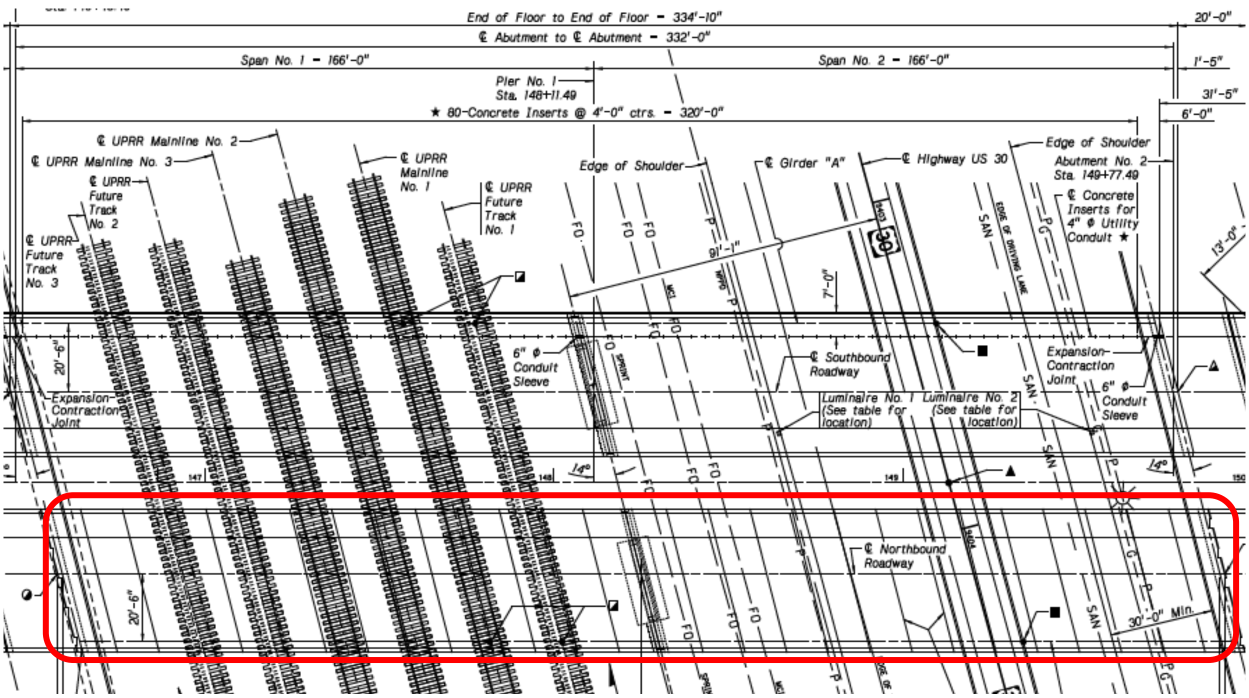
End of Floor to End of Floor - 334'-10"
℄ Abutment to ℄ Abutment - 332'-0"
Span No. 1 - 166'-0"
Span No. 2 - 166'-0"
20'-0"
1'-5"
31'-5"
6'-0"
Pier No. 1
Sta. 148+11.49
★ 80-Concrete Inserts @ 4'-0" ctrs. - 320'-0"
℄ UPRR Mainline No. 2
℄ UPRR Mainline No. 3
℄ UPRR Future Track No. 2
℄ UPRR Future Track No. 3
℄ UPRR Mainline No. 1
℄ UPRR Future Track No. 1
Edge of Shoulder
℄ Girder "A"
℄ Highway US 30
Edge of Shoulder
Abutment No. 2
Sta. 149+77.49
℄ Concrete Inserts for 4" ϕ Utility Conduit ★
13'-0"
91'-1"
7'-0"
30
FO
P
SAN
PG
EDGE OF DRIVING LANE
6" ϕ Conduit Sleeve
℄ Southbound Roadway
Luminaire No. 1 (See table for location)
Luminaire No. 2 (See table for location)
Expansion-Contraction Joint
6" ϕ Conduit Sleeve
20'-6"
Expansion-Contraction Joint
14°
147
148
149
150
℄ Northbound Roadway
20'-6"
30'-0" Min.
G

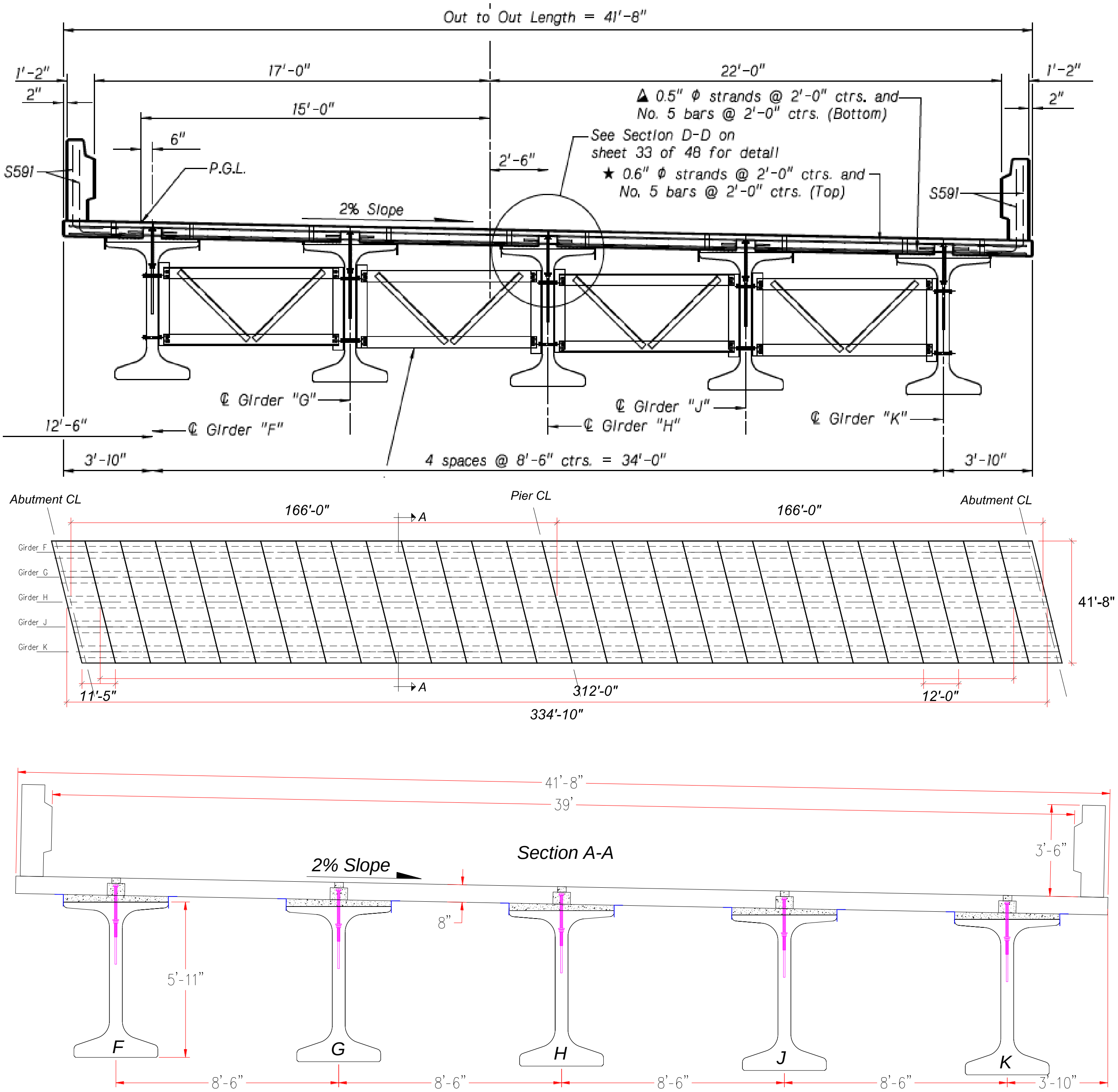
Out to Out Length = 41'-8"
1'-2"
2"
17'-0"
22'-0"
1'-2"
2"
15'-0"
6"
P.G.L.
S591
▲ 0.5" Φ strands @ 2'-0" ctrs. and
No. 5 bars @ 2'-0" ctrs. (Bottom)
See Section D-D on
sheet 33 of 48 for detail
★ 0.6" Φ strands @ 2'-0" ctrs. and
No. 5 bars @ 2'-0" ctrs. (Top)
2'-6"
2% Slope
S591
℄ Girder "G"
℄ Girder "J"
12'-6"
℄ Girder "F"
℄ Girder "H"
℄ Girder "K"
3'-10"
4 spaces @ 8'-6" ctrs. = 34'-0"
3'-10"
Abutment CL
Pier CL
Abutment CL
166'-0"
A
166'-0"
Girder F
Girder G
Girder H
Girder J
Girder K
41'-8"
A
11'-5"
312'-0"
12'-0"
334'-10"
41'-8"
39'
3'-6"
Section A-A
2% Slope
8"
5'-11"
F
G
H
J
K
8'-6"
8'-6"
8'-6"
8'-6"
3'-10"

FIGURE 1.1 Plan and cross section views of the northbound bridge

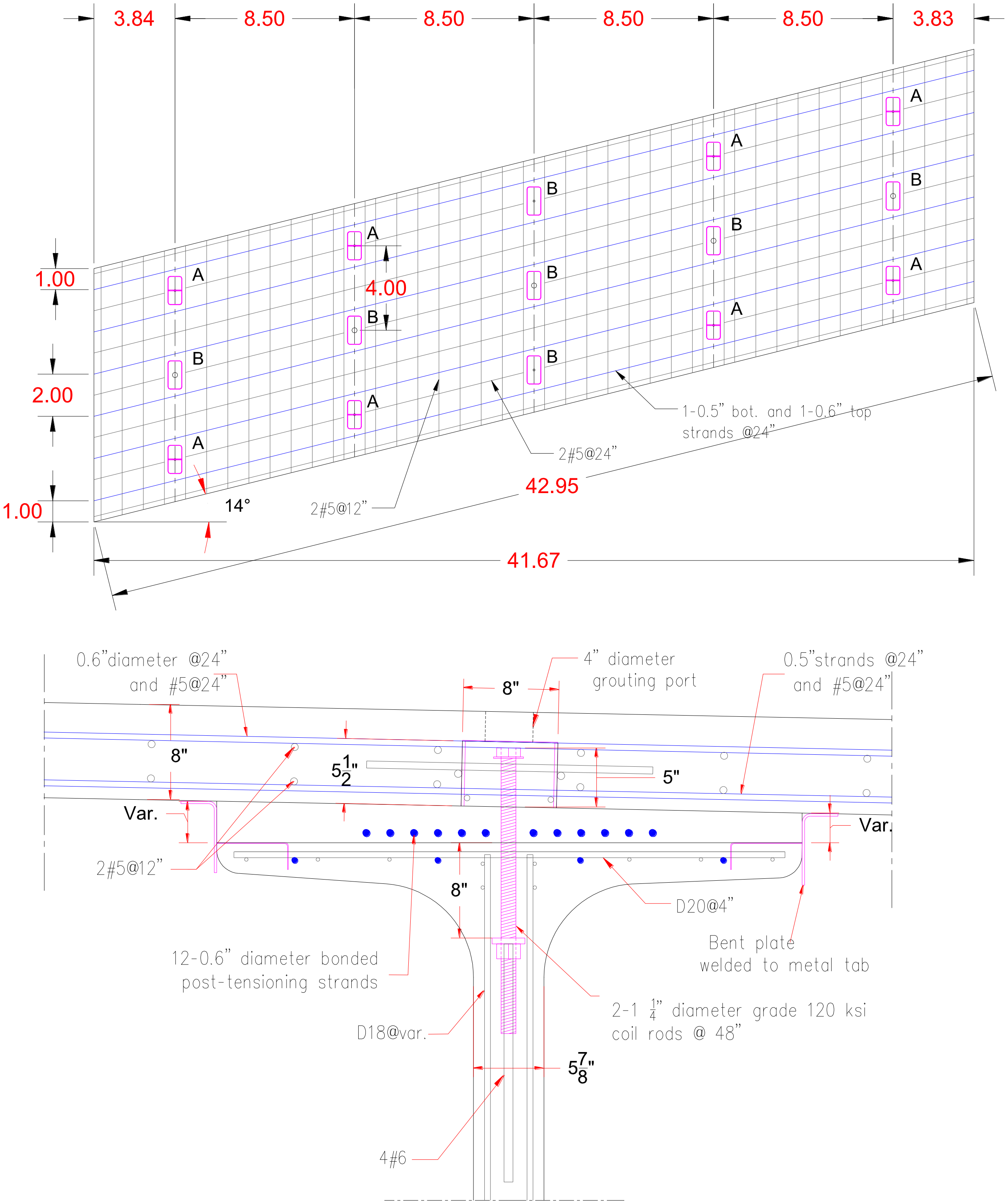
3.84
8.50
8.50
8.50
8.50
3.83
A
B
A
A
B
A
B
B
B
A
B
A
A
B
A
1.00
4.00
2.00
1.00
14°
2#5@12"
2#5@24"
1-0.5" bot. and 1-0.6" top
strands @24"
42.95
41.67
0.6"diameter @24"
and #5@24"
4" diameter
grouting port
0.5"strands @24"
and #5@24"
8"
8"
$5\frac{1}{2}$"
5"
Var.
Var.
2#5@12"
8"
D20@4"
Bent plate
welded to metal tab
12-0.6" diameter bonded
post-tensioning strands
2-1 $\frac{1}{4}$" diameter grade 120 ksi
coil rods @ 48"
D18@var.
$5\frac{7}{8}$"
4#6

FIGURE 1.2 Typical precast concrete deck panel and its connection to concrete girder

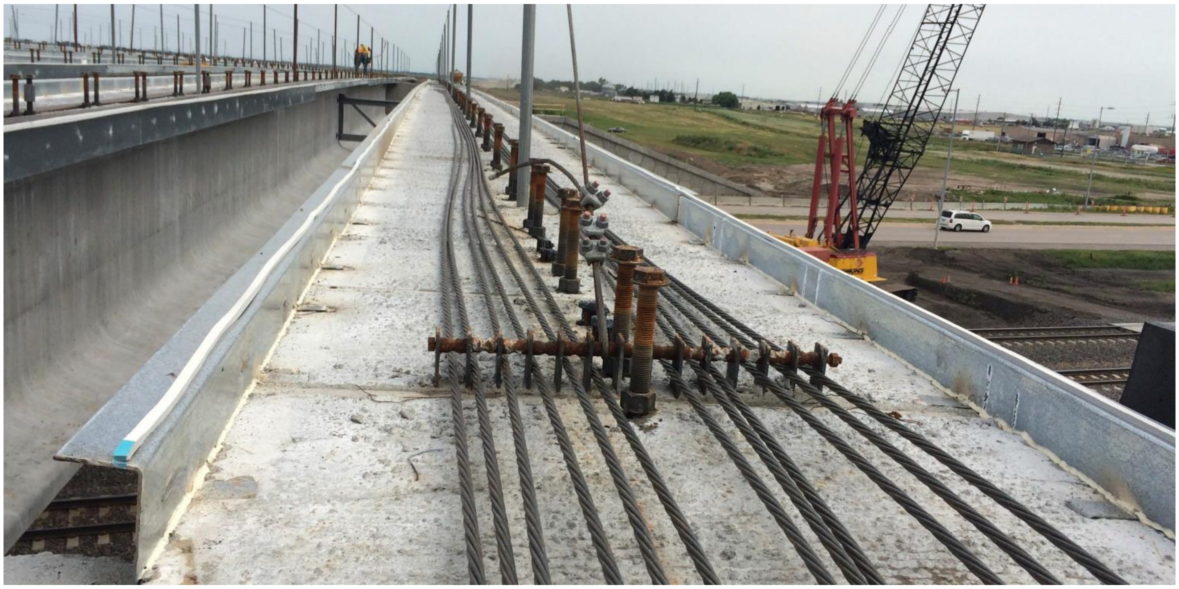

FIGURE 1.3 Deck support system, shear connectors, and PT deviators

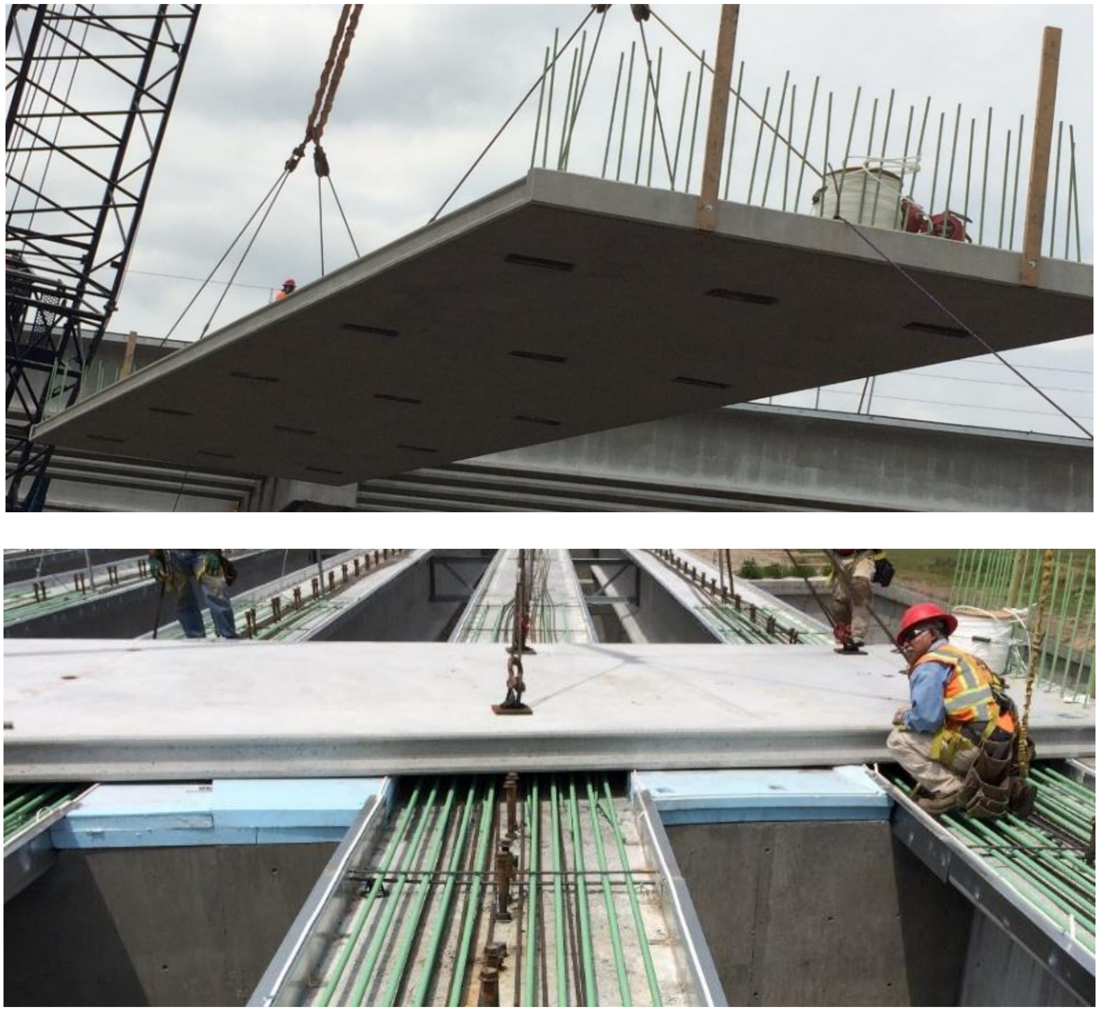

FIGURE 1.4 Deck panel erection

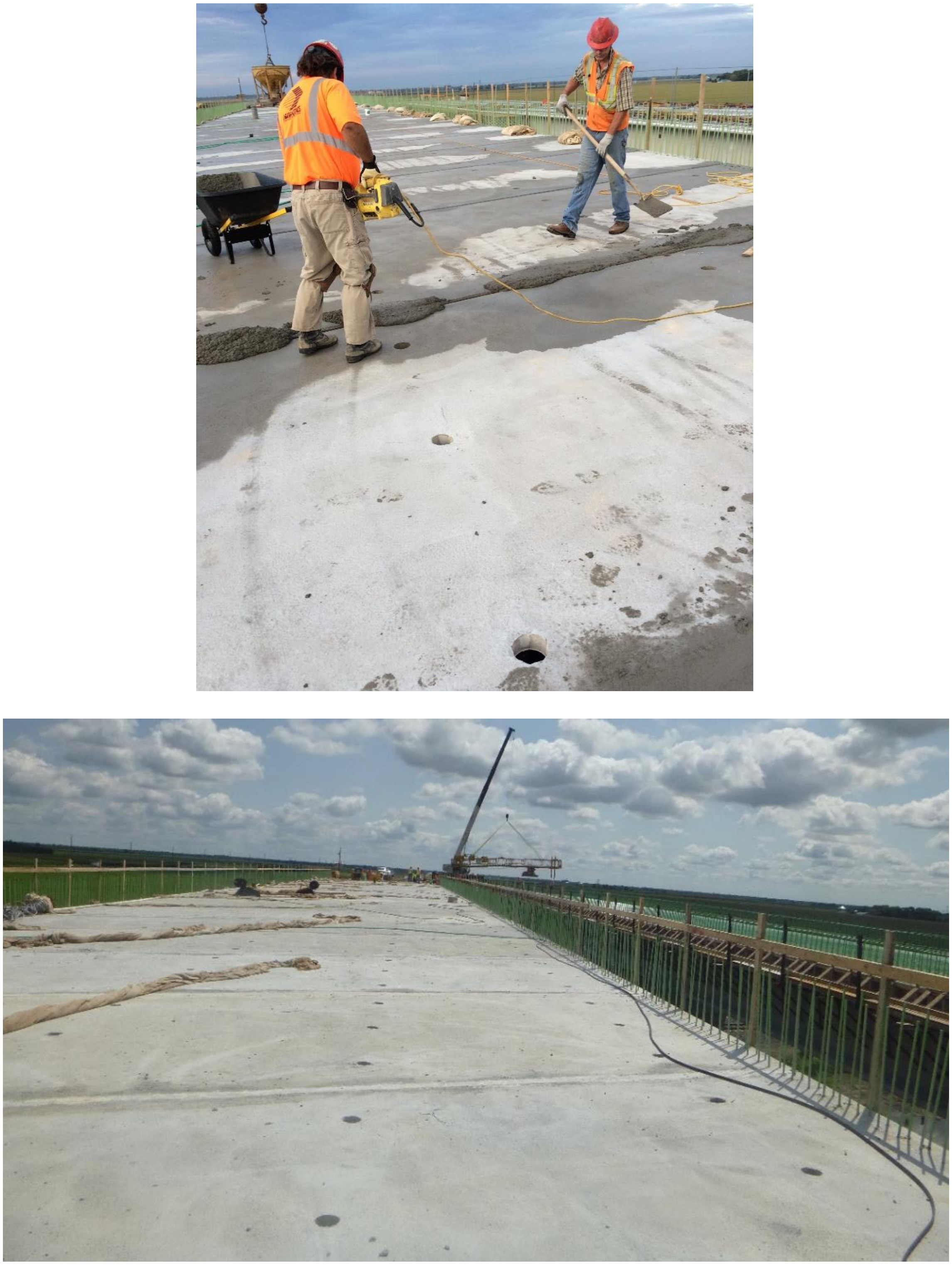

FIGURE 1.5 Precast concrete deck during and after grouting transverse joints

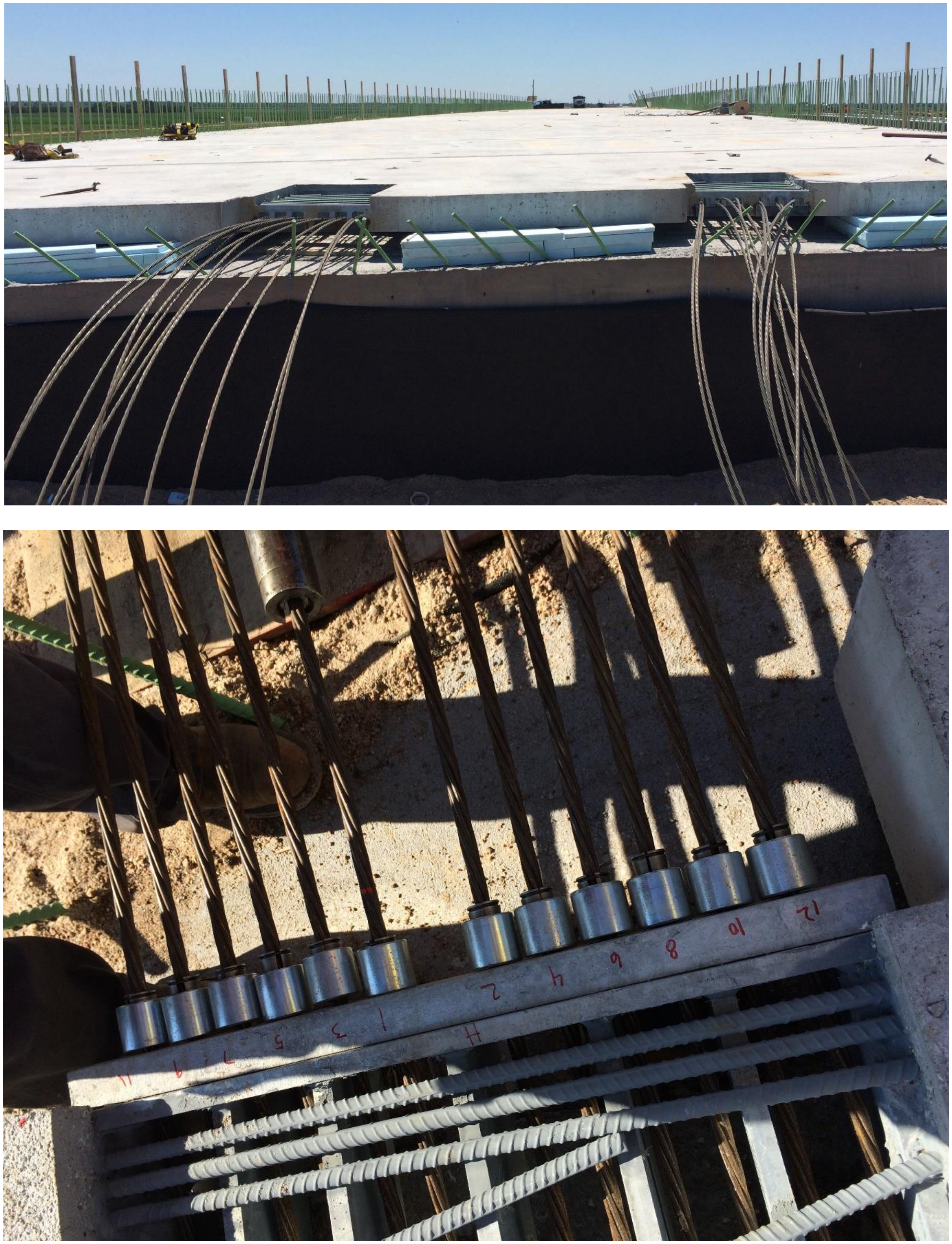
11
9
7
5
3
1
H
2
4
6
8
10
12

FIGURE 1.6 Post-tensioning the deck panels longitudinally using a new system

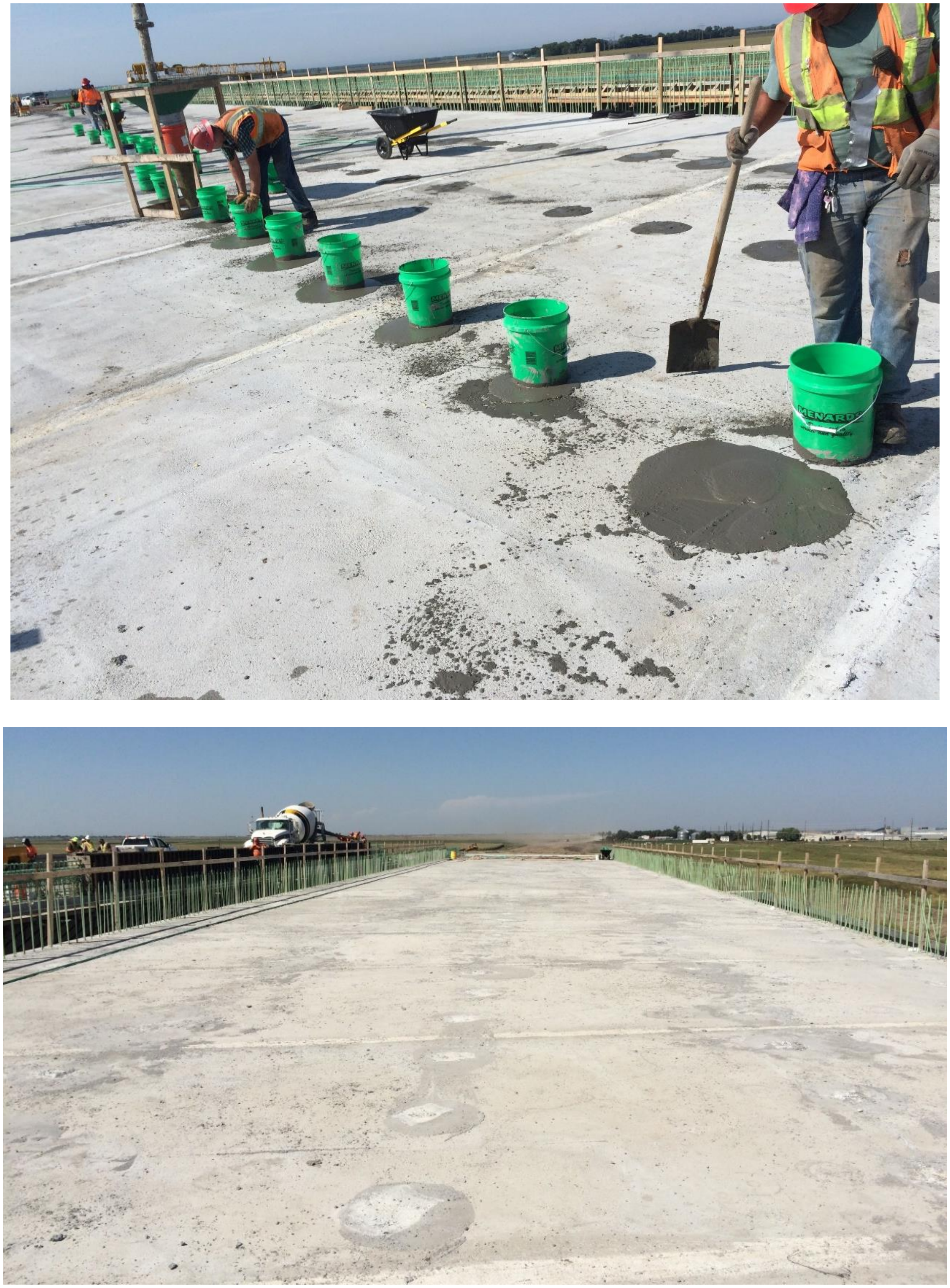

FIGURE 1.7 Precast concrete deck during and after grouting shear pockets and haunches

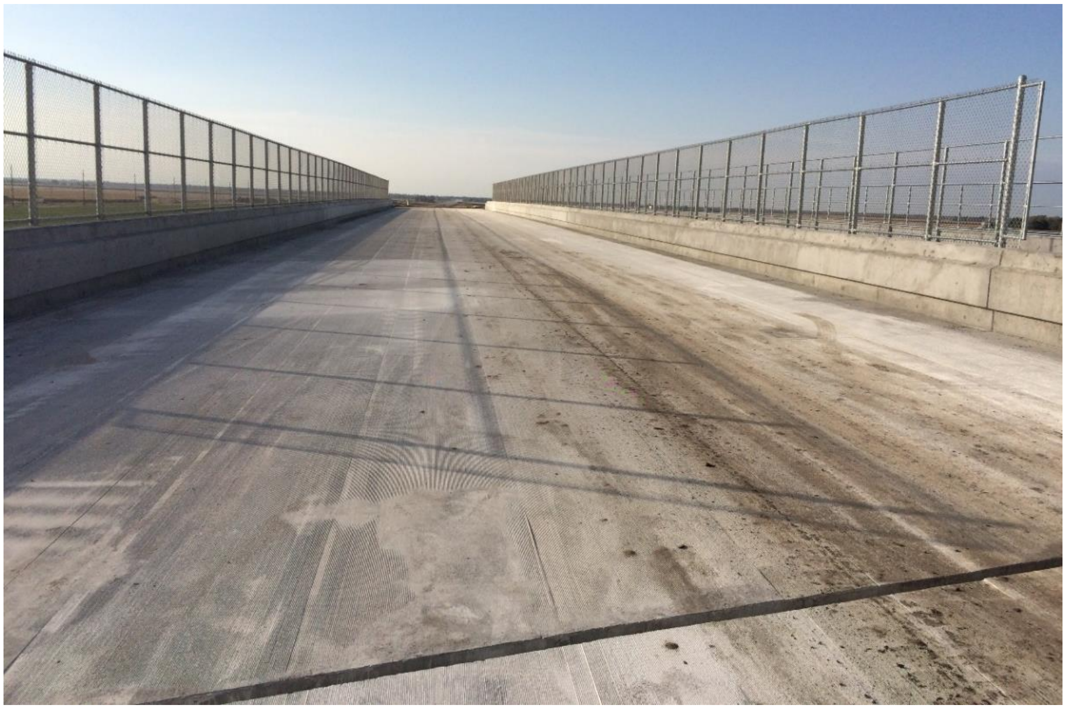

FIGURE 1.8 Precast concrete deck surface after grinding and casting the rail

1.3 Objectives

The main objective of the research project is to inspect, monitor, and evaluate the performance of the Kearney East Bypass bridge project for 3 years after completion. During this period, the bridge deck will be exposed (no-overlay) to allow visual inspections. Wired and wireless gauges will be used to monitor deck behavior during live load test and under service loads. Data collected from long-term monitoring as well as those obtained from finite element analysis (FEA) will be used to evaluate the performance of the new deck system in comparison to the performance of the conventional cast-in-place deck system.

The following sections of the report present: a) deck visual inspection records; b) instrumentation plan and live load testing conducted for both CIP concrete deck and PC deck systems as well as results comparison with finite element analysis; c) long-term monitoring of the new deck system under traffic loads; and d) summary of project conclusions. Appendixes present additional photos of bridge construction, inspection, and instrumentation as well as prestress loss calculations.

2 DECK VISUAL INSPECTIONS

In order to evaluate the durability of the new precast concrete deck system, several visual inspections were conducted by the project investigators and their graduate students for both cast-in-place (CIP) concrete deck precast concrete (PC) deck. In these inspections, the bridge deck surface was examined for cracking at critical locations, such as the joint with the approach slab, mid-span section, over the intermediate pier for the CIP concrete deck; and transverse joints, anchorage blocks, and grouting holes for the PC deck. In some cases where a man lift was available, the underside of the deck was also inspected.

The following visits were conducted, which are presented in their chronological order as follows:

1. October 7, 2015: Directly after the construction was completed and before the bridge was opened to traffic.
2. June 6, 2016: After the first winter and before the bridge was opened to traffic. The bridge was only used for road construction traffic. This visit was done during the bridge instrumentation and load testing
3. June 22, 2017 Visit: After the second winter and seven months after the bridge was opened to traffic.
4. October 16, 2018: After the third winter and almost two years after the bridge was opened to traffic.
5. July 24, 2019: After the fourth winder and two years and eight months after the bridge was opened to traffic.

2.1 October 7, 2015 Visit

This visit was conducted after the construction of the twin bridges was completed. The research team requested that the contractor removes the exterior galvanized bent plates used to support the precast deck panels during construction. This was conducted to inspect the consolidation of the concrete cast to grout the shear pockets and haunches using the new technique (i.e. highly flowable SCC cast through 4 in. diameter grout holes located at 4 ft spacing). Figure 2.1 shows the proper consolidation of haunch concrete at the girder ends. Figures 2.2 and 2.3 show the transverse joints and grout holes after grinding the deck surface respectively. The coarse aggregate shown at the ground joints and grout holes indicate the stability of the concrete used. Figures 2.4 and 2.5 show the underside of the deck at intermediate and end diaphragms respectively. These photos indicate that there was no leakage at neither the transverse joints nor the deck-to-girder connections.

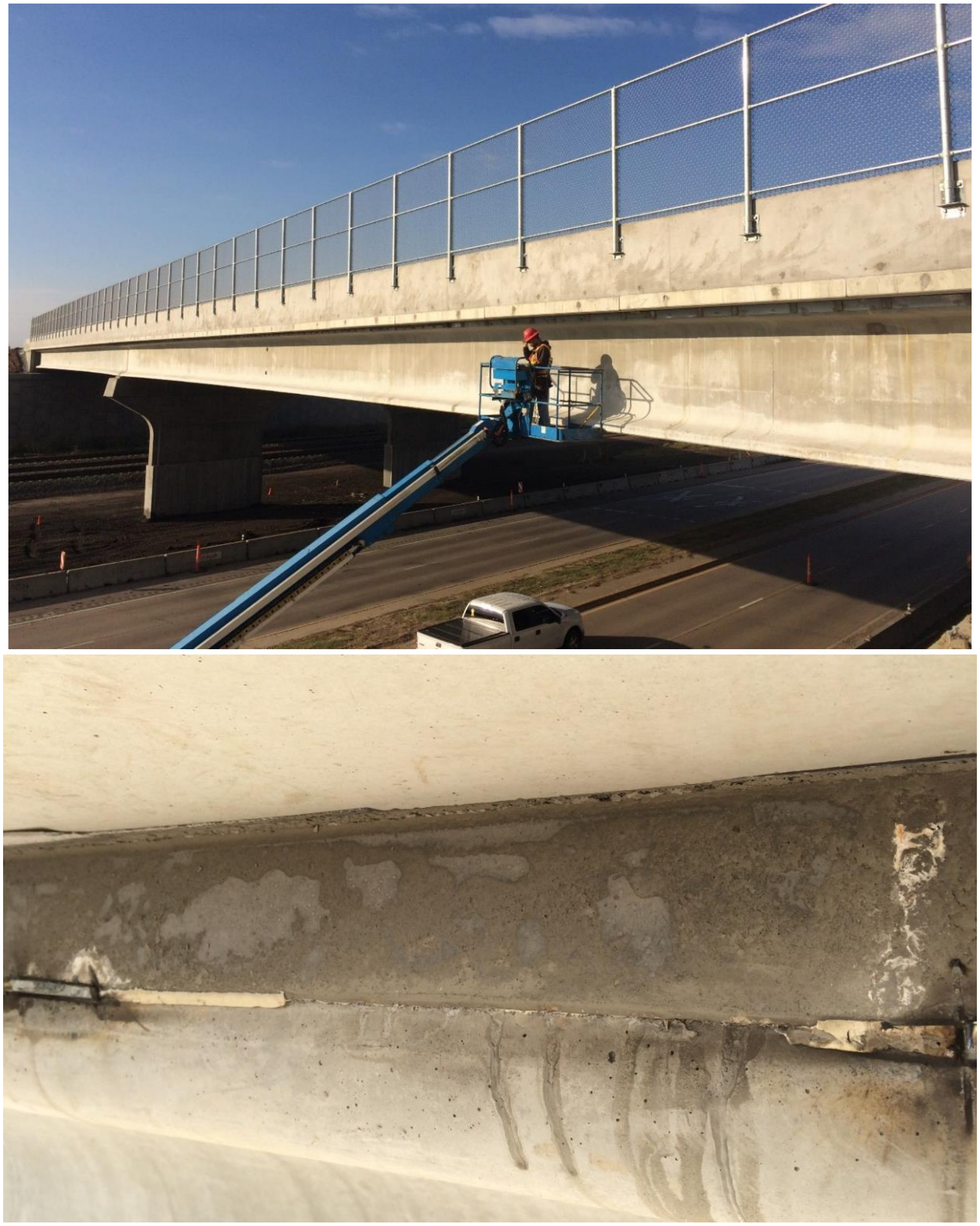

FIGURE 2.1 Removal of deck support system to inspect the SCC haunch

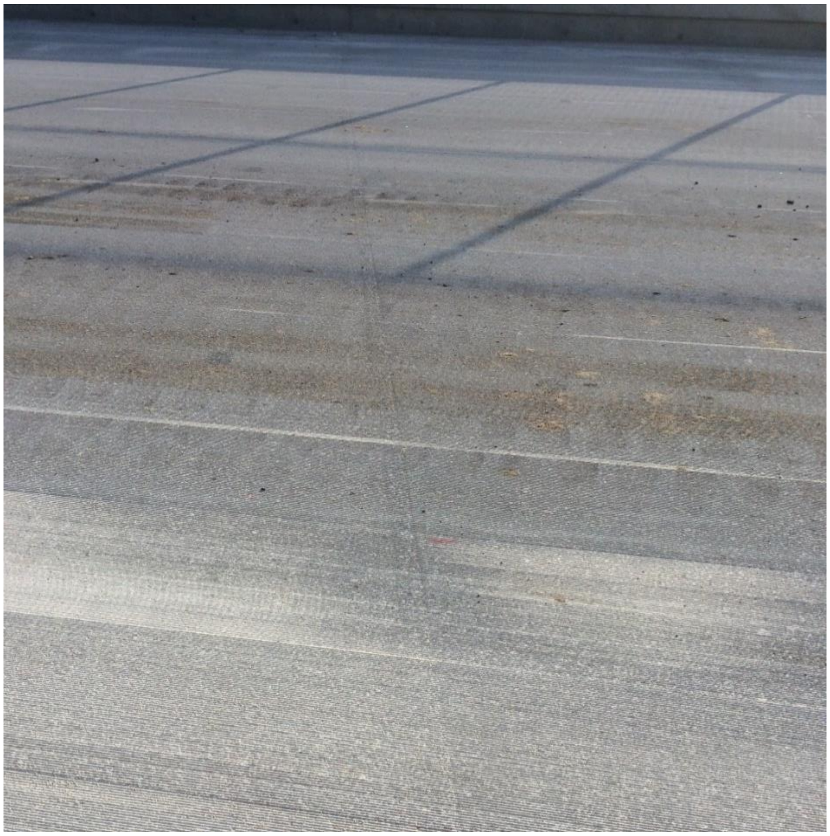

FIGURE 2.2 Transverse joint between adjacent precast concrete deck panels

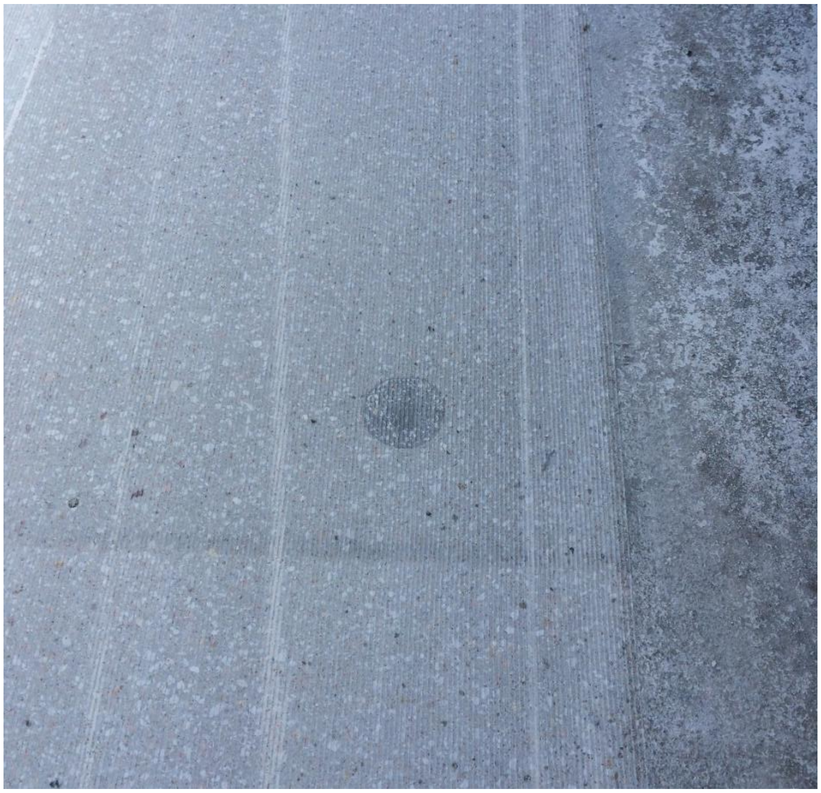

FIGURE 2.3 Grouting hole in precast concrete deck panels

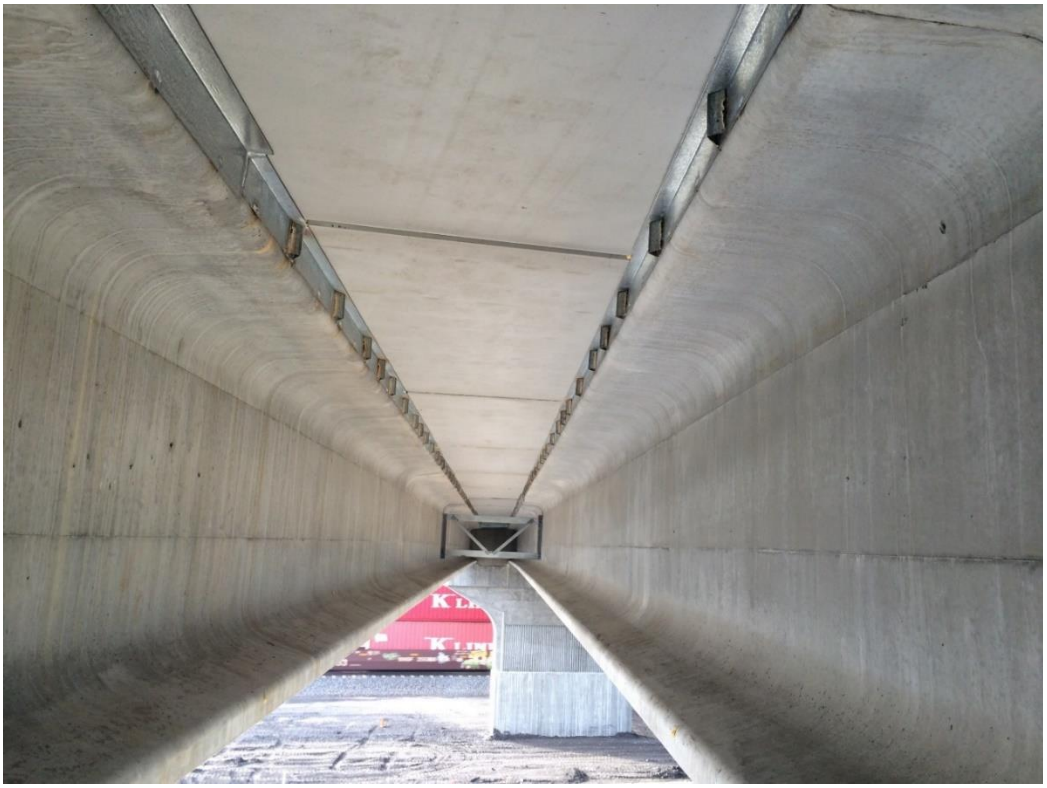
FIGURE 2.4 Underside of the precast concrete deck panels and intermediate diaphragm

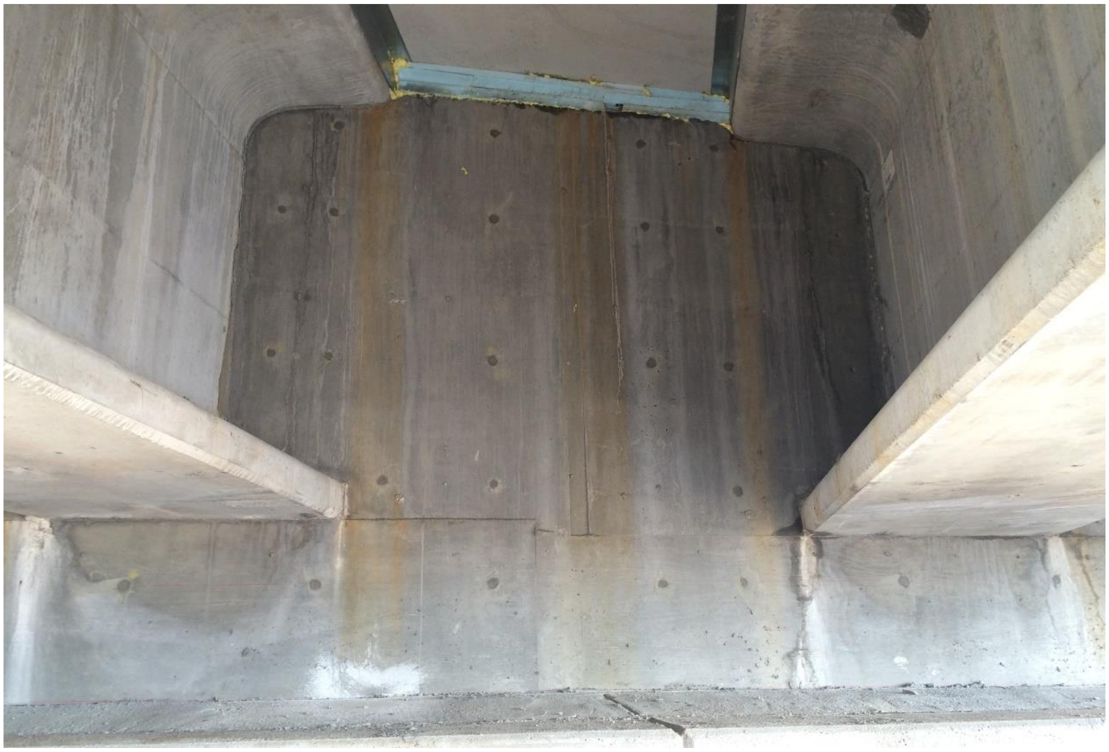
FIGURE 2.5 Girder ends and deck soffit at end diaphragm

2.2 June 6, 2016 Visit

This visit was conducted almost one year after construction was completed and the same time the research time instrumented the bridge for live load testing. Figures 2.6, 2.7, and 2.8 show an anchorage block, transverse joint, and grouting hole, respectively, which are the locations of field cast concrete. In general, these locations looked fine with the exception of slight difference in color and pour lines between precast and cast-in-place concrete in some places. Figure 2.9 shows a side-by-side comparison between cast-in-place deck and precast deck surfaces indicating similar riding surface texture and color. Figure 2.10 shows a photo of another location at an exterior girder where the deck support system was removed to evaluate the consolidation of the haunch concrete.

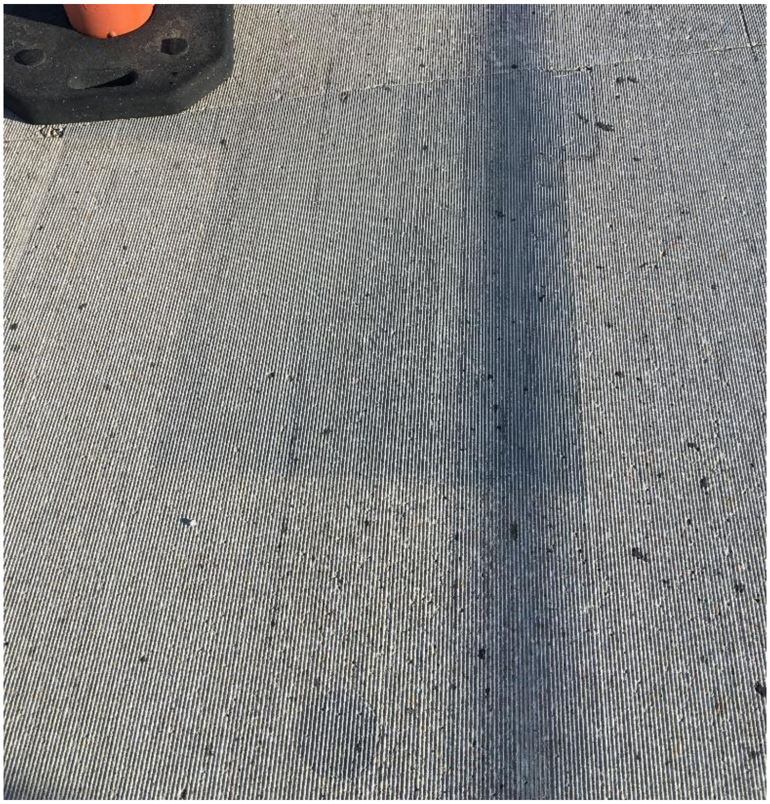

FIGURE 2.6 Anchorage block and grouting hole in the precast concrete deck

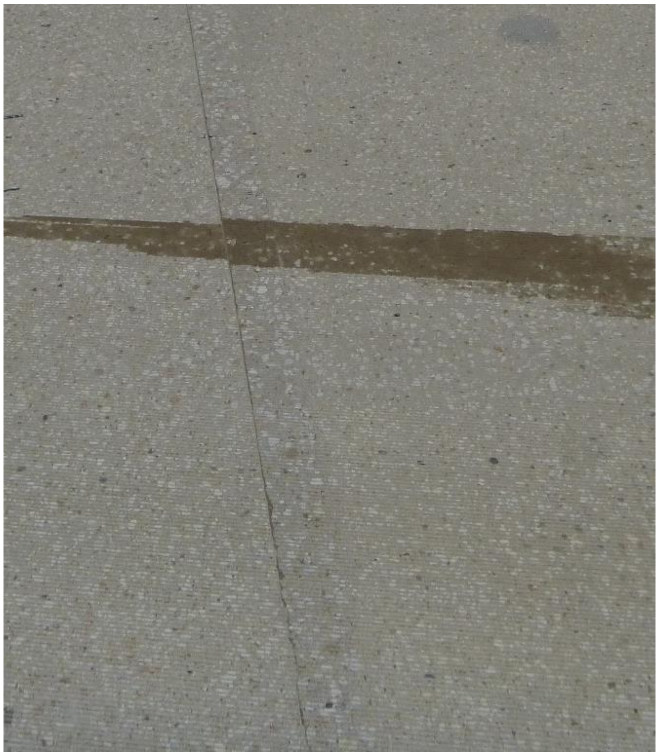

FIGURE 2.7 Transverse joint with pour line between cast-in-place and precast concrete at the intermediate pier

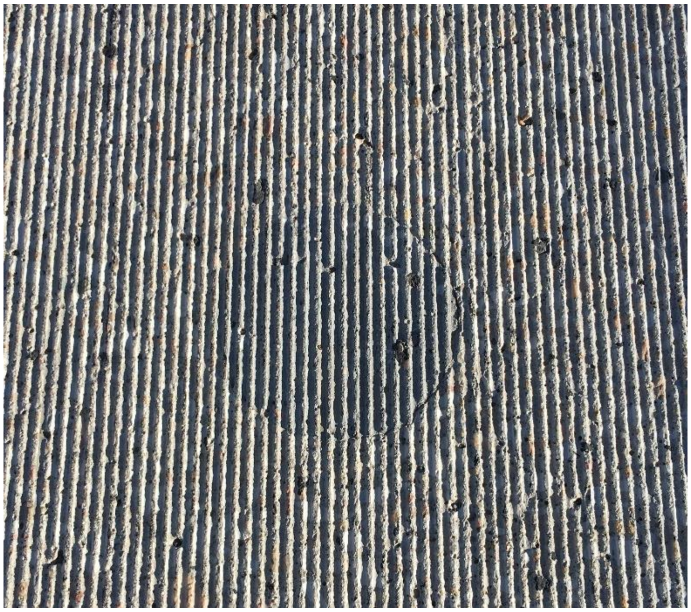

FIGURE 2.8 Grouting hole with fine pour line at its circumference

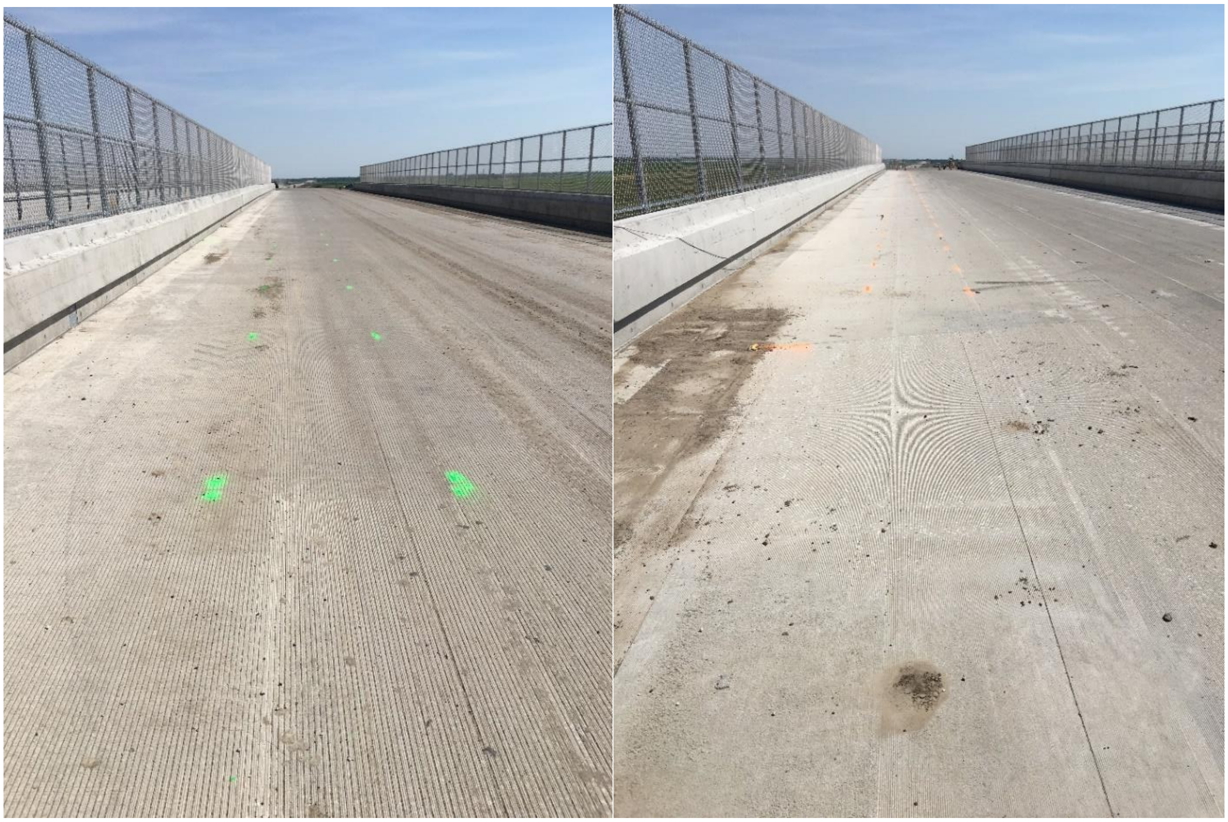

FIGURE 2.9 Cast-in-place concrete deck (left) and precast concrete deck (right)

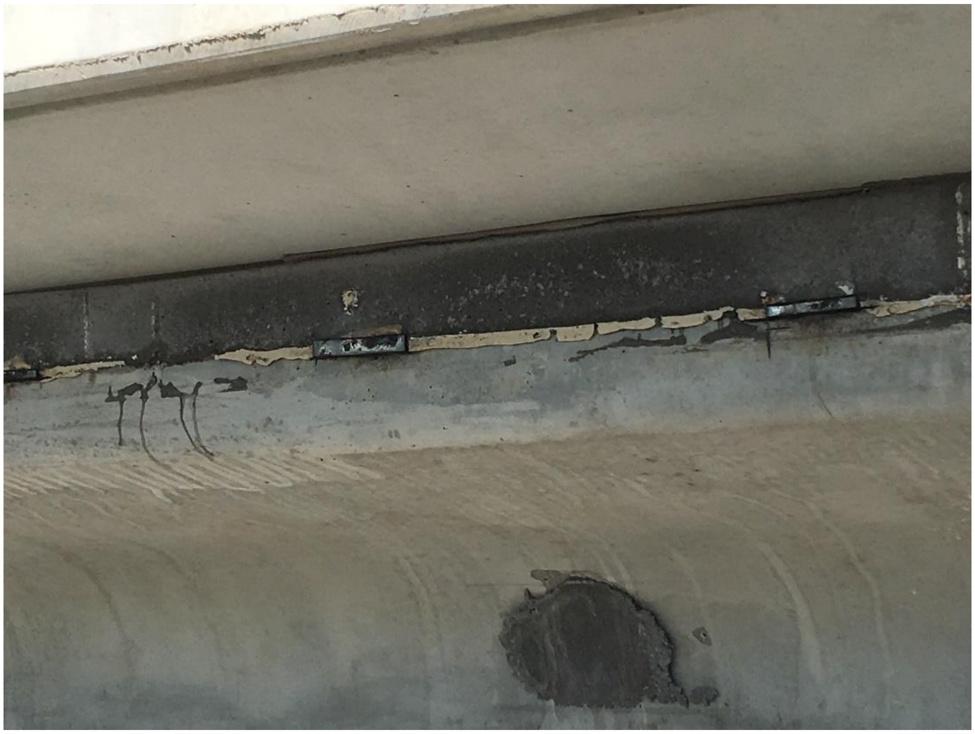

FIGURE 2.10 Exterior girder haunch cast using SCC

2.3 June 22, 2017 Visit

This visit was conducted seven months after the bridge was opened to traffic (almost two years after construction). Figures 2.11, 2.12, and 2.13 show the cast-in-place deck constructed at the same time on the southbound bridge at three different locations: end of floor, mid span, and pier section, respectively. These figures show cracking in all these locations. Random cracking at joint between deck and approach slab, and transverse cracks at the mid-span and pier section. Figures 2.14 and 2.15 show that there is no cracking in the precast deck panels at any of these locations. However, there is a noticeable uniform pour line at the interface between the cast-in-place transverse joint and precast deck panels. The width of this line is approximately 0.04 in. and was found to remain constant over time. Minor cracks were also observed in few grouting holes and south anchorage blocks as shown in Figures 2.16, 2.17, and 2.18. No cracks were detected in the north anchorage blocks as shown in Figure 2.19.

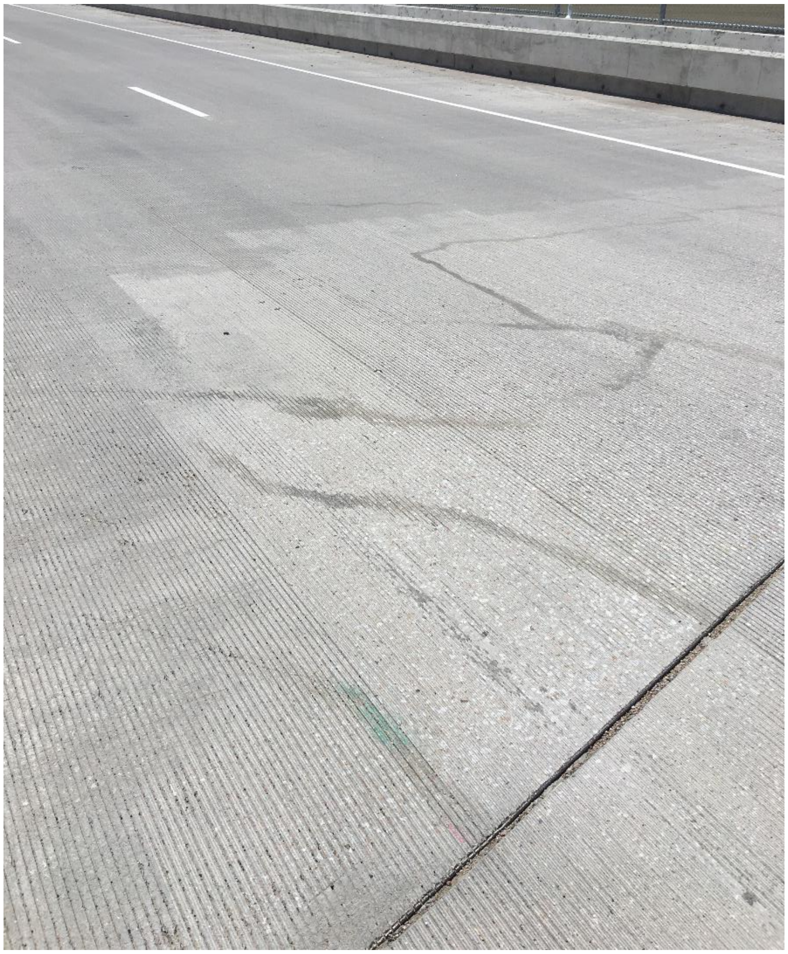

FIGURE 2.11 Diagonal cracks at the end of the skewed cast-in-place concrete deck

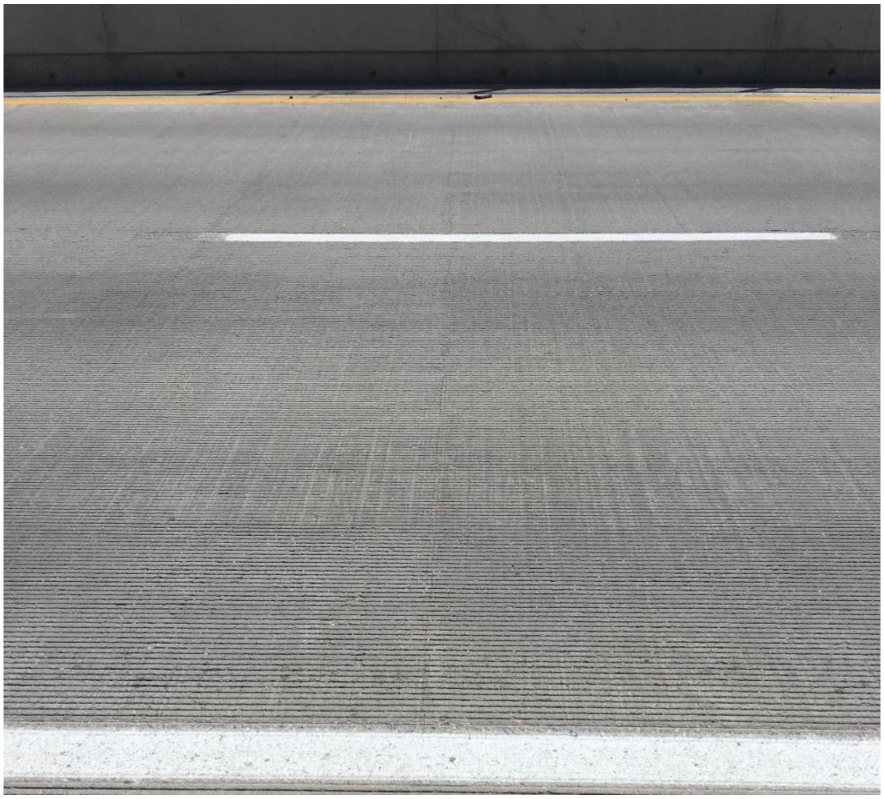
FIGURE 2.12 Transverse cracks in the cast-in-place concrete deck at mid-span section

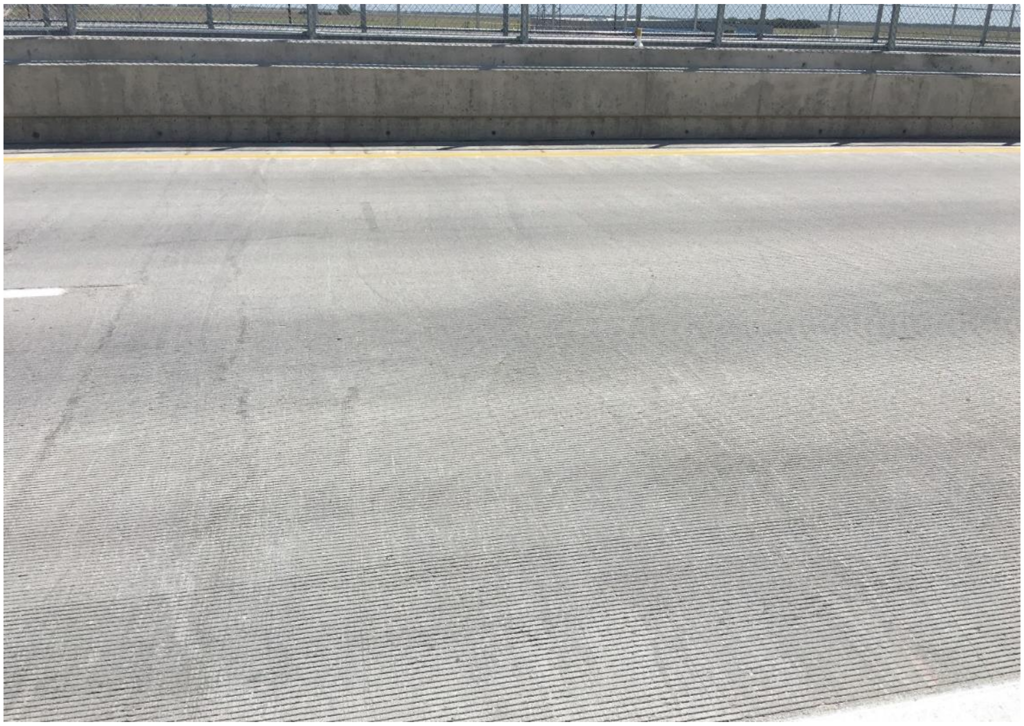
FIGURE 2.13 Transverse cracks in the cast-in-place concrete deck at the intermediate pier

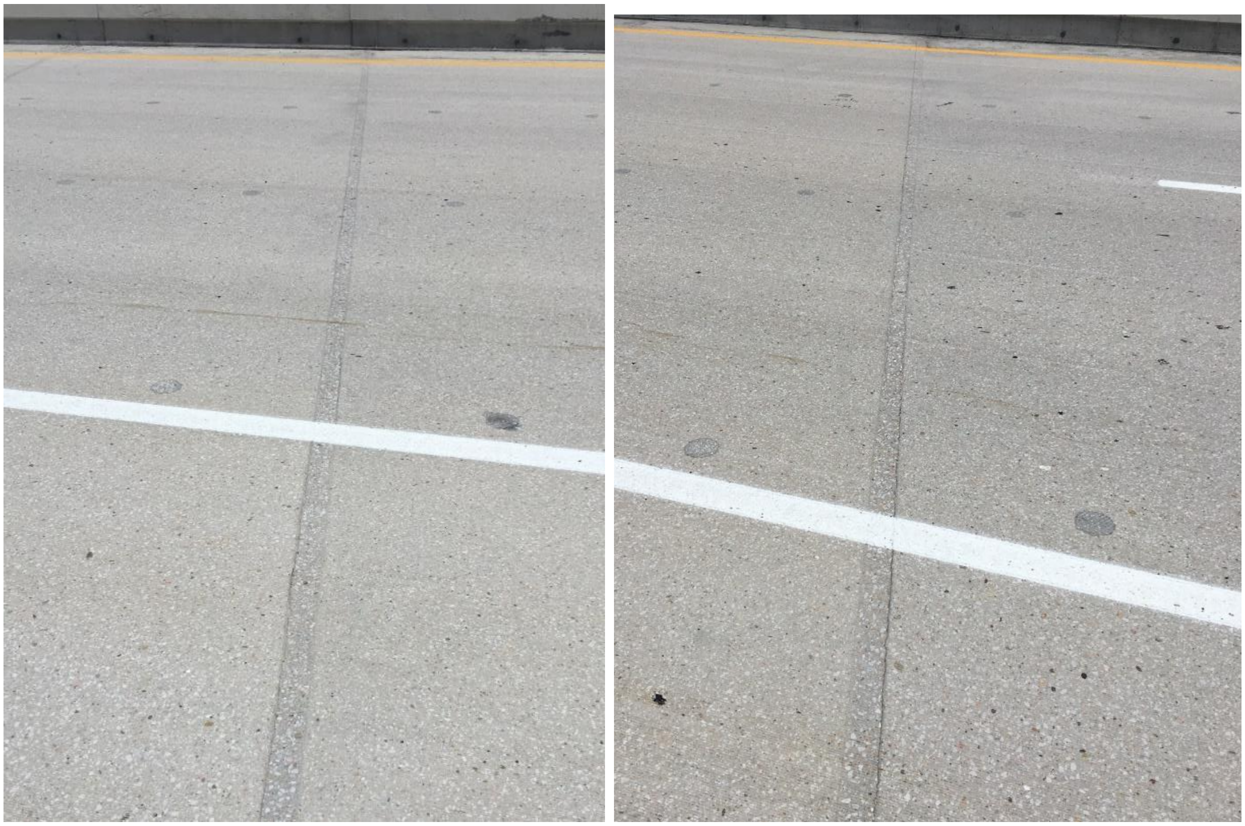

FIGURE 2.14 Transverse joints between precast concrete deck panels at the intermediate pier section (left) and mid-span section (right)

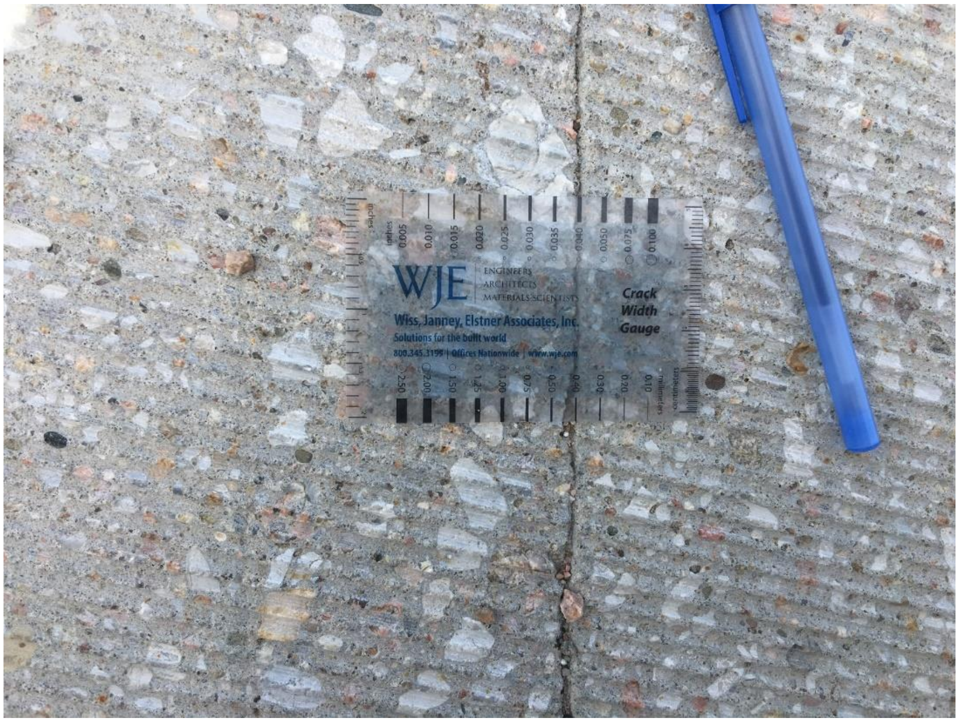
WJE
Wiss, Janney, Elstner Associates, Inc.
Crack Width Gauge

FIGURE 2.15 Measurement of the crack width at the intermediate pier joint

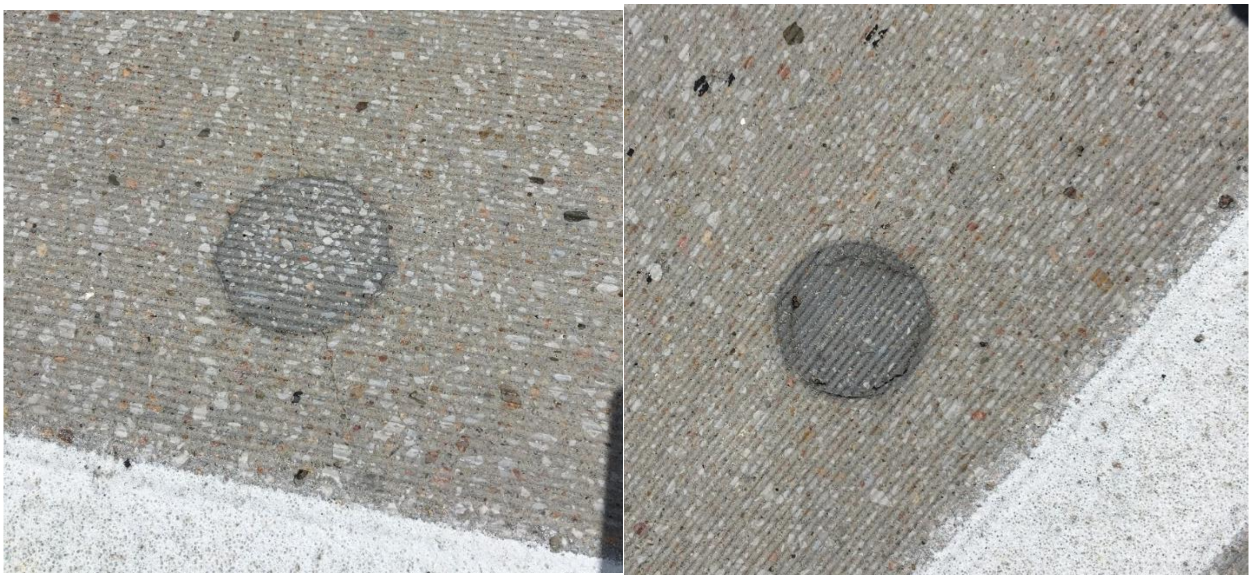

FIGURE 2.16 Fine cracks inside some of the grouting holes of the precast concrete deck

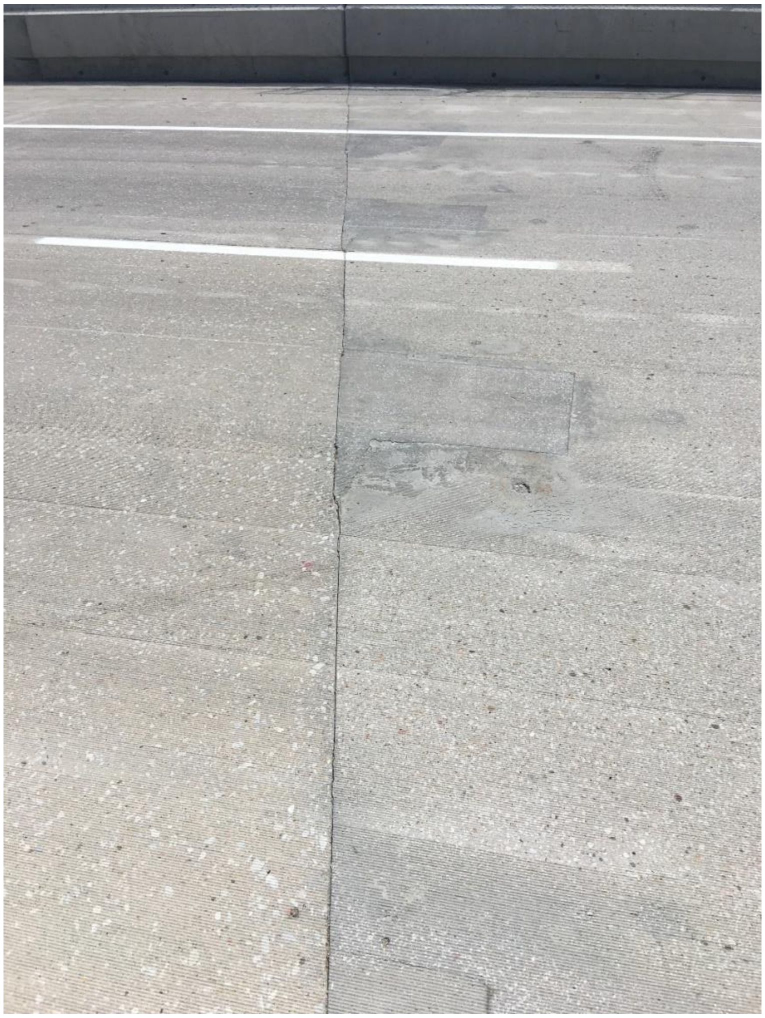

FIGURE 2.17 End panel joint with the approach slab and south anchorage blocks

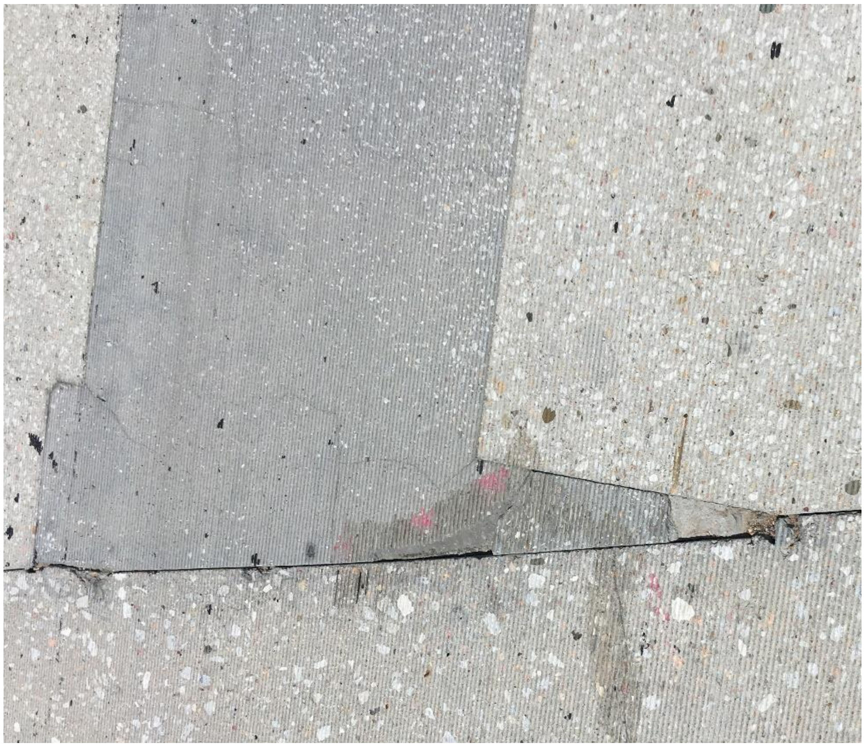

FIGURE 2.18 Random cracking at one of the south anchorage blocks

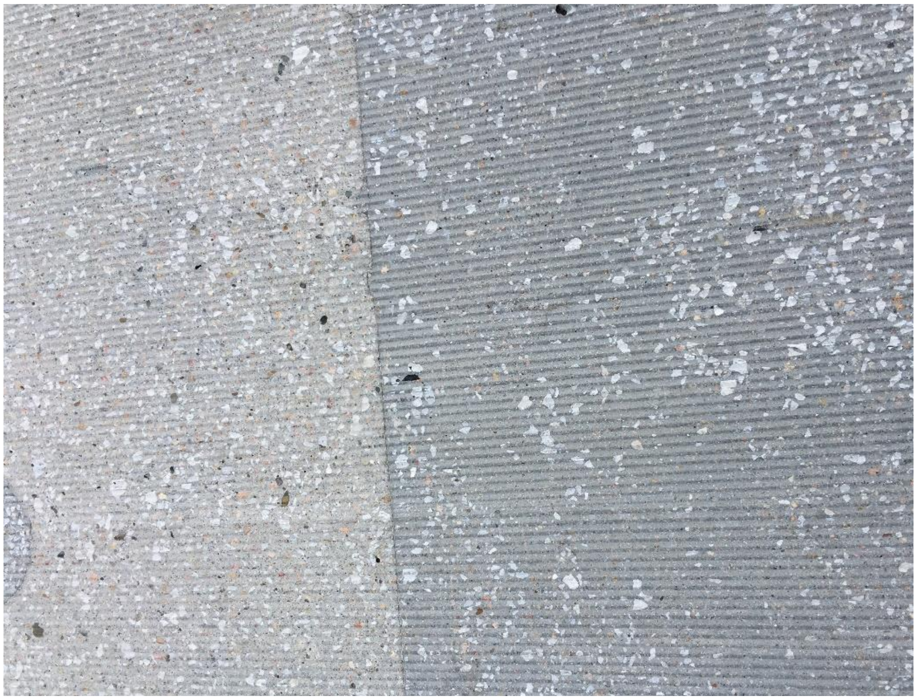

FIGURE 2.19 No cracking at the north anchorage blocks of precast concrete deck

2.4 October 16, 2018 Visit

This visit was conducted almost two years after the bridge was opened to traffic (more than three years after construction). Figures 2.20, and 2.21 show the cast-in-place deck cracking at the negative moment region, which is more noticeable than those in the previous visual inspection. Figures 2.22 shows the pier section transverse joint, which is in the same condition observed in earlier inspections. This means there is no increase in the width of the pour line or any signs of progressive deterioration. Figure 2.23 shows the PT anchorage blocks on the south and north ends of the precast deck with signs of progressive deterioration at the wedge-like corner of the blocks, while Figure 2.24 shows similar type of distress at one of the grouting holes. These isolated incidents could be attributed to the effect of freeze-thaw cycles on such unreinforced portions of concrete. It could also be aggravated during the snow removal operations.

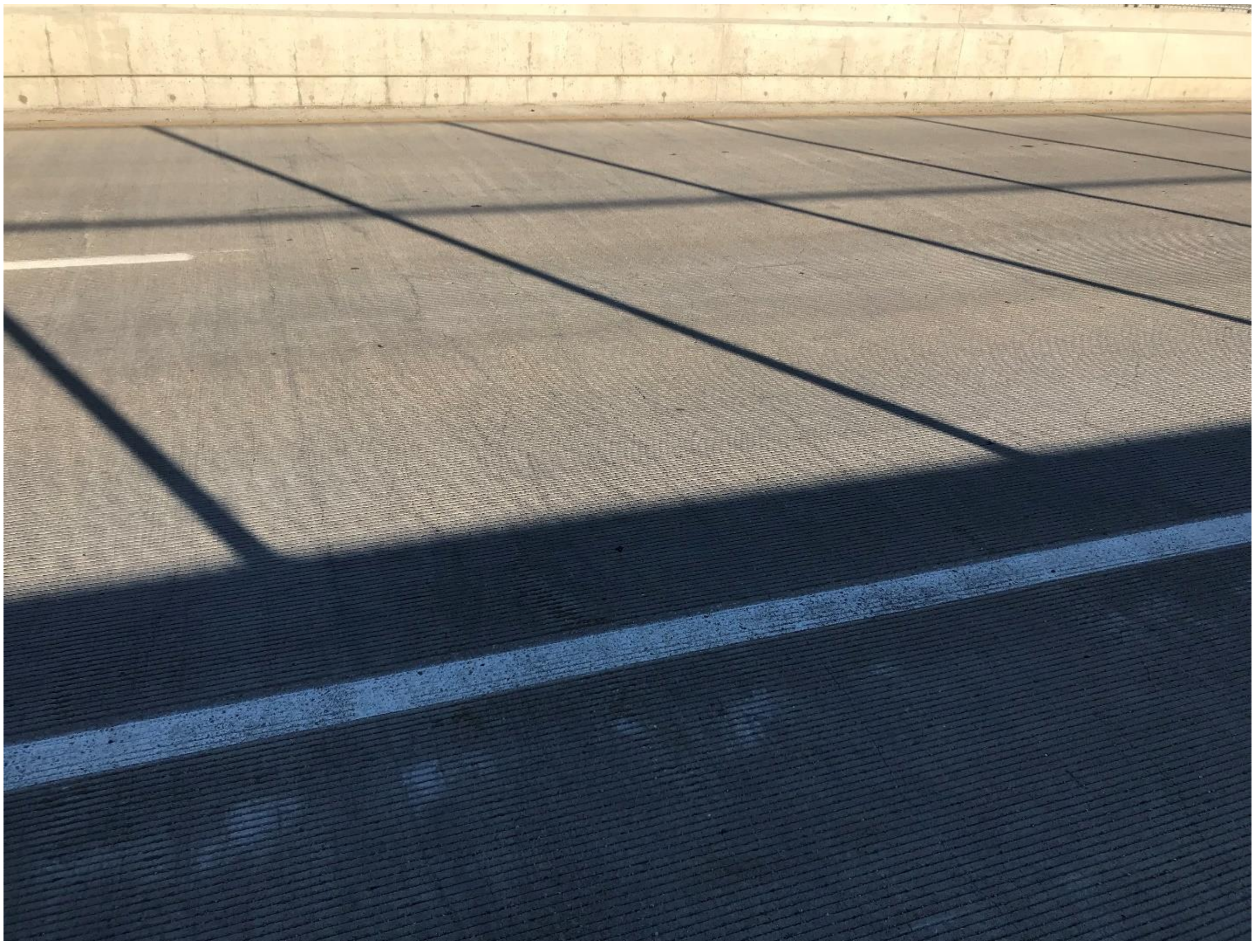

FIGURE 2.20 Multiple transverse cracks at the negative moment region of CIP deck

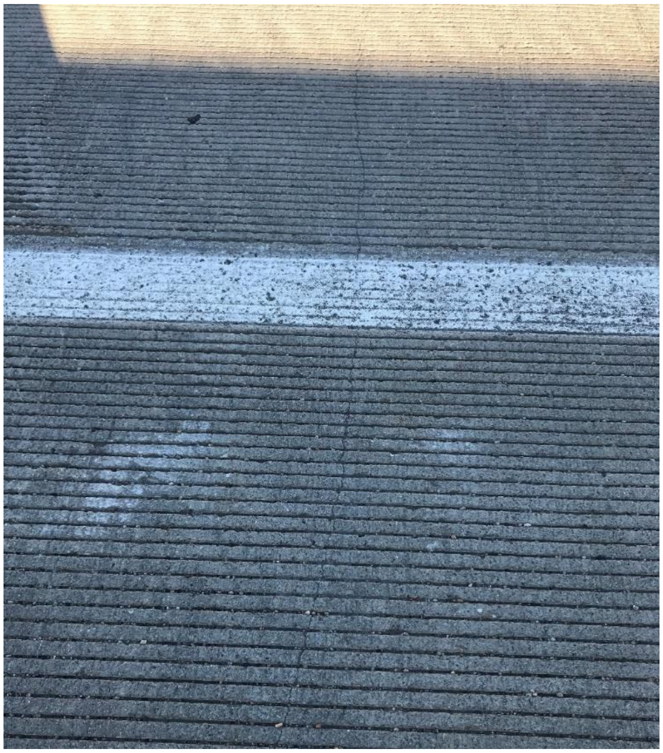

FIGURE 2.21 One of the transverse cracks extending the full width of CIP deck

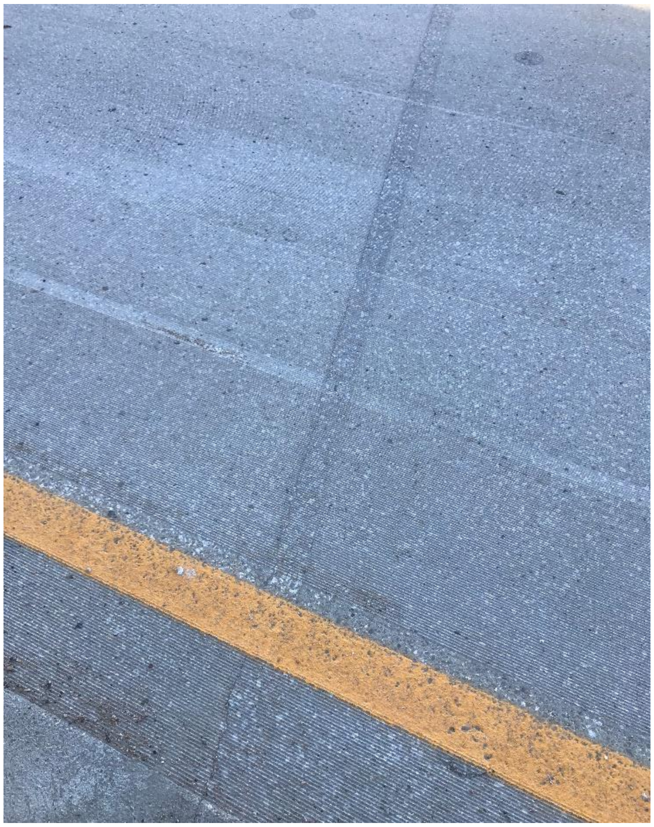

FIGURE 2.22 Pier section transverse joint in precast deck

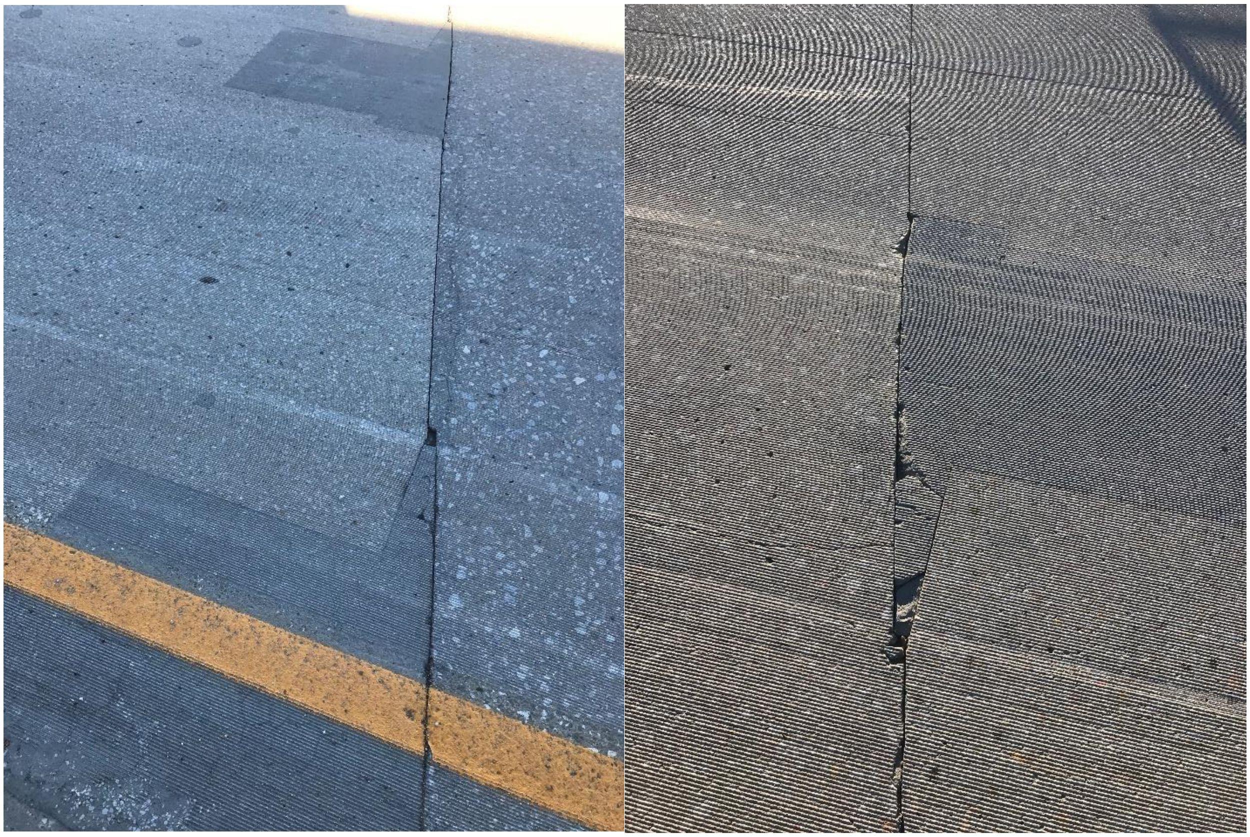

FIGURE 2.23 North (left) and south (right) PT anchorage blocks of the precast deck

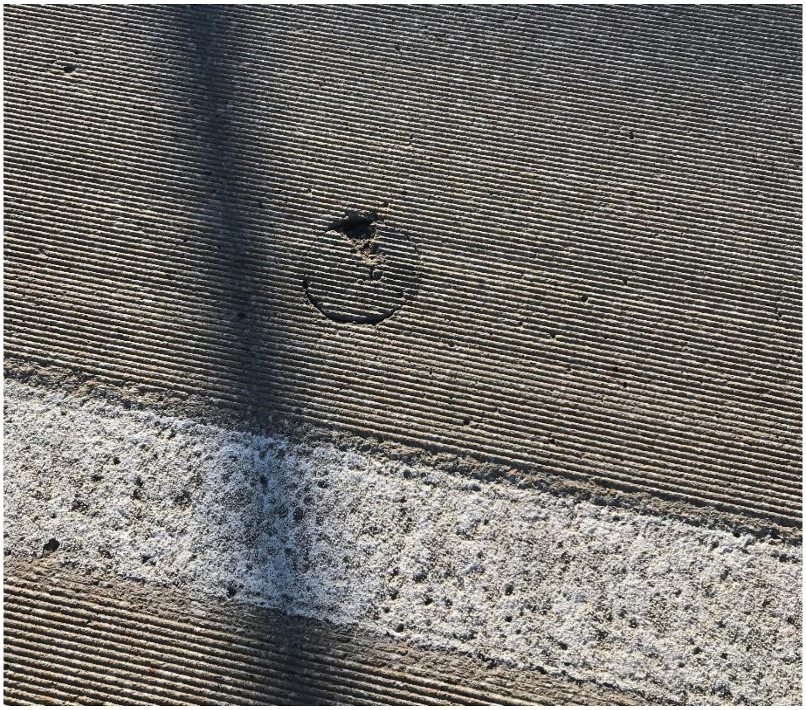

FIGURE 2.24 One of the grouting holes with signs of distress

2.5 July 24, 2019 Visit

This visit was conducted almost four years after the bridge was completed. Figures 2.25 and 2.26 show the cast-in-place deck cracking at the negative moment region and at the end of the deck, respectively, which are similar to those observed in the previous visual inspection. Figures 2.27 shows the pier section transverse joint, which is in the same condition observed in earlier inspections. This means there is no increase in the width of the pour line or any signs of progressive deterioration. Figure 2.28 shows the PT anchorage blocks on the south and north ends of the precast deck with signs of progressive deterioration at the wedge-like corner of the blocks, while Figure 2.29 shows cracking at one of the grouting holes, which is also similar to observations made in earlier inspections. No additional cracking or damaged was observed in this visit. Below are the condition ratings obtained from the bi-annual routine inspections conducted by NDOT.

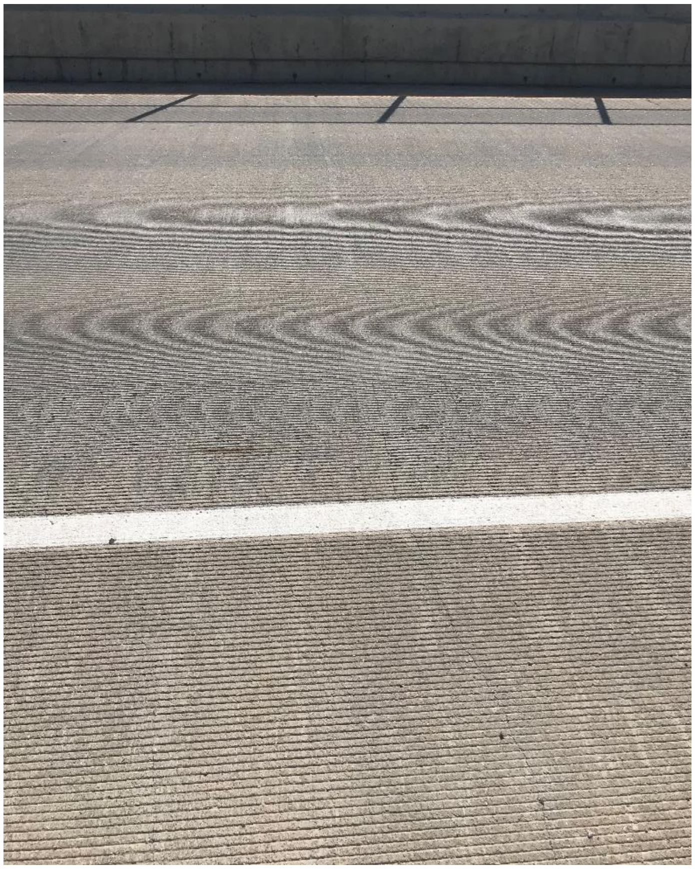

FIGURE 2.25 Multiple transverse cracks at the negative moment region of CIP deck

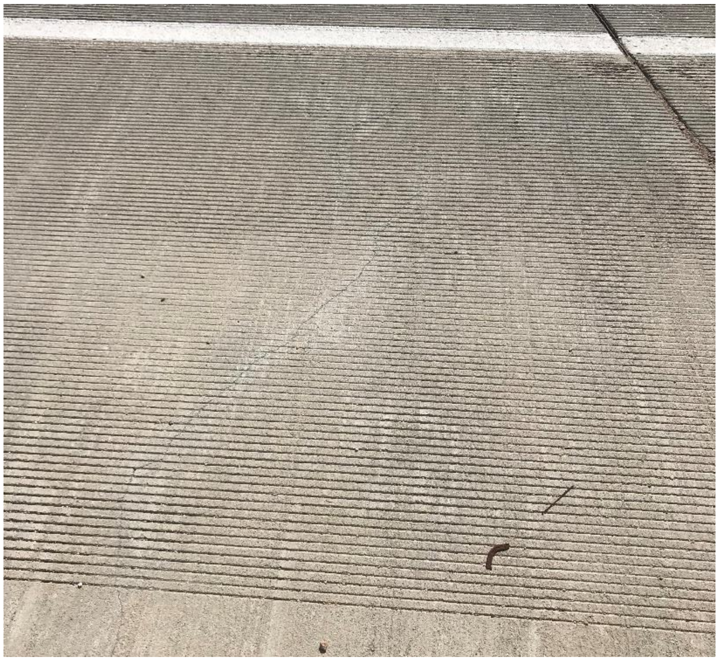

FIGURE 2.26 One of the transverse cracks extending the full width of CIP deck

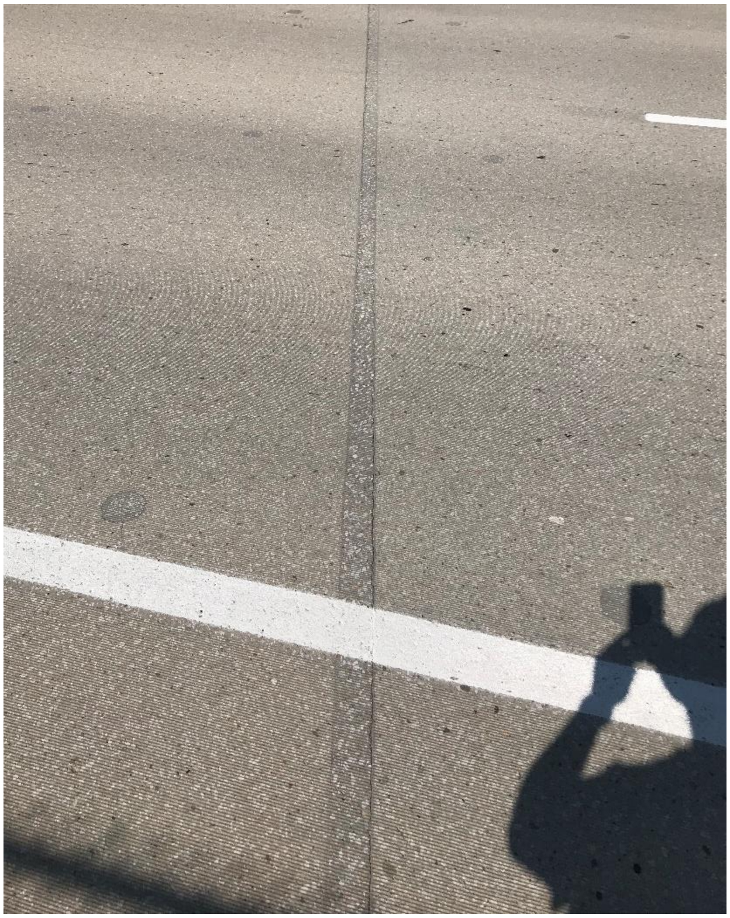

FIGURE 2.27 Pier section transverse joint in precast deck

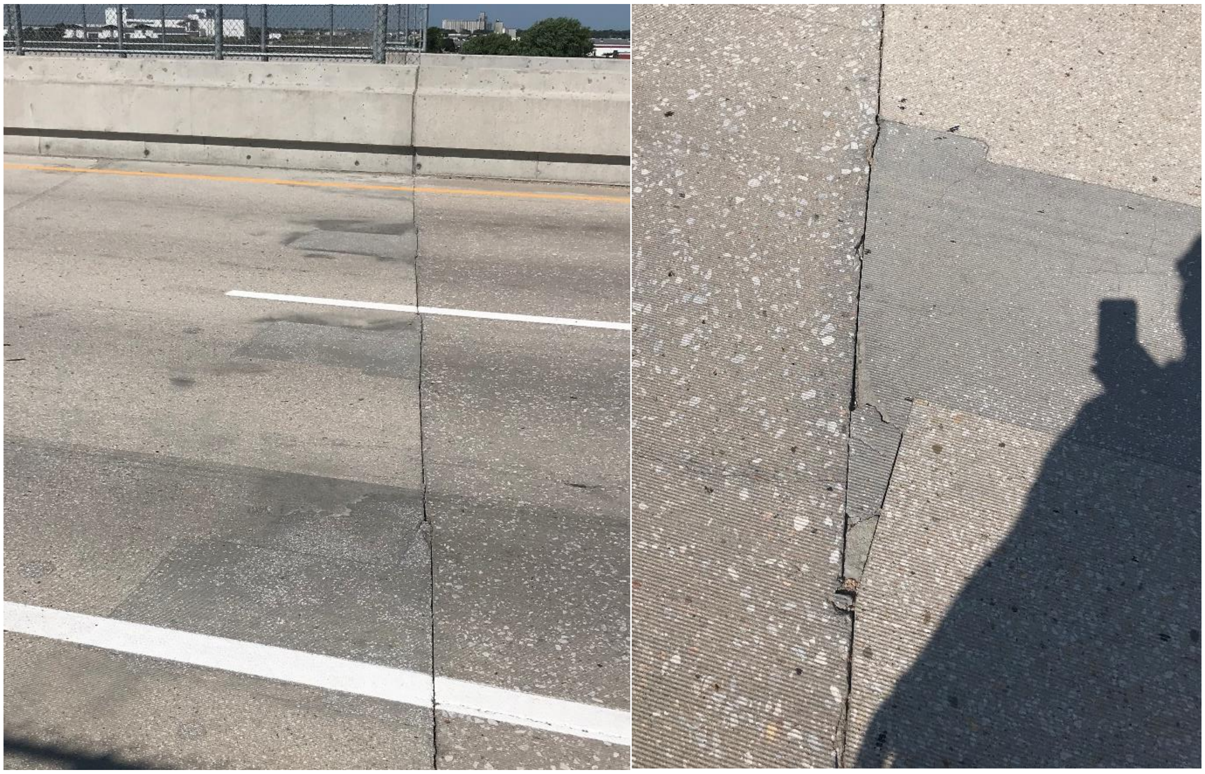

FIGURE 2.28 North (left) and south (right) PT anchorage blocks of the precast deck

FIGURE 2.29 One of the grouting holes with cracking

3 LOAD TESTING

3.1 Bridge Instrumentation

In order to ensure that the new precast concrete deck system is performing as designed, a monitoring system was installed for short-term and long-term performance of the precast concrete (PC) deck bridge and the short-term performance of the cast-in-place (CIP) concrete deck bridge for comparison. Figure 3.1 shows the proposed monitoring system that comprises short-term and long-term plans. The short-term plan includes instrumenting the CIP concrete and PC deck systems to compare their behavior under live load. The long-term plan focuses on instrumenting the PC deck system using vibrating wire (VW) strain gauges to evaluate its behavior under traffic loads over three-year period. The Bridge Diagnostic, Inc. (BDI) wireless structural testing system (STS) was used for short-term monitoring of strains and deflections in each bridge in addition to linear variable differential transformers (LVDTs) used to measure relative displacement between adjacent components in the PC deck system.

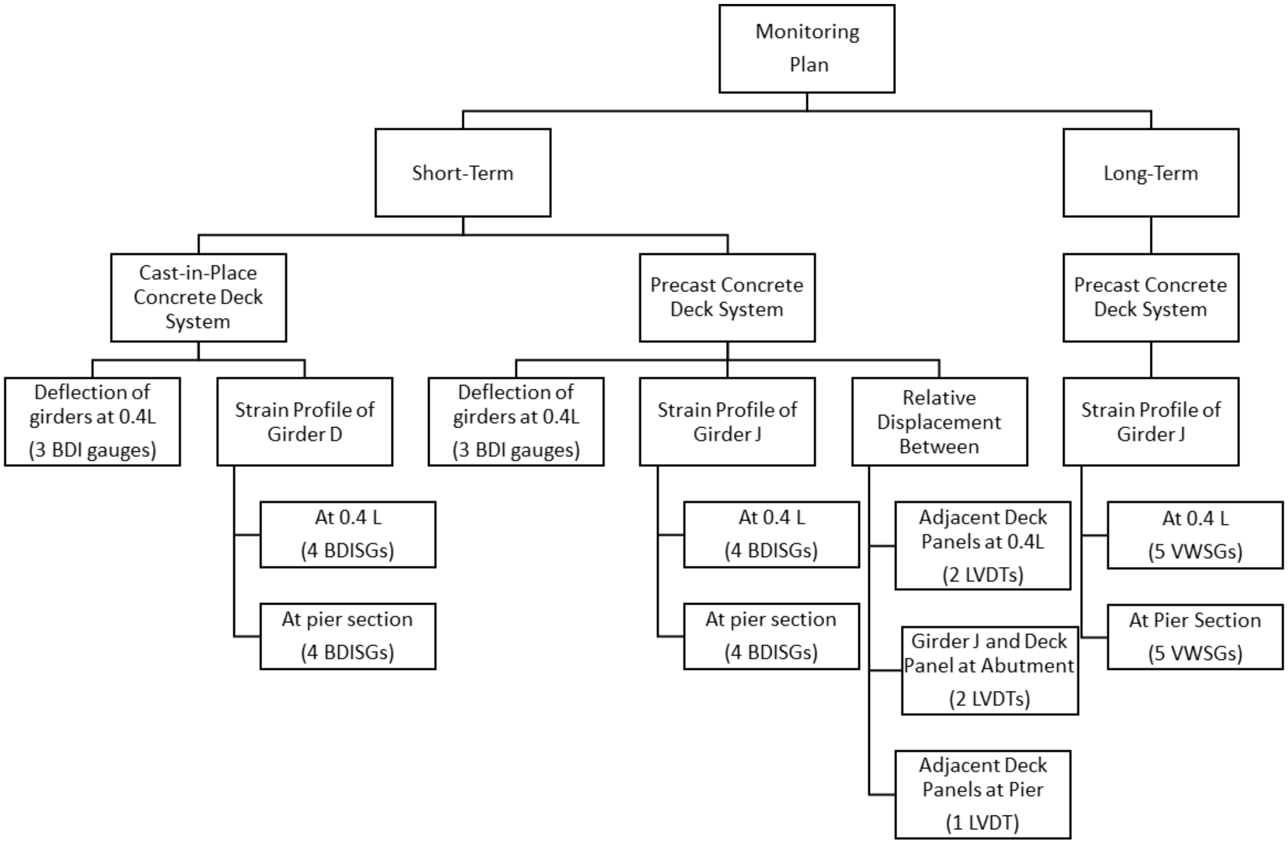
Monitoring Plan
Short-Term
Long-Term
Cast-in-Place Concrete Deck System
Precast Concrete Deck System
Precast Concrete Deck System
Deflection of girders at 0.4L (3 BDI gauges)
Strain Profile of Girder D
Deflection of girders at 0.4L (3 BDI gauges)
Strain Profile of Girder J
Relative Displacement Between
Strain Profile of Girder J
At 0.4 L (4 BDISGs)
At pier section (4 BDISGs)
At 0.4 L (4 BDISGs)
At pier section (4 BDISGs)
Adjacent Deck Panels at 0.4L (2 LVDTs)
Girder J and Deck Panel at Abutment (2 LVDTs)
Adjacent Deck Panels at Pier (1 LVDT)
At 0.4 L (5 VWSGs)
At Pier Section (5 VWSGs)

FIGURE 3.1 Short-term and long-term monitoring plans of the PC and CIP deck systems

Figure 3.2 shows a plan view of the PC deck bridge and the three instrumented sections of the north span: pier section (P), middle section (M), and abutment section (A). The location of these sections were selected to maximize the response of the bridge under live load. Section P was located 14 ft (4.27 m), which is approximately 2d, from the face of the pier and instrumented with four BDI strain gauges placed on the first interior girder “J”. These gauges were mounted on the top flange (B2612), web (B1983), bottom flange (B1993), and soffit (B1976). Also, five wired VW strain gauges were installed at deck soffit, top flange, web, bottom flange, and girder soffit for long-term monitoring. One LVDT was placed at the top surface of the deck across the pier joint, as shown in Figure 3.3, to measure the effectiveness of the live load continuity reinforcement placed in the haunch area. Section M was located at 71 ft 5 in. (21.77 m), which is 0.4L, from the north abutment where the maximum positive moment in the composite cross section is expected. The same girder was instrumented with four BDI strain gauges at the top flange (B1971), web (B1987), bottom flange (B2290), and soffit (B1981) as shown in Figure 3.4. Also, five wired VW strain gauges were installed at deck soffit, top flange, web, bottom flange, and girder soffit for long-term monitoring. Two LVDTs were mounted at this location on the soffit of the deck across the transverse joint. One of these LVDTs was placed horizontally and the other was placed vertically to measure the relative displacement between two adjacent deck panels under live load to evaluate the effectiveness of the unreinforced transverse joint. Three BDI deflection gauges (#3, #6, and #2) were placed at this section on the soffit of girders K, J, and H, respectively, as shown in Figure 3.4, to measure deflection changes during loading. Section A was located 6 ft (1.83 m) from the face of the abutment where the maximum interface shear between the deck panel and the girder is expected. Two LVDTs were placed at this section to measure the relative displacement between the precast concrete girder and end deck panel in the horizontal and the vertical directions as shown in Figure 3.3.

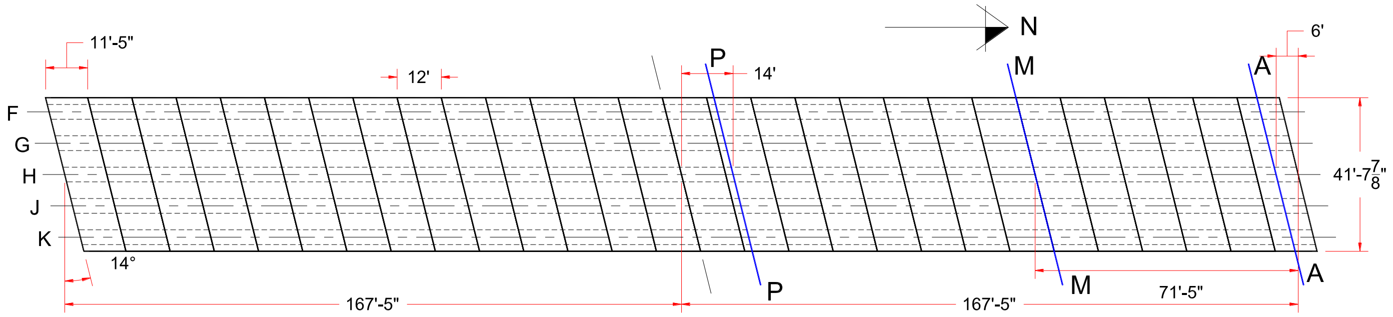

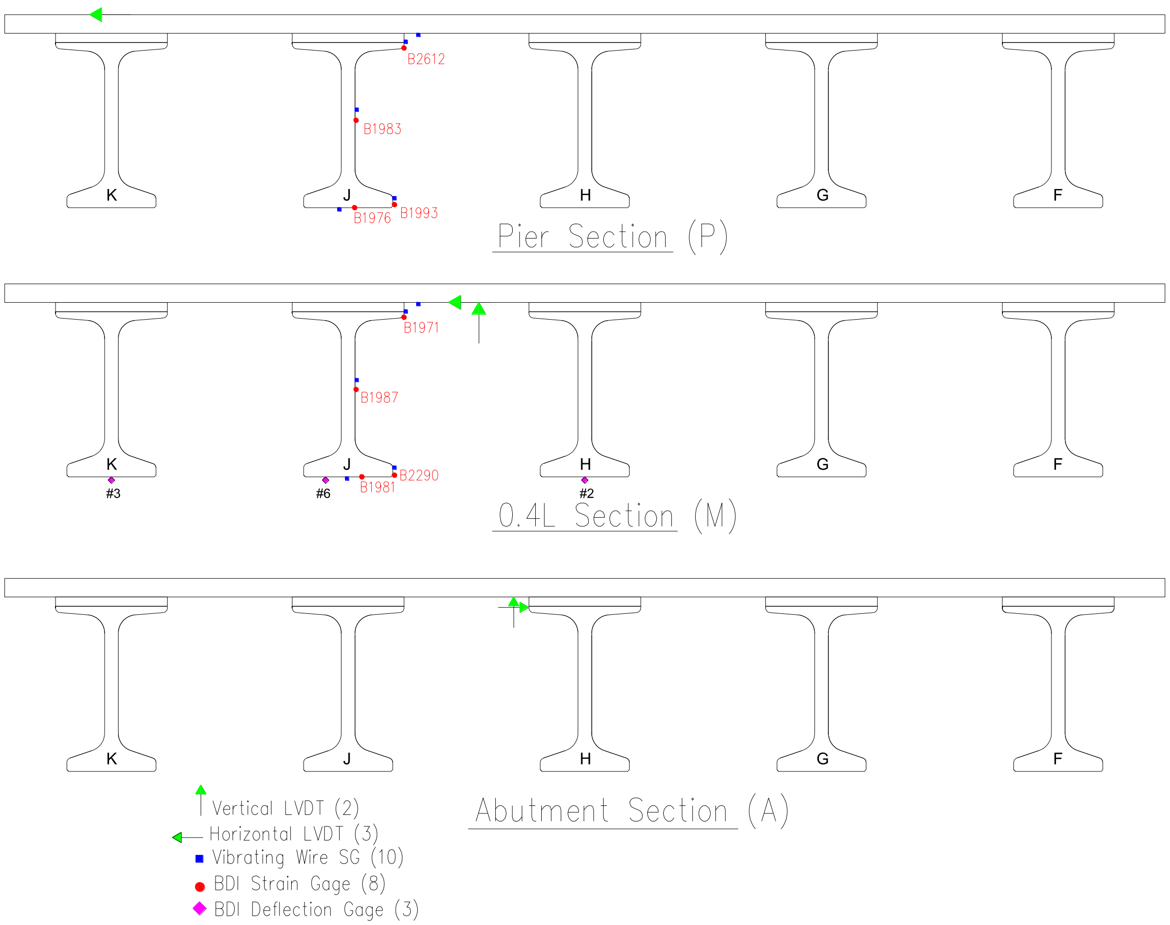
B2612
B1983
K
J
H
G
F
B1976
B1993
Pier Section (P)
B1971
B1987
K
J
H
G
F
B2290
B1981
#3
#6
#2
0.4L Section (M)
K
J
H
G
F
Vertical LVDT (2)
Horizontal LVDT (3)
Vibrating Wire SG (10)
BDI Strain Gage (8)
BDI Deflection Gage (3)
Abutment Section (A)

FIGURE 3.2 Instrumentation of bridge superstructure of PC deck

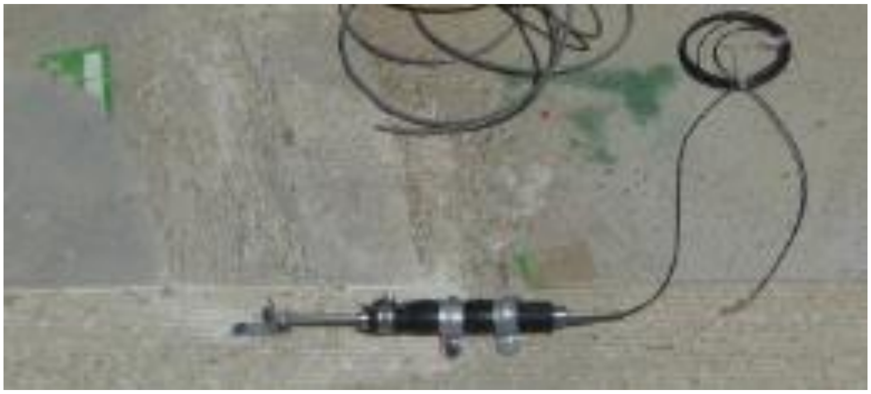

(a) LVDT installed at pier section

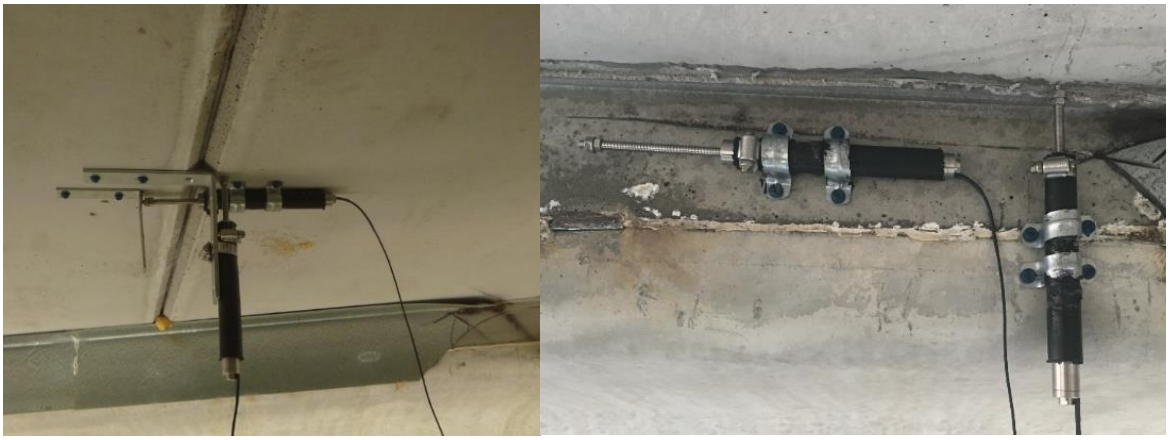

(b) LVDT installed at pier section (c) LVDT installed at pier section

FIGURE 3.3 LVDTs installed at pier section (a), middle section (b), and pier section (c)

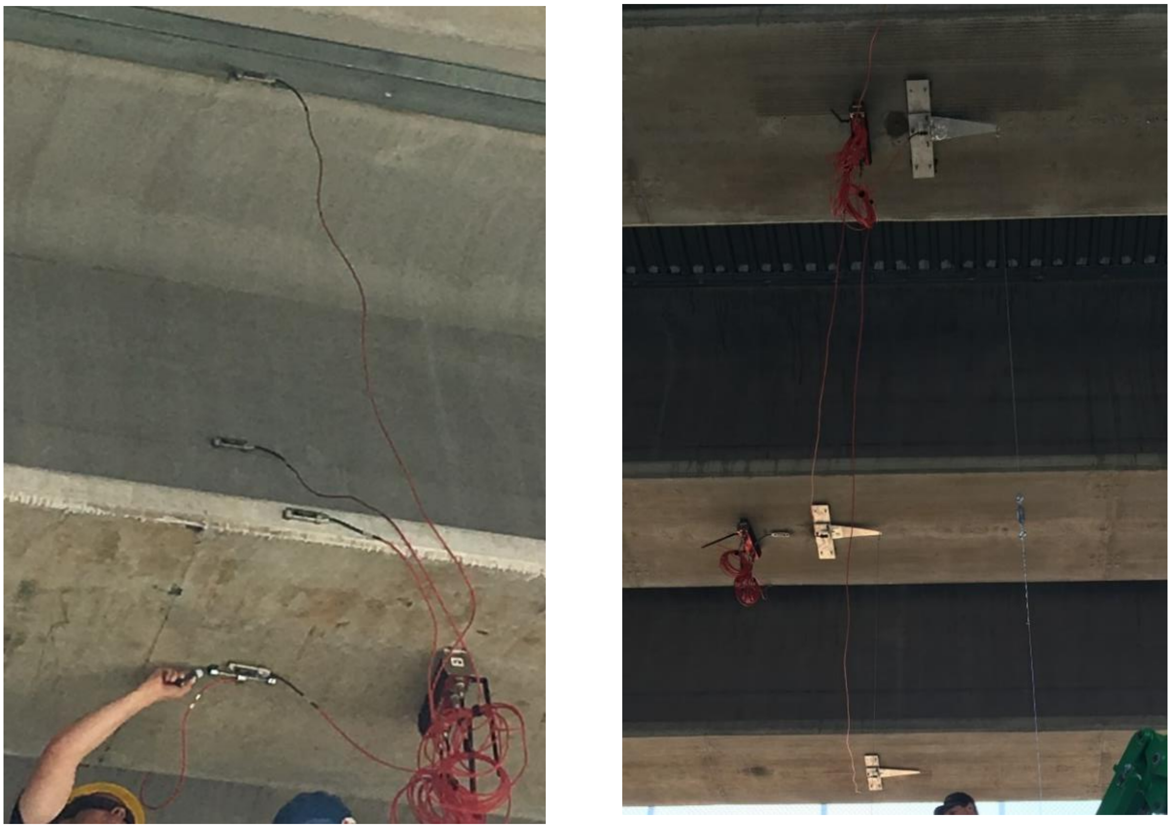

FIGURE 3.4 Installing strain gauges (left) and deflection gauges (right) at the middle section

Figure 3.5 shows the two instrumented sections for the short-term monitoring of the CIP concrete deck bridge: pier section (P) and middle section (M). The location of these sections are the same as those of the PC deck bridge shown in Figure 3.2. Section P was located 14 ft (4.27 m), which is approximately 2d, from the face of the pier and instrumented with four BDI strain gauges placed on the first interior girder “D”. These gauges were mounted on the top flange (B4981), web (B1989), bottom flange (B1977), and soffit (B1972). Section M was located at 71 ft 5 in. (21.77 m), which is 0.4L, from the north abutment where the maximum positive moment in the composite cross section is expected. The same girder was instrumented with four BDI strain gauges at the top flange (B1992), web (B2611), bottom flange (B1988), and soffit (B1996) as shown in Figure 3.5. Three BDI deflection gauges (#5, #4, and #7) were placed at this section on the soffit of girders E, D, and C, respectively, as shown in Figure 3.5, to measure deflection changes during loading.

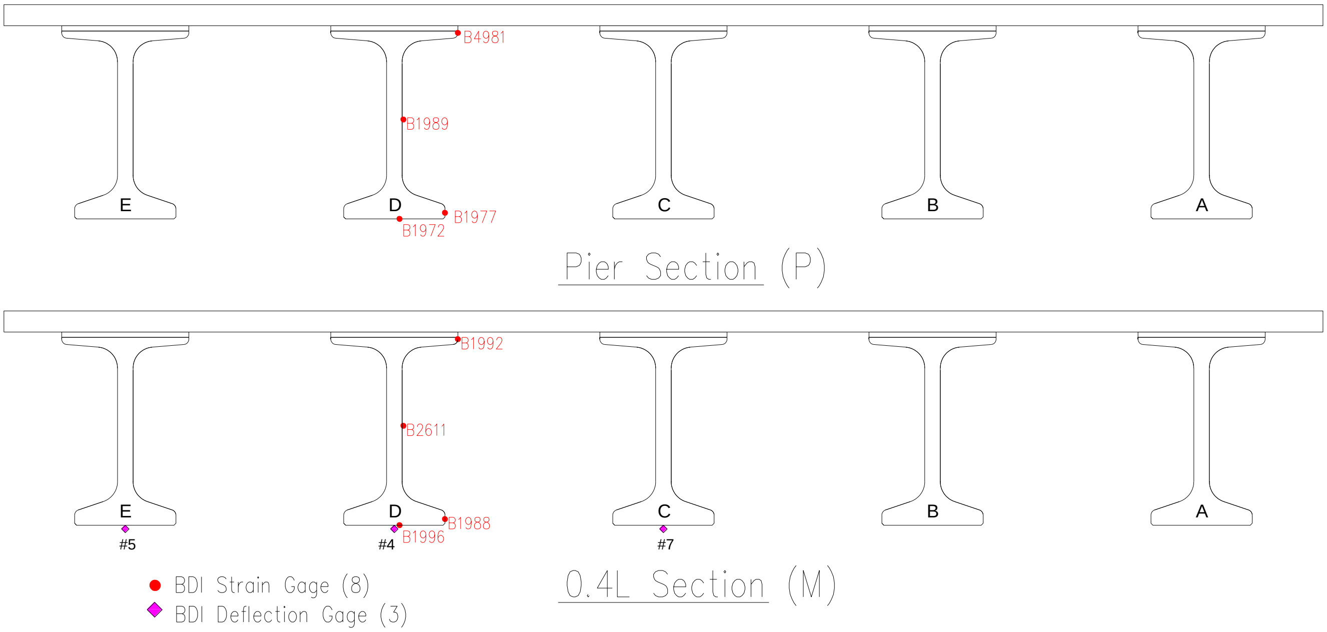
B4981
B1989
E
D
C
B
A
B1977
B1972
Pier Section (P)
B1992
B2611
E
D
C
B
A
B1988
#5
#4
B1996
#7
● BDI Strain Gage (8)
◆ BDI Deflection Gage (3)
0.4L Section (M)

FIGURE 3.5 Instrumentation of bridge superstructure of CIP concrete deck

3.2 Live Load Test

The live load testing of the Kearney East Bypass Bridge was conducted during the summer of 2016 and consisted of four load paths using one-truck and two-truck loadings as shown in Figure 3.6. Each path was repeated twice: one time in the north-south direction and the other time in the south-north direction. These load paths were selected to maximize the moment and deflection of bridge deck and girders. The two trucks used in this testing were identically loaded dump trucks that have axle weights as shown in Table 3.1. Figure 3.7 presents the spacing between axles of the trucks. Trucks were driven at a very low speed (approximately 2.3 km/hr or 1.43 mph) to simulate live load without dynamic effects. Trucks were spaced approximately 5 ft between the centers of the adjacent wheels. Each path was color marked on the deck surface to ensure the accuracy of the loading location. The rate of data recording was approximately once per 1 in. of the loading path (sampling frequency is 25). It should be noted that similar loading paths were applied to the CIP concrete deck bridge.

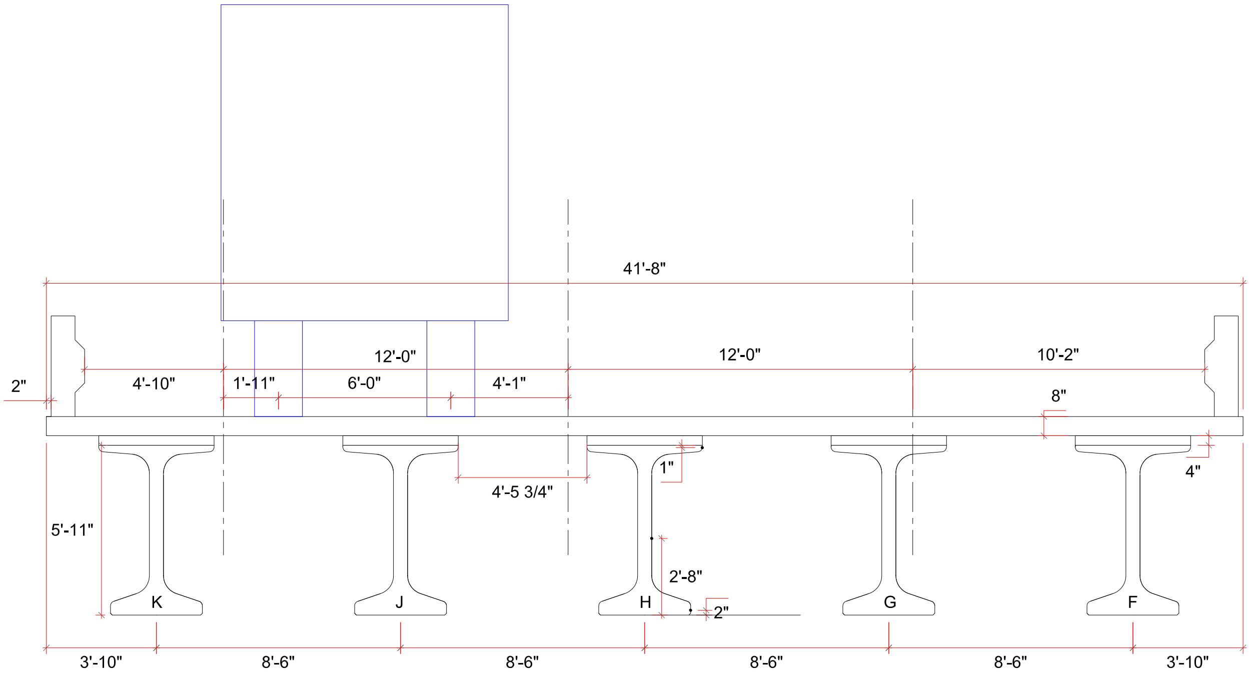

(a) Path #1

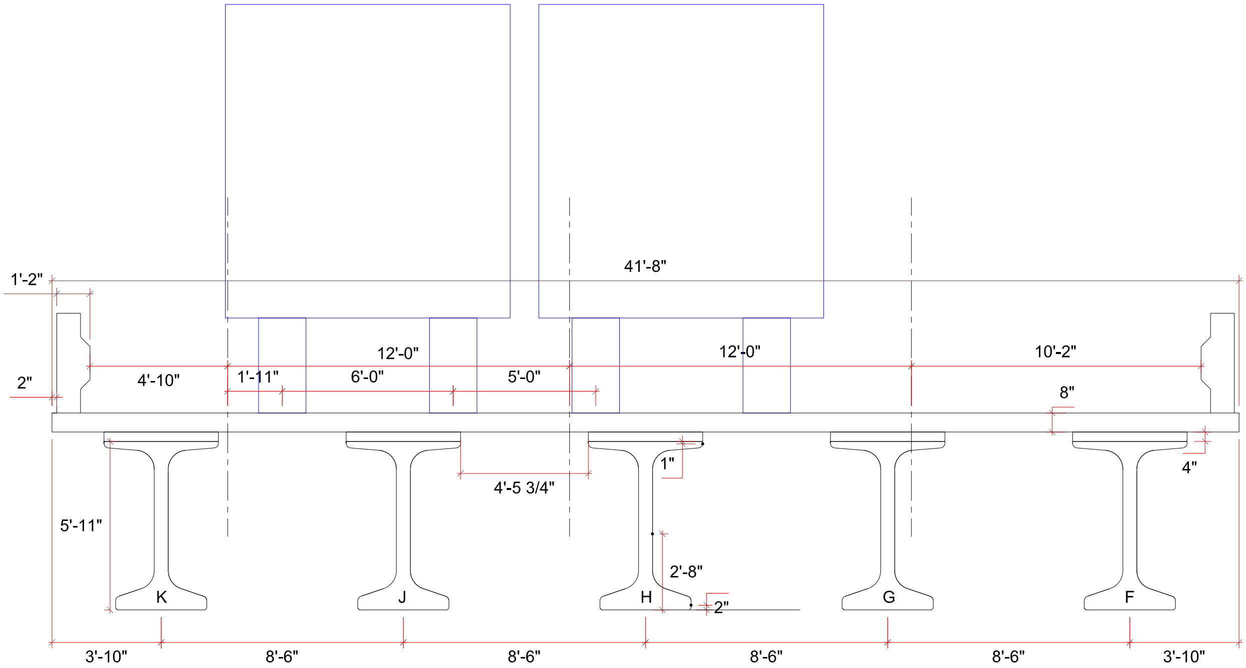
41'-8"
1'-2"
12'-0"
12'-0"
10'-2"
4'-10"
1'-11"
6'-0"
5'-0"
2"
8"
4"
1"
4'-5 3/4"
5'-11"
2'-8"
2"
K
J
H
G
F
3'-10"
8'-6"
8'-6"
8'-6"
8'-6"
3'-10"

(b) Path #2

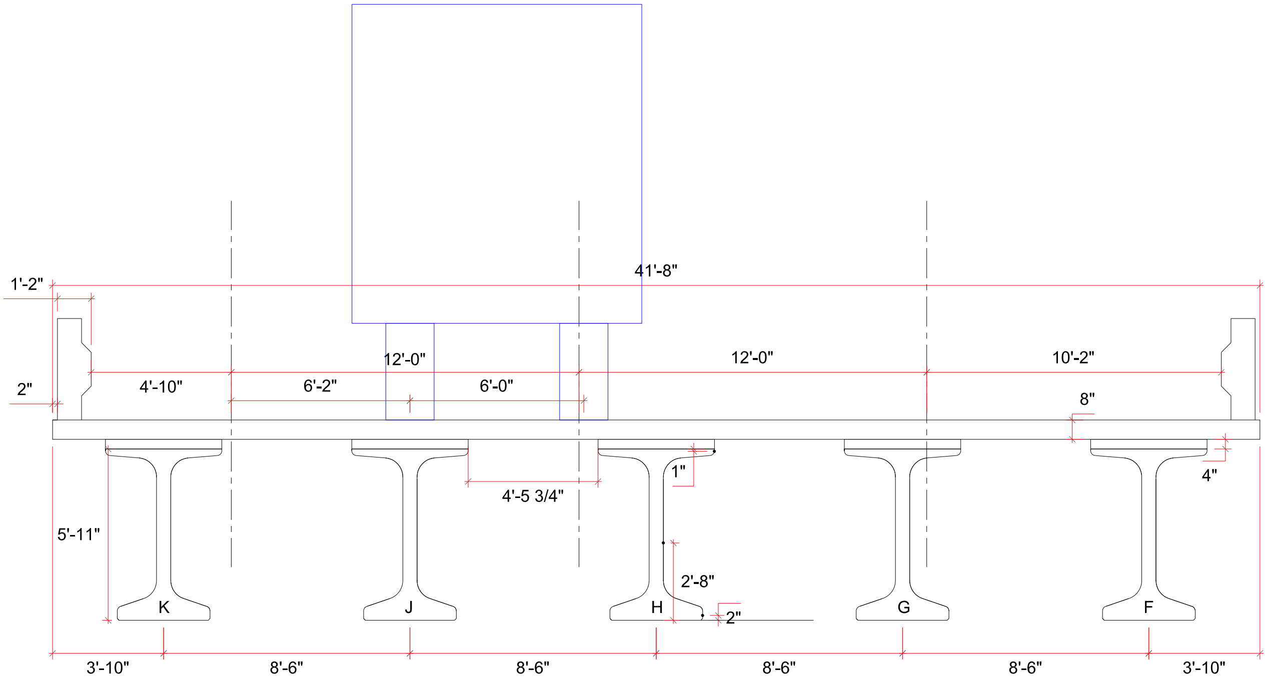
41'-8"
1'-2"
12'-0"
12'-0"
10'-2"
4'-10"
6'-2"
6'-0"
2"
8"
4"
1"
4'-5 3/4"
5'-11"
2'-8"
2"
K
J
H
G
F
3'-10"
8'-6"
8'-6"
8'-6"
8'-6"
3'-10"

(c) Path #3

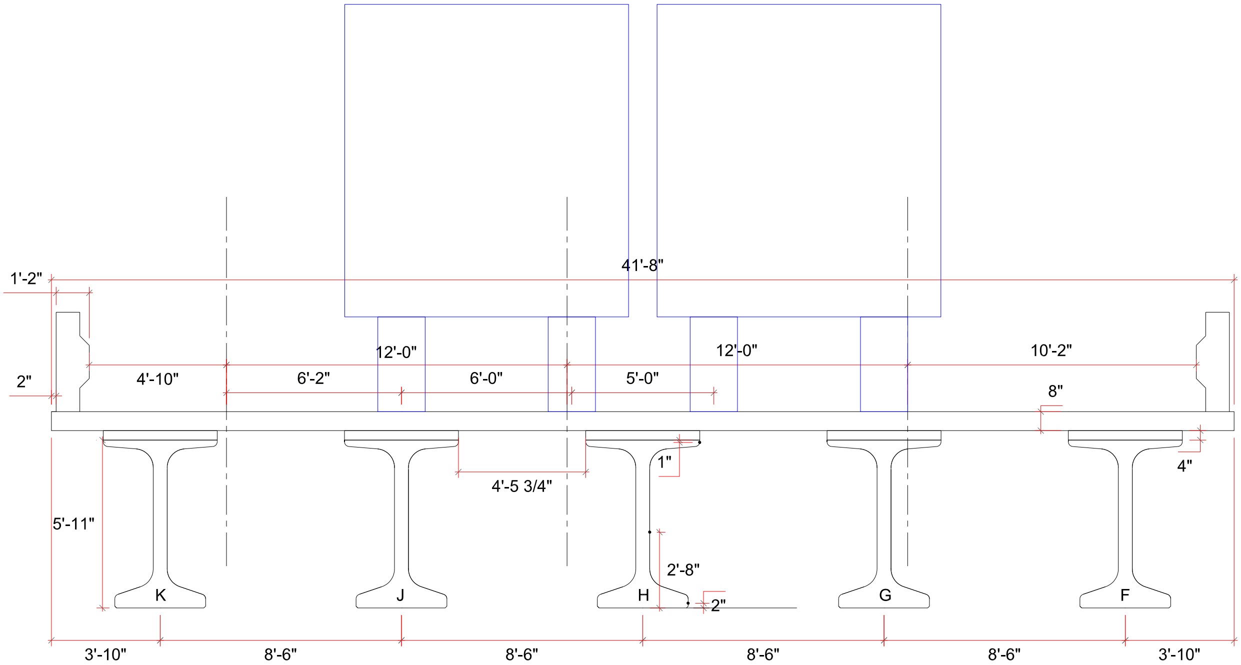
1'-2"
41'-8"
2"
4'-10"
6'-2"
12'-0"
6'-0"
5'-0"
12'-0"
10'-2"
8"
4"
1"
4'-5 3/4"
5'-11"
2'-8"
2"
K
J
H
G
F
3'-10"
8'-6"
8'-6"
8'-6"
8'-6"
3'-10"

(d) Path #4

Figure 3.6: Truckload positions on bridge

TABLE 3.1 Dump Truck Axle and Total Weight

Truck No.	Steering Axle (lb) [kg]	Rear Axle #1 (lb) [kg]	Rear Axle #2 (lb) [kg]	TOTAL (lb) [kg]
Truck #1	15,440 [7,004]	16,700 [7,575]	16,700 [7,575]	48,840 [22,154]
Truck #2	14,460 [6,560]	17,770 [8,060]	17,770 [8,060]	50,000 [22,680]

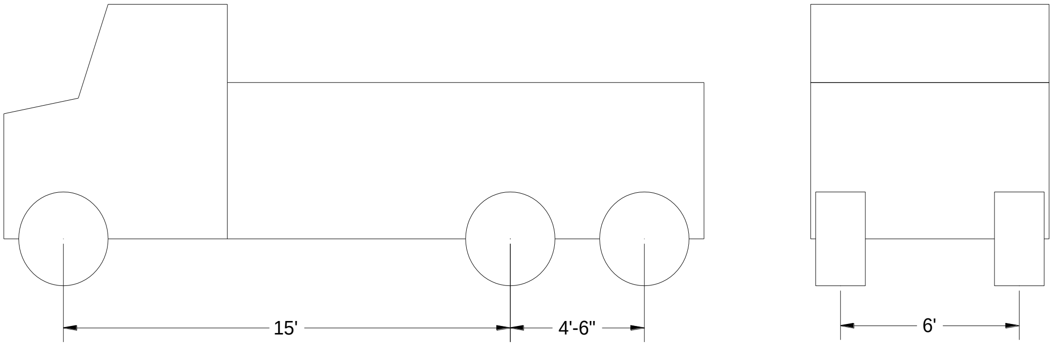

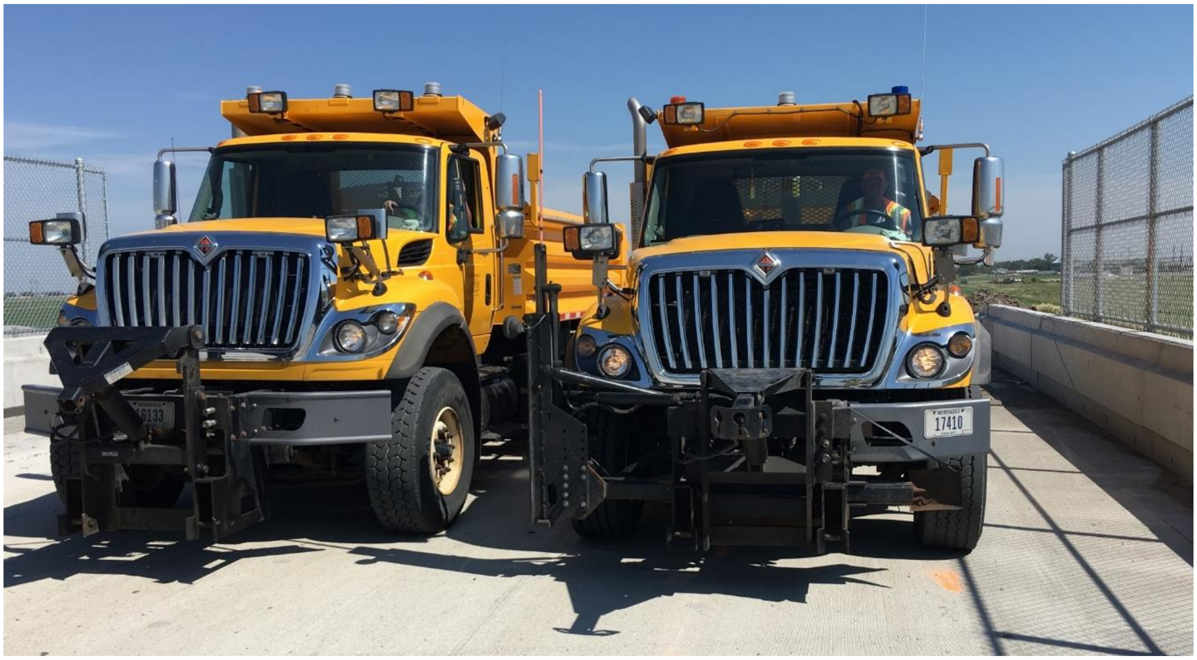

FIGURE 3.7 Dump truck axle configuration and photo

3.3 Finite Element Analysis (FEA)

Different Finite Element (FE) modeling techniques were presented in the literature for multi-girder bridges utilizing different modeling elements for girder and deck components. Chung (2003) concluded that modeling the girder using beam elements and deck using shell/plate elements provided the simplest solution with satisfactory accuracy. Analysis results were within 1% when it was compared to the theoretical solution. The FE analysis of the Kearney East Bypass Bridge was conducted using commercial FE package, STAAD Pro. (V.20.07.11.82) software. Plate elements were used to model the precast concrete deck panels using four-node quadrilateral elements with six degrees of freedom at each node (three translational and three rotational degrees of freedom). Beam elements used to model the girders consisted of two nodes with six degrees of freedom at each node.

The Kearney East Bypass Bridge was designed as non-composite simply supported spans for girder and deck weights and composite two-span continuous for superimposed dead load and live loads. In order to mimic the actual bridge behavior, full connectivity between the precast concrete deck and girders was used in the model utilizing offset feature in STAAD pro. The offset feature prevented the overlap between the deck and girder elements and eliminated the need for a rigid link between the centers of gravity of the two elements. The beam was modeled as a prismatic I-shape utilizing the un-cracked transformed section shown in Figure 3.8, which is a valid assumption for fully prestressed concrete girders. Similarly, the barrier rails were modeled as beam elements and the offset feature was used to adjust the rail location with respect to the concrete deck. Figure 3.9 presents a schematic shape of different elements of the FE model. The concrete diaphragms at the pier and abutments were modeled using beam elements to simulate the integral system. Pin supports were considered at the pier location while roller supports were considered at the abutment locations. Although actual bridge supports are neither pinned or roller supports, the effect of support type on the rotational stiffness of the girder is not significant due to the use of full-depth concrete diaphragms at these supports. These diaphragms rigidly connect girder ends and provide the rotational stiffness of the superstructure. Table 3.2 lists the material properties for different concrete superstructure components used in the FE model. The modulus of elasticity (MOE) was calculated according to AASHTO LRFD (2014) code provisions. It should be noted that only linear elastic models were used for all materials as the study focuses on the behavior of the bridge under service loads only.

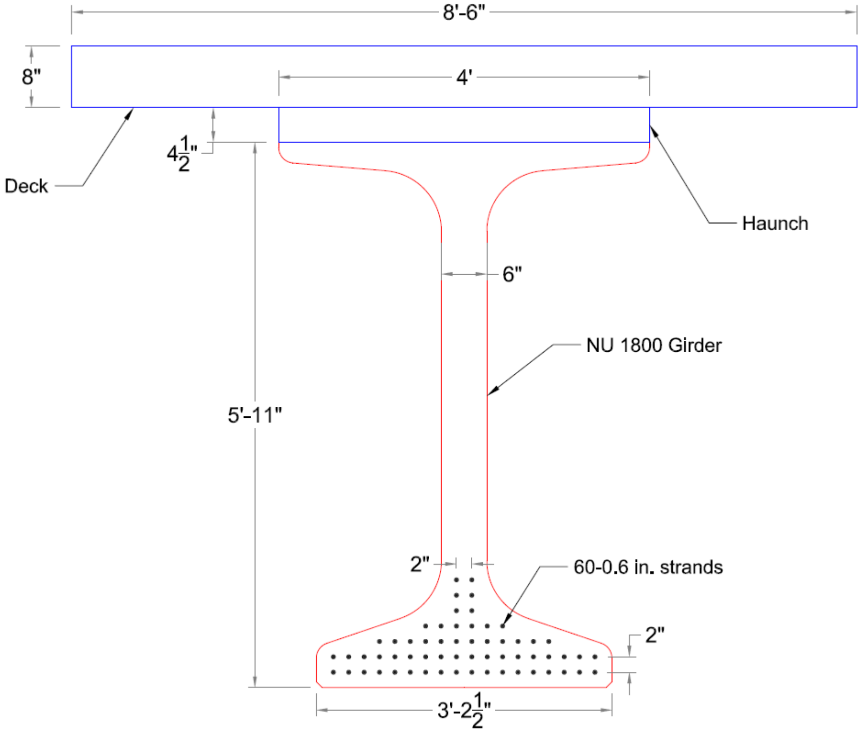

FIGURE 3.8 Bridge girder composite section used in analysis

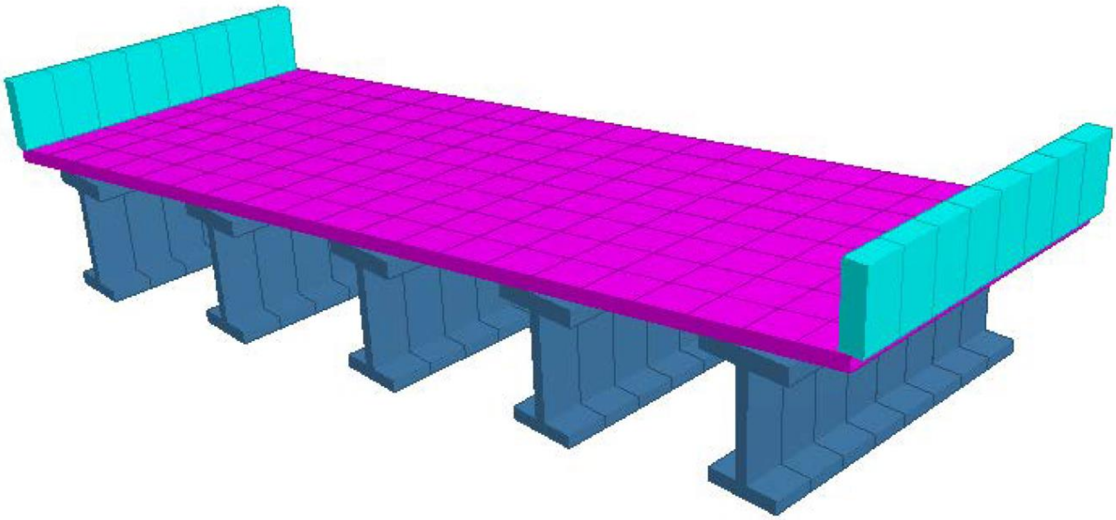

FIGURE 3.9 FEA model of the bridge superstructure

Table 3.2 Specified and Measured Concrete Material Properties used in FEA

Component	Specified f'_c (ksi) [MPa]	Actual f_c (ksi) [MPa]	MOE (ksi) [MPa]
Barrier	4 [27.6]	4 [27.6]	3,834 [26,435]
Deck	6 [41.4]	7 [48.3]	5,072 [34,970]
Haunch	6 [41.4]	9 [62]	5,751 [39,651]
Girder	10 [68.9]	11 [75.8]	6,358 [43,837]

The selection of the element size is an important factor in the efficiency and accuracy of the FE model, which depends on span length, girder spacing and loading positions. In general, the aspect ratio, which is a ratio of element length to element width, should be less than two (Cook et al. (1989)). A parametric study was conducted to evaluate the effect of the plate element size on the overall bridge behavior. Two element sizes were investigated: 24 x 24 in. (0.6 x 0.6 m) and 12 x 12 in. (0.3 x 0.3 m), and deflection and strains of the middle girder (H) at 0.4L location (section M) were compared when the two element sizes are used. Comparison results indicated no significant difference and, therefore, the element size 24 x 24 in. (0.6 x 0.6 m) was used to improve analysis efficiency. Element sizes smaller than 12 in. (0.3 m) were not investigated because the length and width of the modeled bridge made it computational prohibitive.

3.4 Testing and Analysis Results

Strains measured at the critical sections (M and P sections) of an interior girder in the twin bridges due to live load were compared to each other and to those predicted by the FE model at the same locations to evaluate the performance of the bridge with the new deck system. Since the outputs of this FE model are typical moments rather than strains, calculations were made using un-cracked transformed section properties and concrete properties listed in Table 3.2 in accordance to AASHTO LRFD provisions. Figure 3.10 shows the measured versus predicted girder soffit strains (in micro-strain) at both M and P sections due to load paths #3 and #4. Strains at other locations of the girder (top, web, and bottom) follow the same trend but with smaller values. In middle sections, the strains measured from the PC deck bridge matched very well those predicted by FEA as shown in Figures 3.10a and 3.10c, which indicate that the FE model accurately simulate the new deck system with respect to composite behavior and moment distribution. On the other hand, significant differences exist between strains measured from the PC deck bridge and those measured from the CIP concrete deck bridge. This could be attributed to the higher stiffness of the 7 ksi (48 MPa) precast/prestressed concrete deck panels and 9 ksi (62 MPa) haunch compared to the 4 ksi (27 MPa) conventionally reinforced CIP concrete deck and haunch, which results in better live load distribution in the transverse direction to adjacent girders and lower moment distribution factor. More discussion on moment distribution factors will be presented later. In pier sections, some differences exist between strains measured from the PC deck bridge and those predicted by FEA as shown in Figures 3.10b and 3.10d. This could be attributed to using un-cracked transformed cross section properties for the entire girder length when calculating the strain values from the FE model, which is not true for the actual bridge as pier sections are reinforced concrete that could be cracked under service loads. Objective error function analysis (Sanayei and Onipede, 1992) was conducted to evaluate the level of FEA accuracy compared to the test results. Table 3.3 summarizes the maximum measured and calculated (FEA) strain values for each sensor at M and P sections along with the absolute percent error (APE). The analysis shows that FEA results are in close agreement with the measured strain values with mean absolute percent error (MAPE) of 6.93 %. On the other hand, the strains measured from the PC deck bridge match very well those measured from the CIP concrete bridge deck at the pier section, which indicate that the new continuity system behave very similar to that provided in bridges with conventionally reinforced CIP concrete deck.

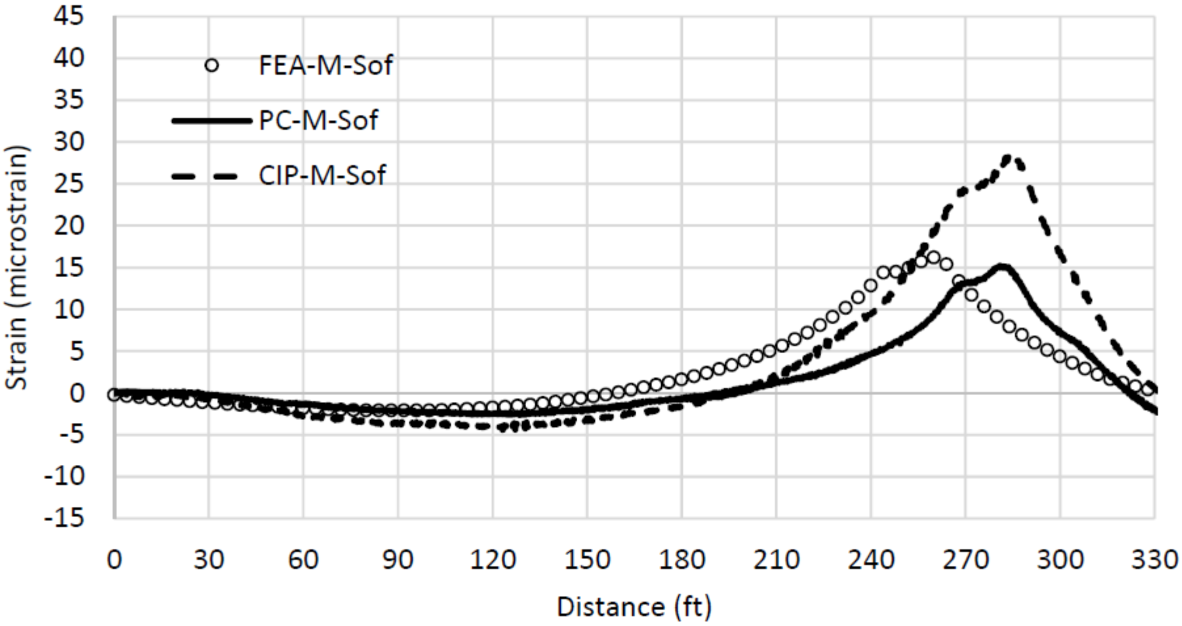

(a) Girder bottom strain at the middle section for load path #3

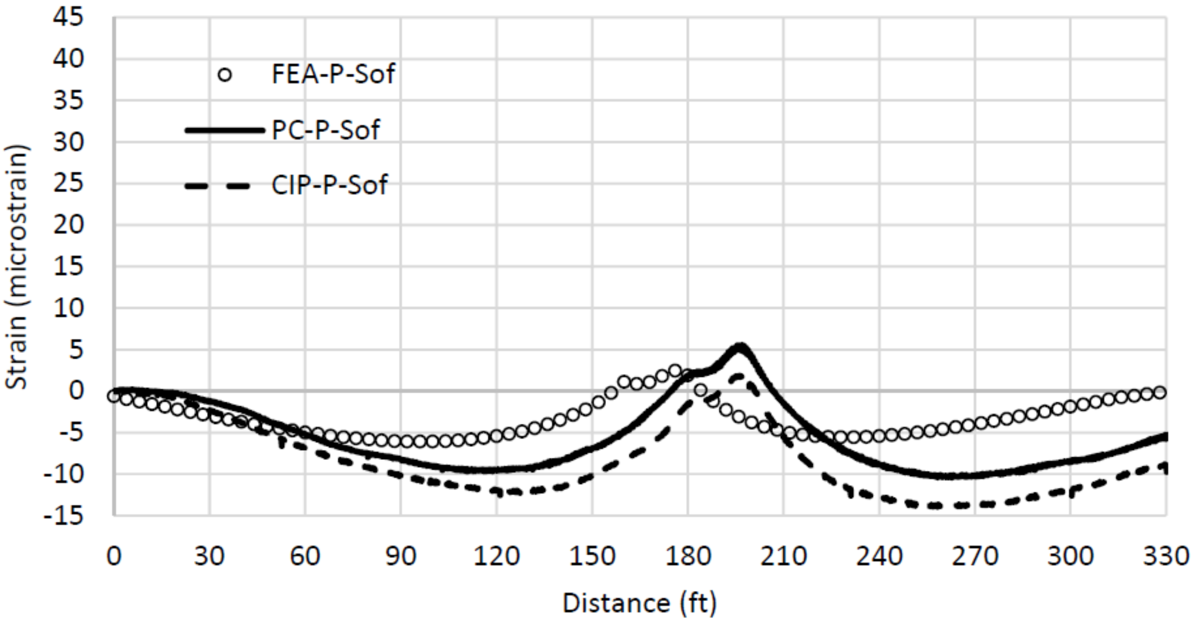

(b) Girder bottom strain at the pier section for load path #3

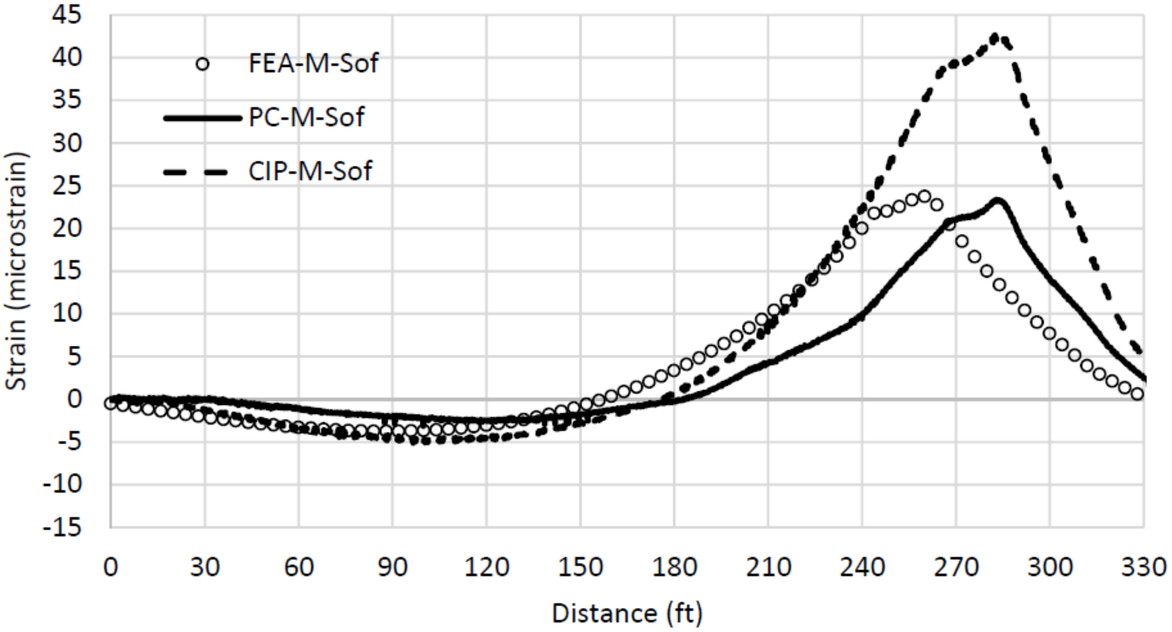

(c) Girder bottom strain at the middle section for load path #4

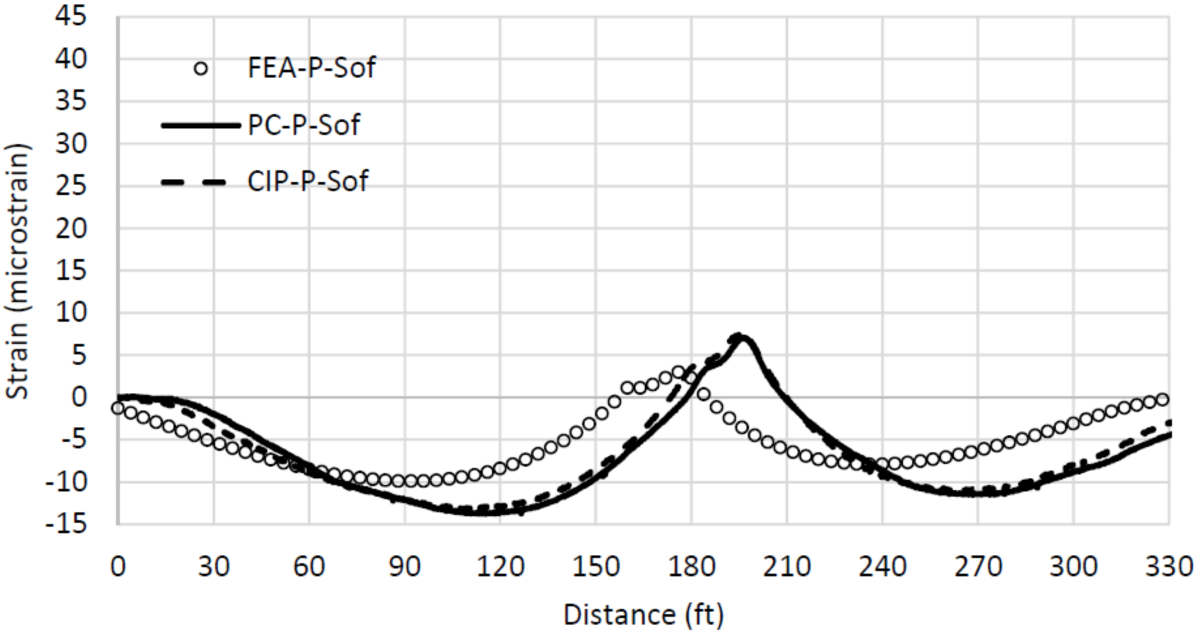

(d) Girder bottom strain at the pier section for load path #4

FIGURE 3.10 Girder bottom strains for load paths #3 and #4

Table 3.3 Objective Error Function

Load Path #	Sensor location	Maximum Strain (με)		APE (%)
		Measured	FEA	
1	M	18.598	16.530	11.12
	P	-11.120	-10.990	1.17
2	M	30.741	27.220	11.45
	P	-16.433	-16.800	2.23
3	M	15.217	16.210	6.53
	P	-10.610	-9.110	14.14
4	M	23.366	23.740	1.60
	P	-13.764	-14.760	7.24
Mean				6.93

Note: APE=Absolute Percent Error; M=Mid-span section; P=Pier section

It should be noted that the measured data was recorded while the live load is moving at approximately 1 in. (25 mm) increment, however, the FE data were obtained by moving wheel loads at 48 in. (1.2 m) increment. Consequently, the FE results were interpolated to match the measured data. A general observation in the strains of the four load paths is a shift/lag between the FE and test plots. This shift/lag may be attributed to inaccuracy of the manual positioning system used to determine the truck location in the longitudinal direction while moving and variability in the truck speed along each path. Position data could be further processed to match the FEA data, however, the authors preferred to use the original one to avoid overlapping the plots. Figure 3.11a presents the strain profile of an interior girder “J” in the PC deck bridge for the four loading paths at the 0.4L section (M). This figure presents that the average location of the neutral axis from the bottom of the girder is 55.4 in. (1.41 m), which is very close to the theoretical location calculated using the un-cracked transformed section, which is 53.14 in. (1.35 m). Figure 3.11b presents the strain profile in the corresponding girder “D” in the CIP concrete deck bridge for the same load paths. This figure presents that the average location of the neutral axis from the bottom of the girder is 55 in. (1.4 m), which is very close to both the PC deck bridge and the theoretical one. It should be noted that the theoretical strain profile for an un-cracked section should be linear, however, measured strain profile had a slight kink that could be due to the sensitivity of the strain gauges and/or the inaccuracy of their locations.

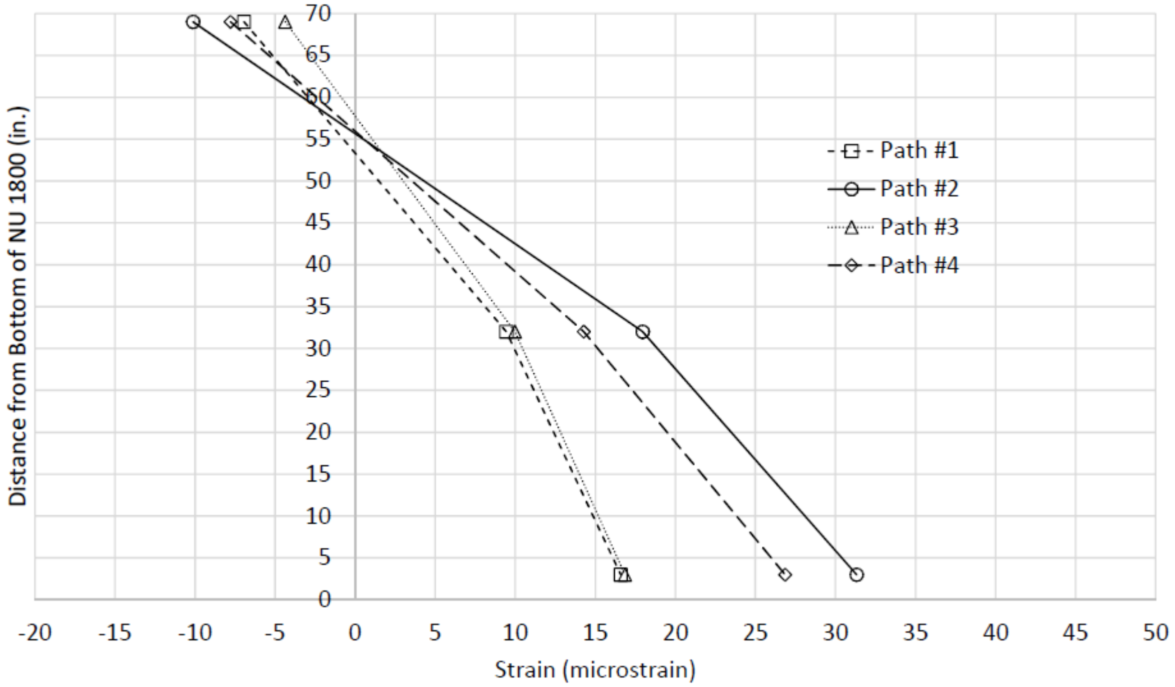

(a) Strain profiles of girder “J” in PC deck bridge at middle section

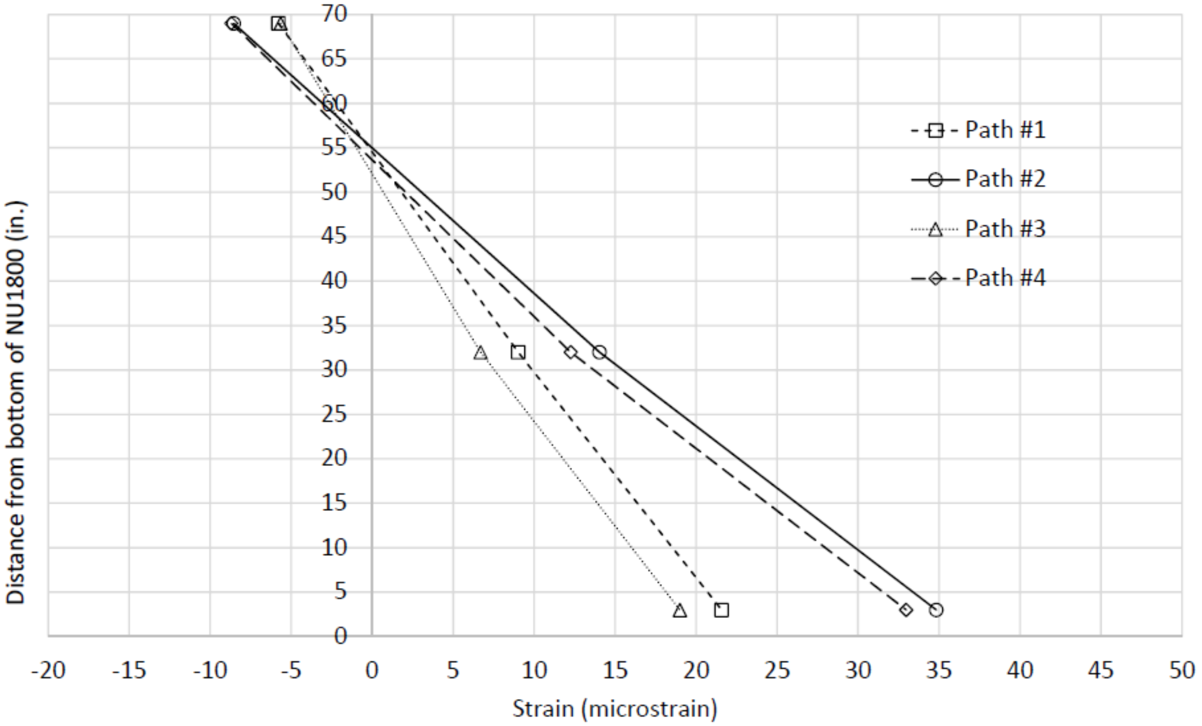

(b) Strain profiles of girder “D” in CIP concrete deck bridge at middle section

FIGURE 3.11 Strain profiles for girders at middle section (M) of PC and CIP bridge decks due to different loading paths

Figure 3.12 presents the deflection at 0.4L of the middle girder (H) for load paths #3 and #4, respectively. In each figure, the deflections predicted by the FEA are plotted against those measured in the twin bridges: PC deck and CIP concrete deck bridges. Comparing deflections at 0.4L of the middle girder (H) in the two bridges indicate that there is no significant difference in the behavior or stiffness of the two bridges. The figures also indicate that measured deflections are very close to the predicted ones with the exception of the slight shift/lag discussed earlier. In general, predicted deflections are slightly higher than measured ones, which could be attributed to differences between the actual bridge and FE model with respect to end conditions and material modulus of elasticity.

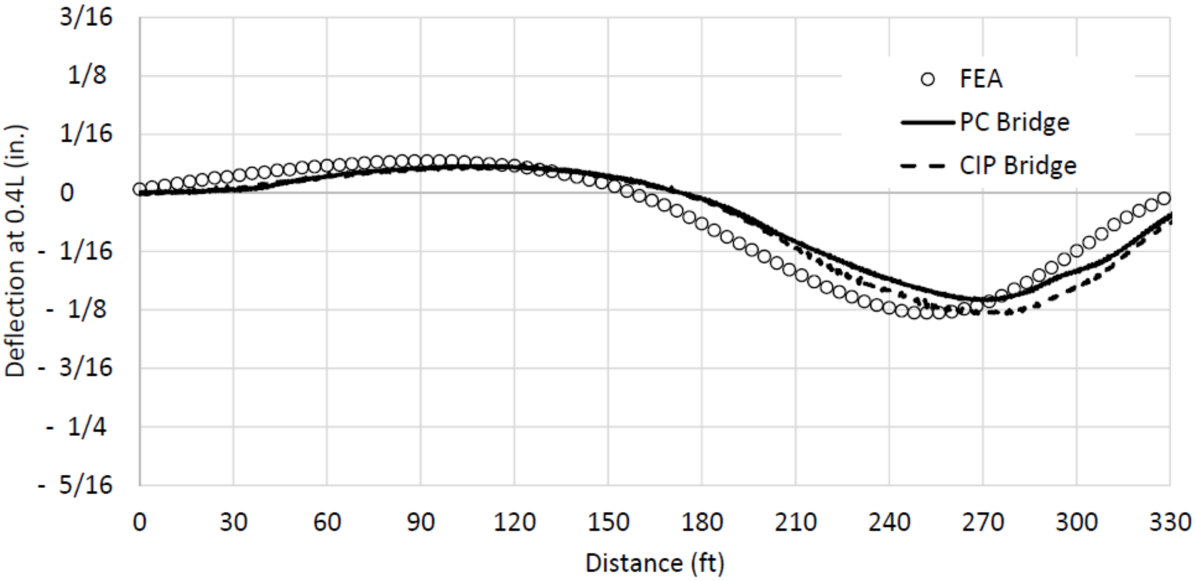

(a) Deflection at 0.4L of the middle girder (H) for load path #3

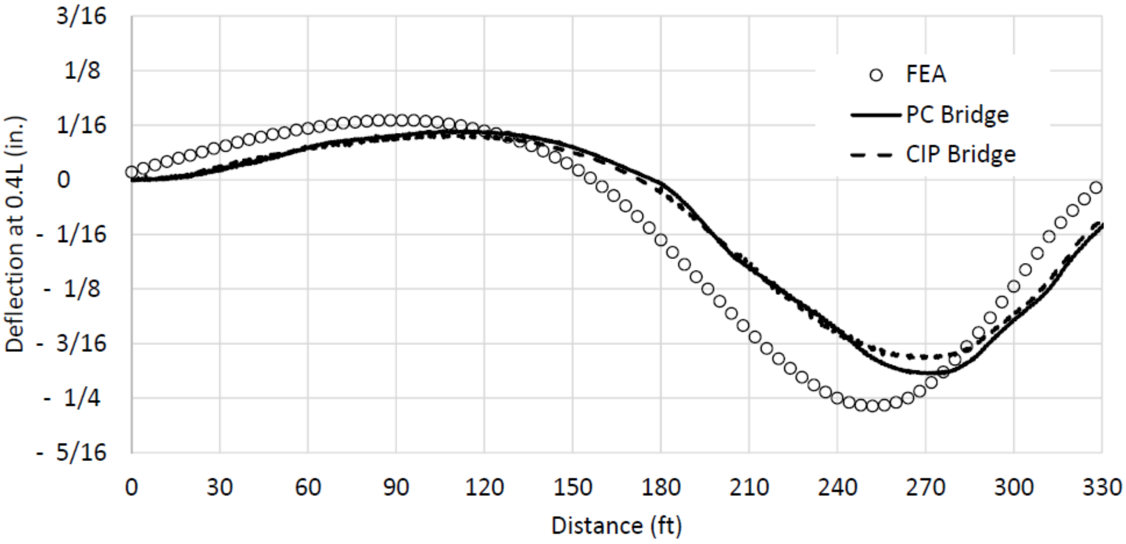

(b) Deflection at 0.4L of the middle girder (H) for load path #4

FIGURE 3.12 Deflections at 0.4L of the middle girder (H) for load paths #3 and #4

Live load distribution factors represent how the applied live load is transversely distributed by the bridge deck and diaphragms (if any) to the supporting girders. In this study, only moment distribution factor (MDF) was calculated based on the available deflection and strain data. Figures 3.13a and 3.13b plot the measured and predicted deflection profiles at M section for the three girders: exterior “K”, interior “J”, and middle “H” due to load paths #3 and #4, respectively. These deflection profiles show insignificant difference between measured values and those predicted by FEA. Figure 3.13c plots the MDFs calculated for those girders based on deflection values against those obtained from FEA. It is worth mentioning that deflection based MDF values provided very close results (within 1% difference) to those calculated using moment values. Figure 3.13c presents excellent correlation between measured and FEA predicted MDF with less than 3% difference. It should be noted that the AASHTO LRFD provisions of MDFs for type “k” bridges (Table 4.6.2.2.2b-1) were applied to this bridge and resulted in much higher values of MDF (0.43 for interior girders) regardless of the number of loaded lanes, which is in agreement with the literature (Laurendeau et al. (2015); Torres and Maguire (2015)).

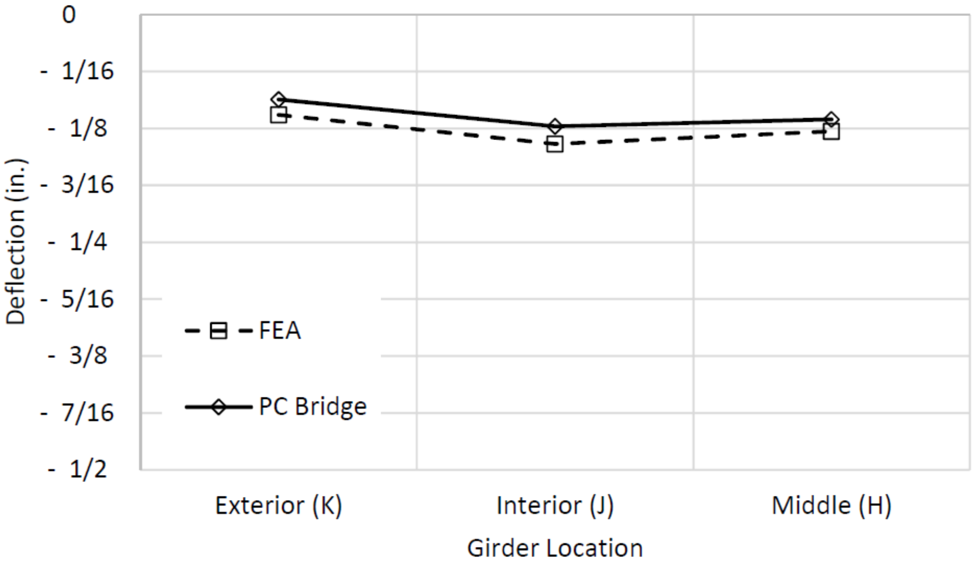

(a) Deflection profile under load path #3

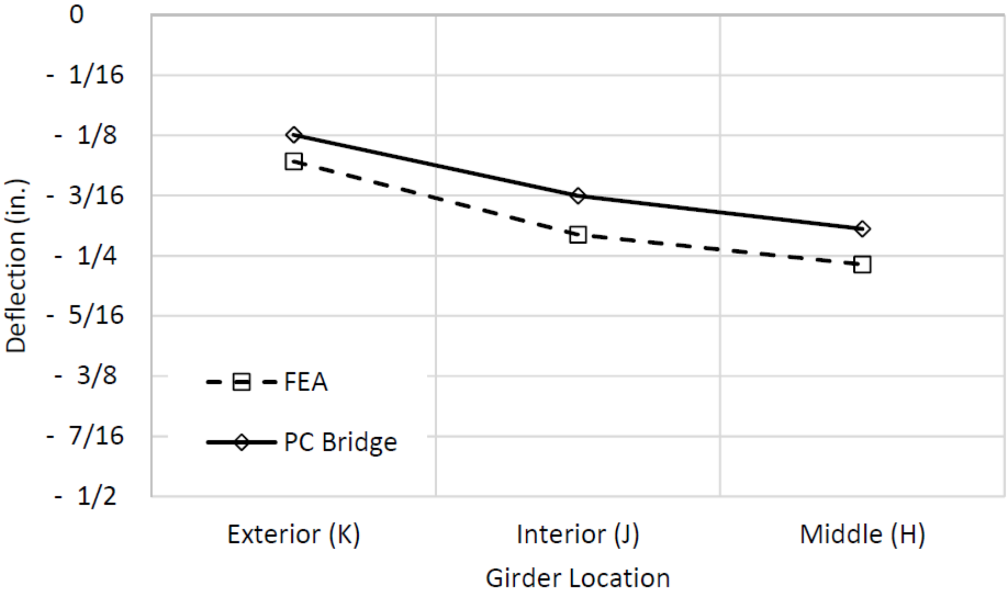

(b) Deflection profile under load path #4

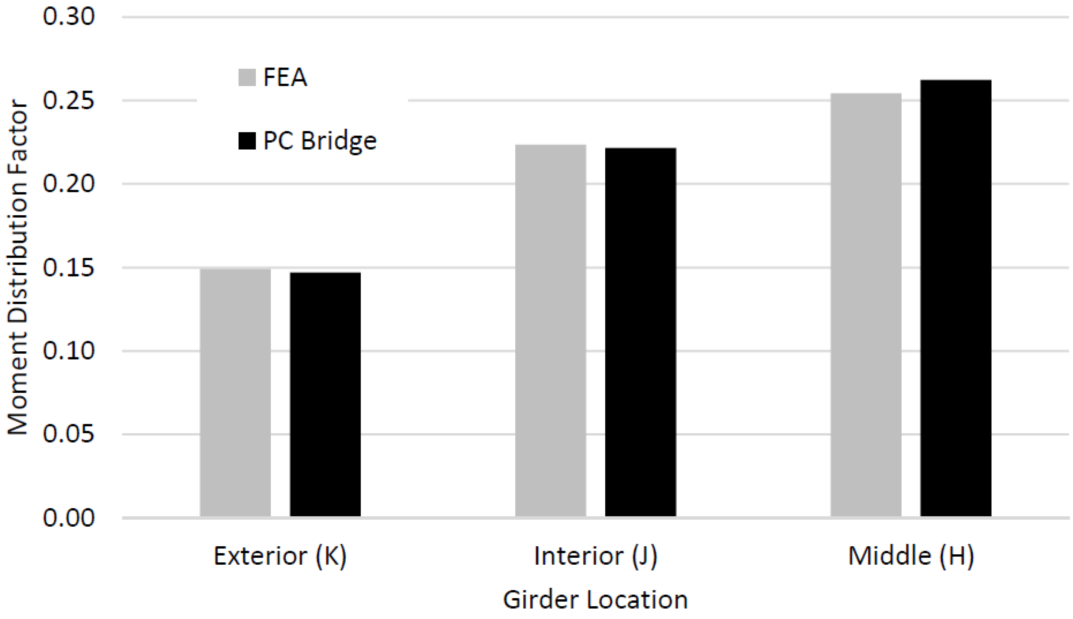

(c) Distribution factor comparison for load path #4

FIGURE 3.13 Deflection profile and distribution factor comparison.

As a part of the monitoring plan, LVDTs were installed at the locations where relative displacement between adjacent components is expected. Figure 3.14 presents the relative displacement recorded by the five LVDTs during the load path #4. These plots indicate insignificant relative movement (< 0.001 in.) between adjacent deck panels in either horizontal or vertical directions at P or M sections. It also indicates no separation between the end deck panel and its supporting girder as the recorded values were less than 0.001 in. (0.025 mm), which is considered within the precision of the LVDTs used. FEA models were not able to capture any relative displacement between deck panels or deck-girder interface because the model assumed full connectivity between the deck panels and supporting girders. This assumption was found to be accurate based on the recorded test data.

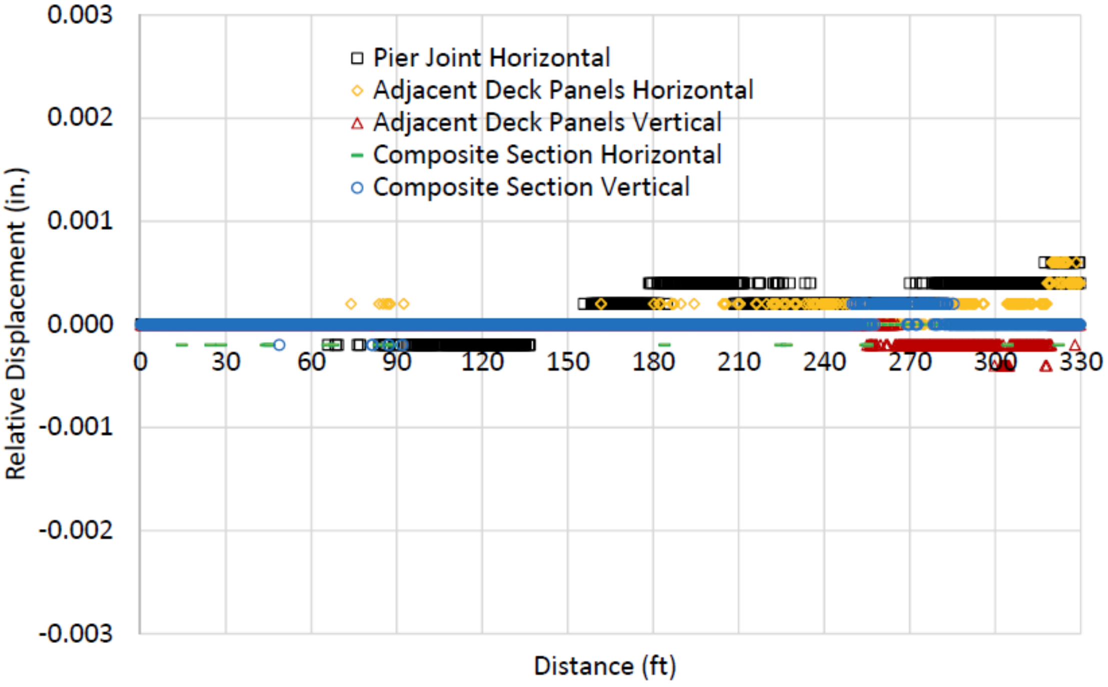

FIGURE 3.14 Relative displacement at different locations for load path #4

4 LONG-TERM MONITORING

In order to evaluate the structural performance of the new precast concrete deck system over a longer duration, strain data were collected at the mid-section (0.4L) and pier section (14 ft from the pier centerline) at different times during the first three years of service. The objective of this monitoring process is to examine whether changes in strain values are normal and within the predicted values of prestress losses due to shrinkage and creep of concrete. Significant changes in girder strains would indicate either deterioration in the composite section or excessive loss of prestressing. A total of ten vibrating wire strain gauges (five in each section) were installed and connected to the data acquisition unit shown in Figure 4.1. The location of these gauges are shown in Table 4.1. This long-term monitoring system was designed to transfer the data wirelessly to the research team, however, due to some internet connectivity problems, the research team used wired connection to collect stored strain data at specific dates. Below are the dates when strain data were collected for approximately four-month period prior to these dates:

1. November 21, 2016: The bridge was just opened to traffic.
2. October 16, 2018: Almost two years after the bridge was opened to traffic.
3. July 24, 2019: Two years and eight months after the bridge was opened to traffic.

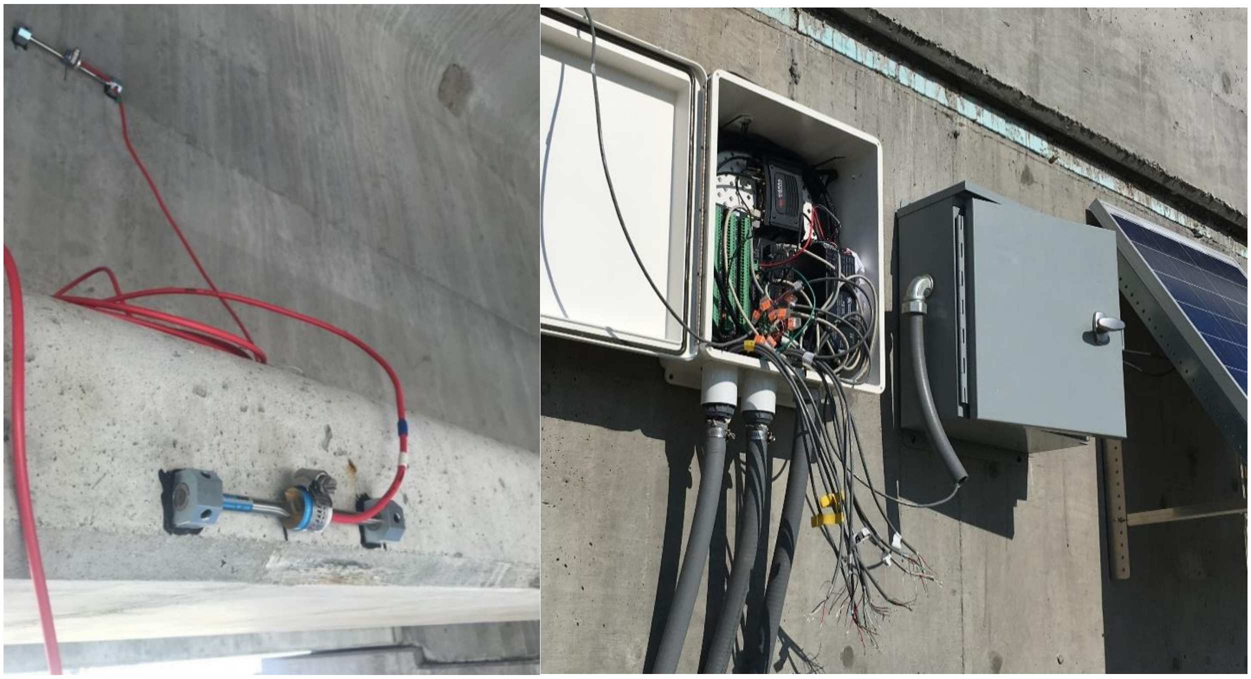

FIGURE 4.1 Vibrating wire strain gauges (VWSG) and data acquisition unit

Table 4.1 Location of VWSGs at pier and mid sections

VWSG Location	Pier Section	0.4 L Section
Deck Soffit	VWG 1	VWG 6
Top Flange	VWG 2	VWG 7
Web	VWG 3	VWG 8
Bot. Flange	VWG 4	VWG 9
Girder Soffit	VWG 5	VWG 10

4.1 November 21, 2016

The data collected at this time covered the period from July 15, 2016 to November 21, 2016. Strain data was recorded every 20 minutes as well as the ambient temperature in degree Celsius. Figures 4.2 and 4.3 show the strain and temperature data respectively. These plots indicate that the average strains remained almost constant during the four-month period. Daily changes in the strain corresponded to the daily changes in temperature. Figures 4.4 and 4.5 clarify that by zooming in to show changes in strain and temperature during a 10-day period. It should be noted that the absolute values of the strain are meaningless as they need to be zeroed. Only changes in the strain values are used to indicate changes in the state of stress in the interior girder.

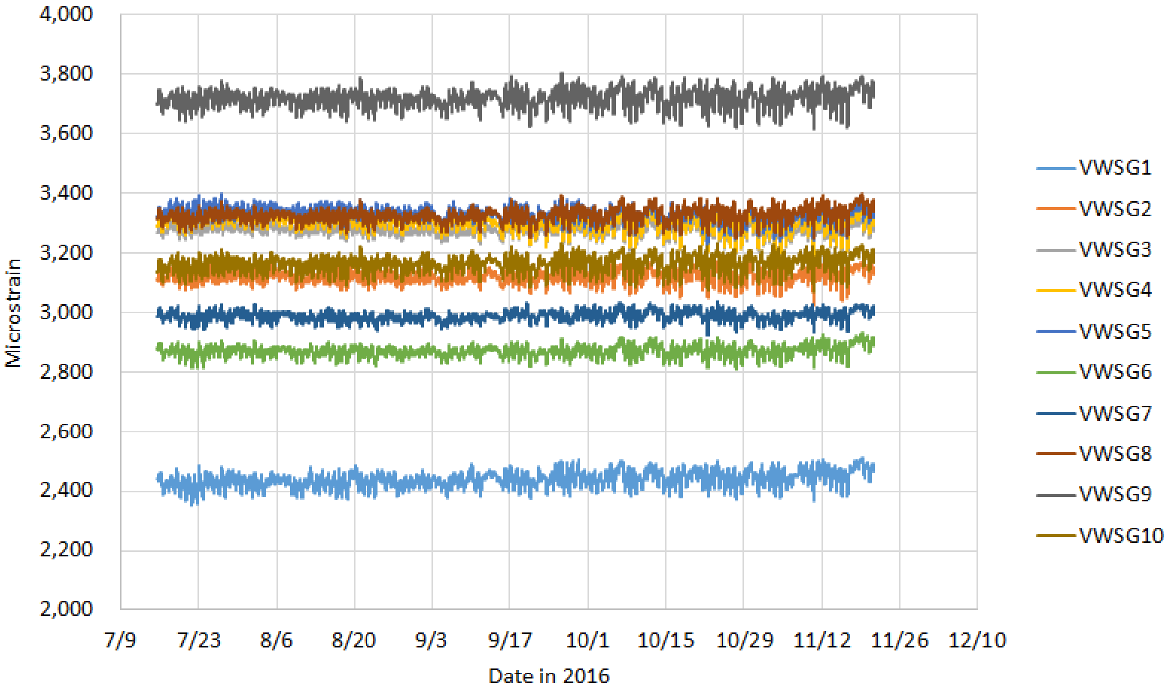

FIGURE 4.2 Strain readings from the 10 VWSGs in 2016

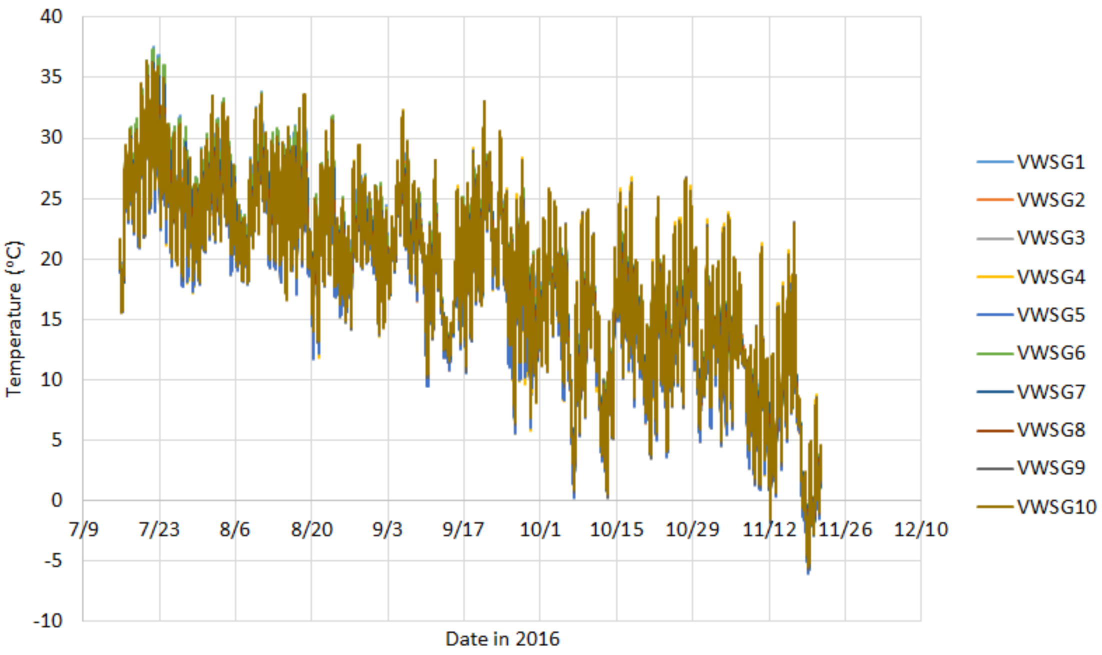

FIGURE 4.3 Temperature readings from the 10 VWSGs in 2016

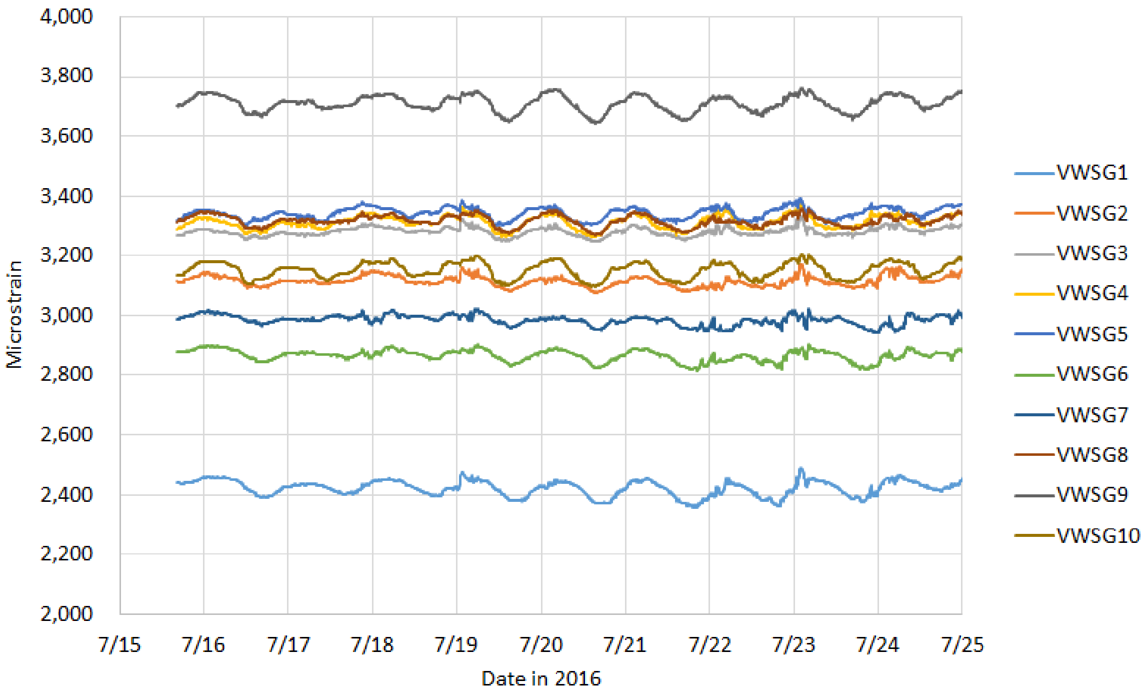

FIGURE 4.4 Strain readings from the 10 VWSGs in July 2016

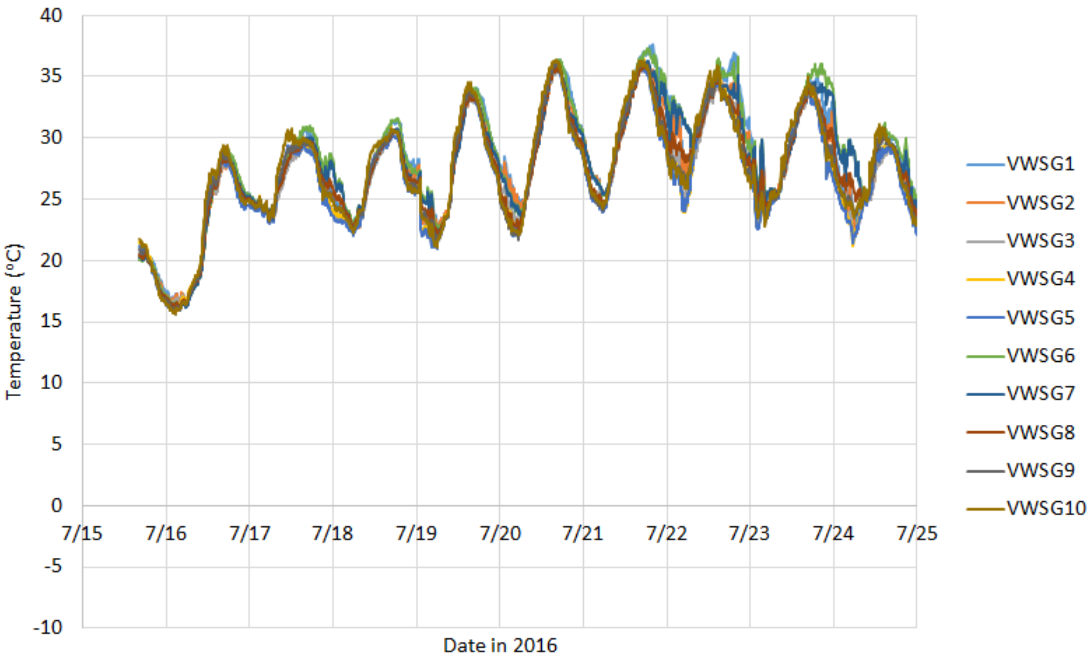

FIGURE 4.5 Temperature readings from the 10 VWSGs in July 2016

4.2 October 16, 2018

The data collected at this time covered the period from June 23, 2018 to October 16, 2018. Strain data was recorded every 20 minutes as well as the ambient temperature in degree Celsius. Figures 4.6 and 4.7 show the strain and temperature data respectively. These plots indicate that the average strains remained almost constant during the four-month period. Daily changes in the strain corresponded to the daily changes in temperature. Figures 4.8 and 4.9 clarify that by zooming in to show changes in strain and temperature during a 10-day period.

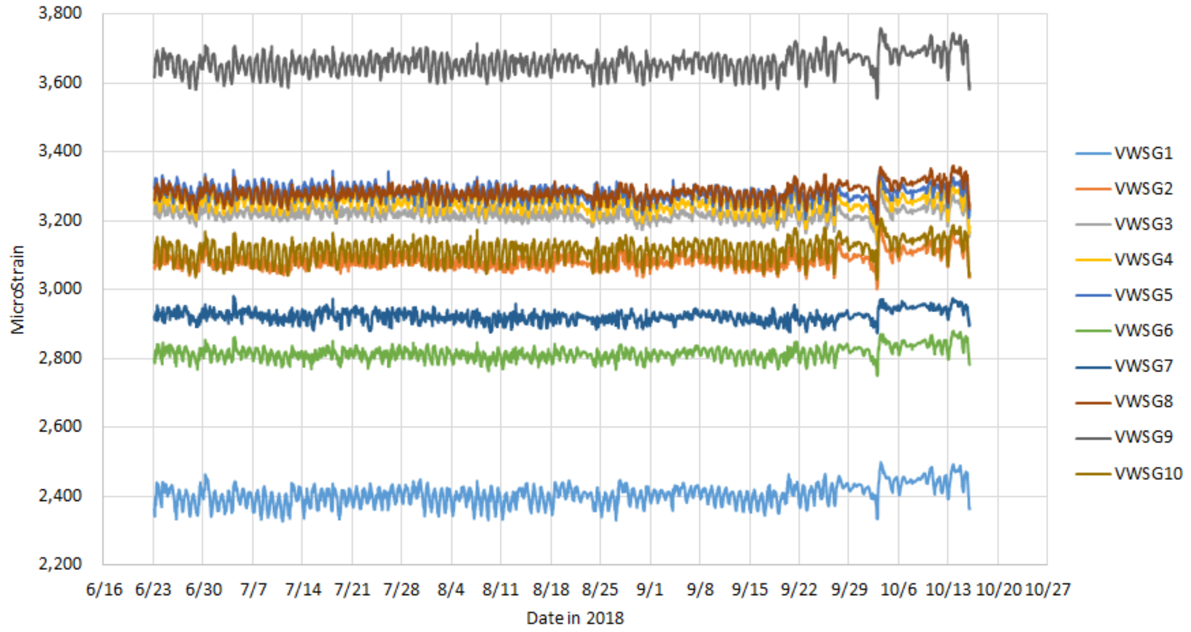

FIGURE 4.6 Strain readings from the 10 VWSGs in 2018

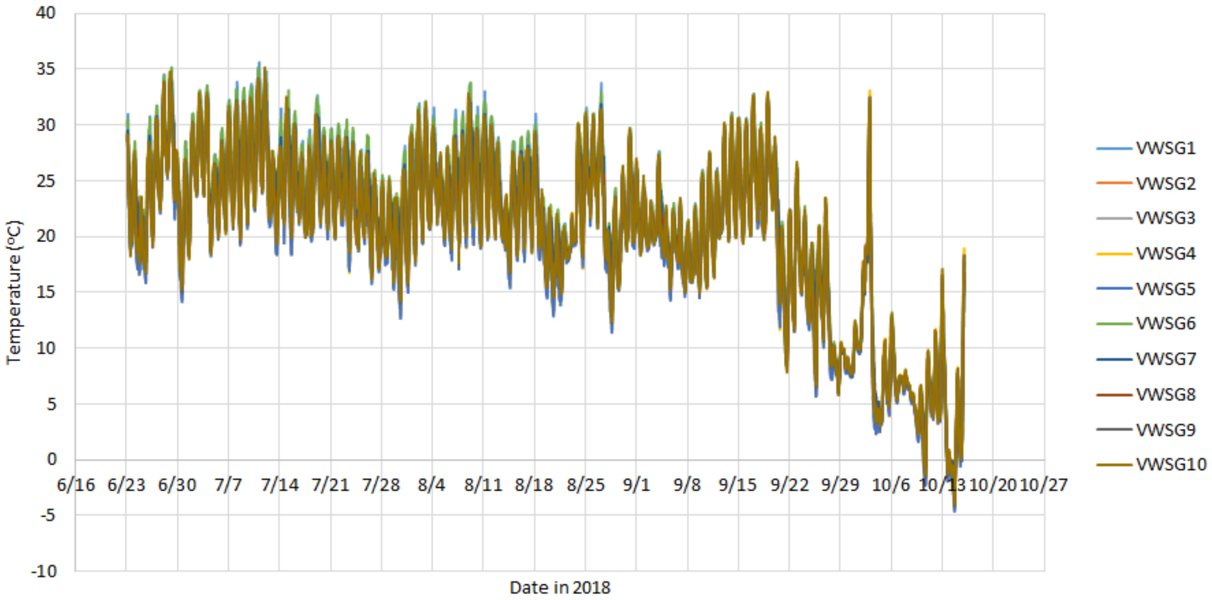

FIGURE 4.7 Temperature readings from the 10 VWSGs in 2018

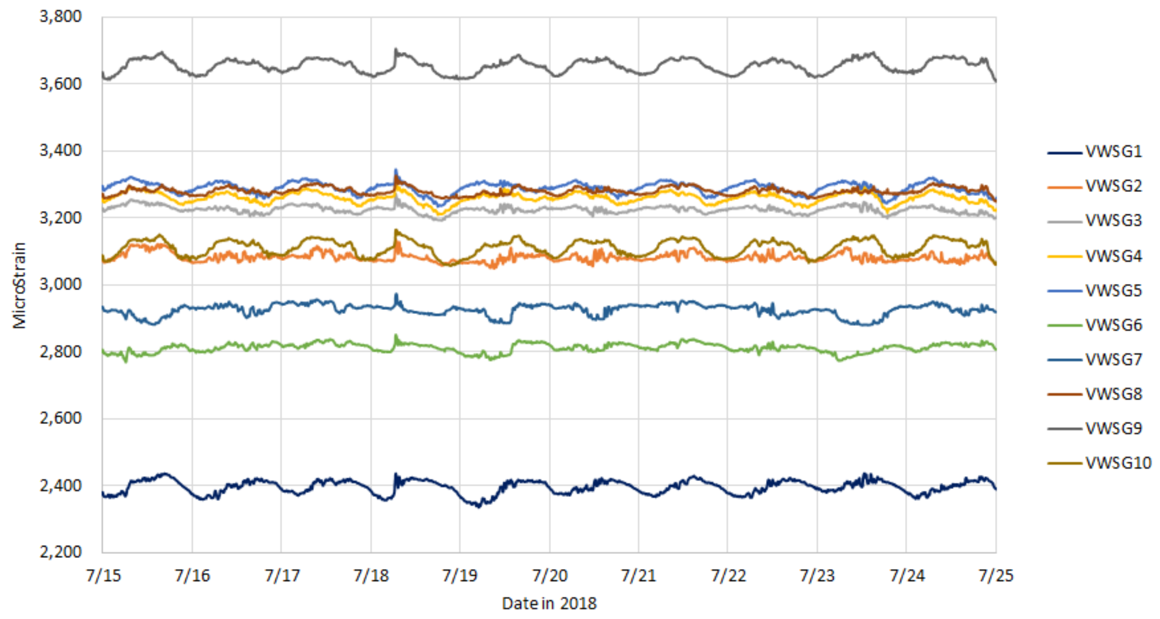

FIGURE 4.8 Strain readings from the 10 VWSGs in July 2018

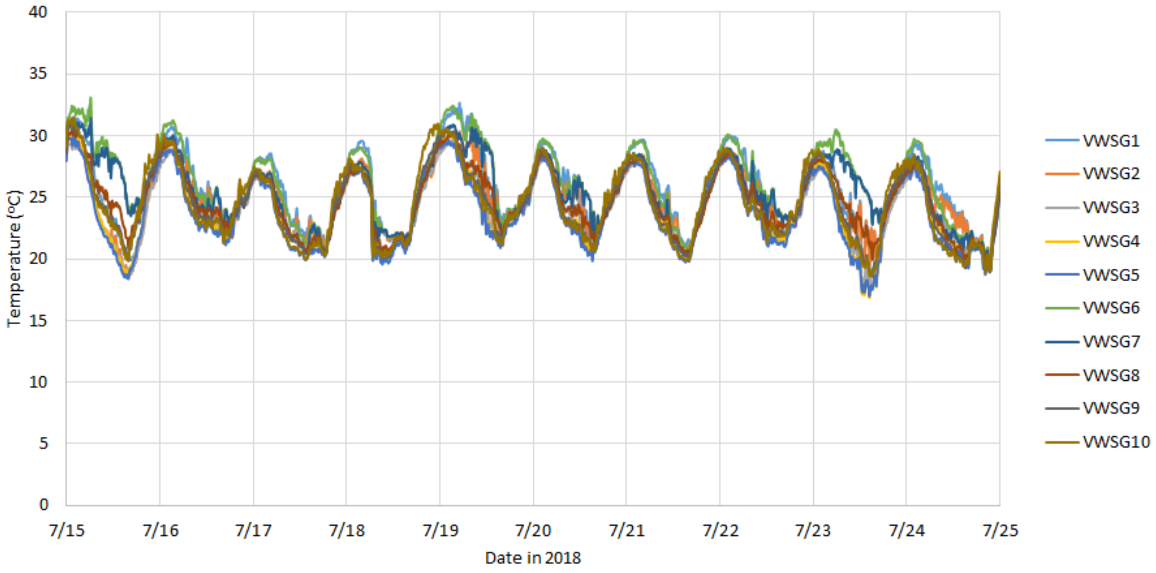

FIGURE 4.9 Temperature readings from the 10 VWSGs in July 2018

4.3 July 24, 2019

The data collected at this time covered the period from March 31, 2019 to July 24, 2019. Strain data was recorded every 20 minutes as well as the ambient temperature in degree Celsius. Figures 4.10 and 4.11 show the strain and temperature data respectively. These plots indicate that the average strains remained almost constant during the four-month period. Daily changes in the strain corresponded to the daily changes in temperature. Figures 4.12 and 4.13 clarify that by zooming in to show changes in strain and temperature during a 10-day period.

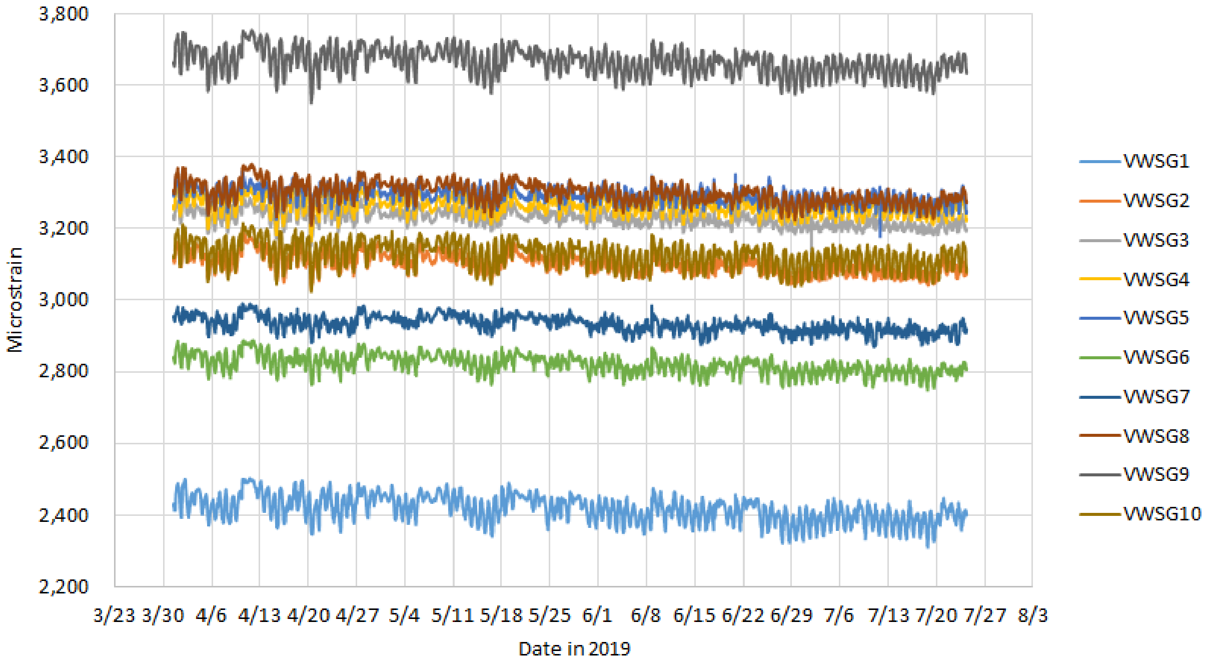

FIGURE 4.10 Strain readings from the 10 VWSGs in 2019

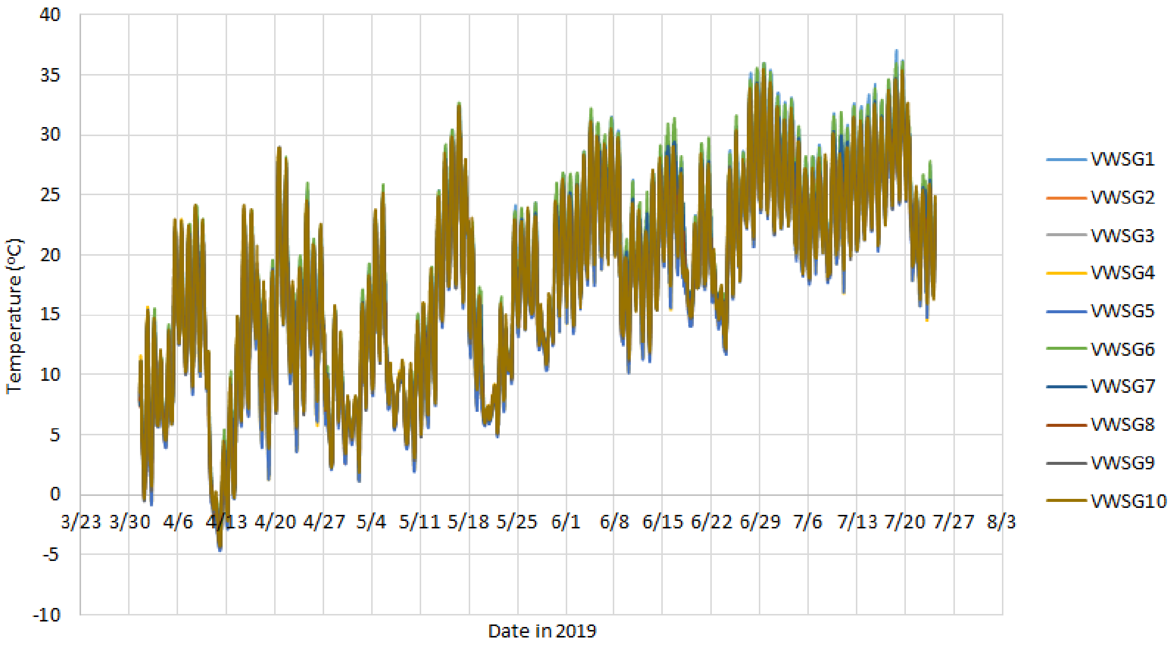

FIGURE 4.11 Temperature readings from the 10 VWSGs in 2019

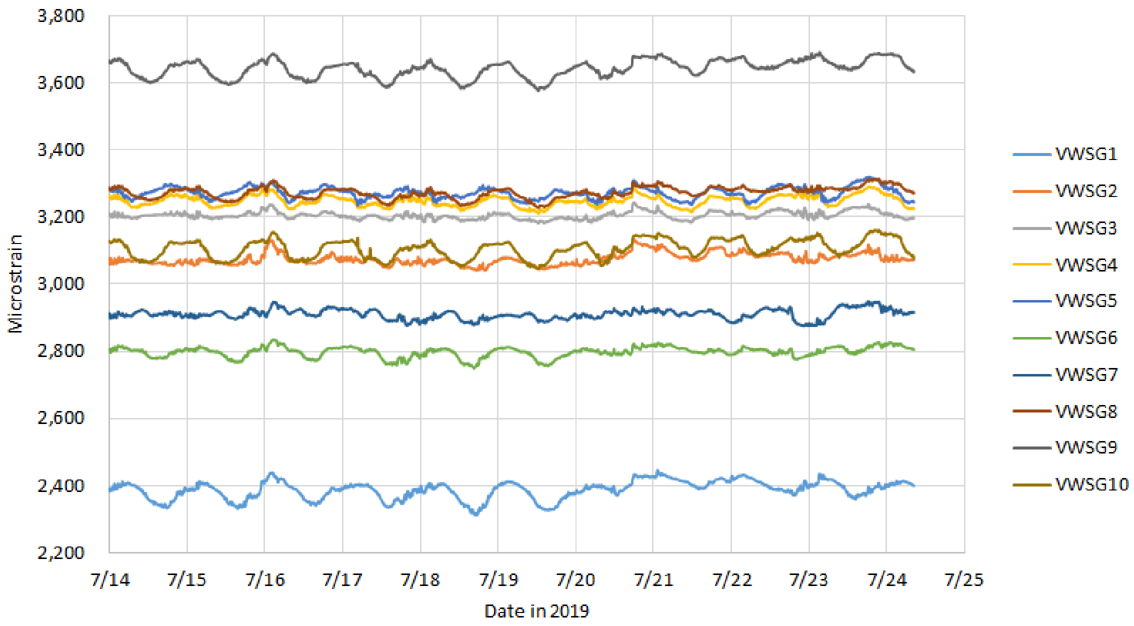

FIGURE 4.12 Strain readings from the 10 VWSGs in July 2019

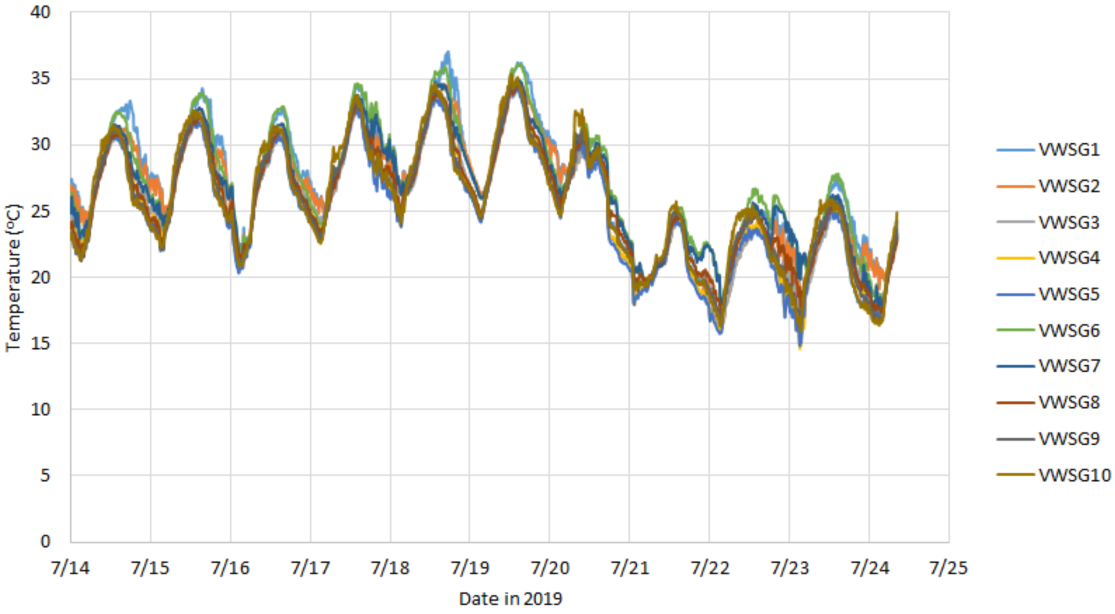

FIGURE 4.13 Temperature readings from the 10 VWSGs in July 2019

In order to make conclusions based on the measured strain values over the three-year period, the minimum and maximum strain values in each of the three periods were plotted versus time for both pier and mid sections. Figure 4.14 plots the changes in minimum and maximum strain values obtained from the five gauges at the pier section, while Figure 4.15 plots the changes in minimum and maximum strain values obtained from the five gauges at the mid section. Table 4.2

lists these values as well as the corresponding temperatures. These plots and table indicate that the largest change in bottom flange strain at the pier section is 48 micro-strain and at the mid-section is 65 micro-strain. These values correspond to a prestress loss of 1.4 ksi and 1.9 ksi respectively, which are considered reasonable for shrinkage and creep after deck placement.

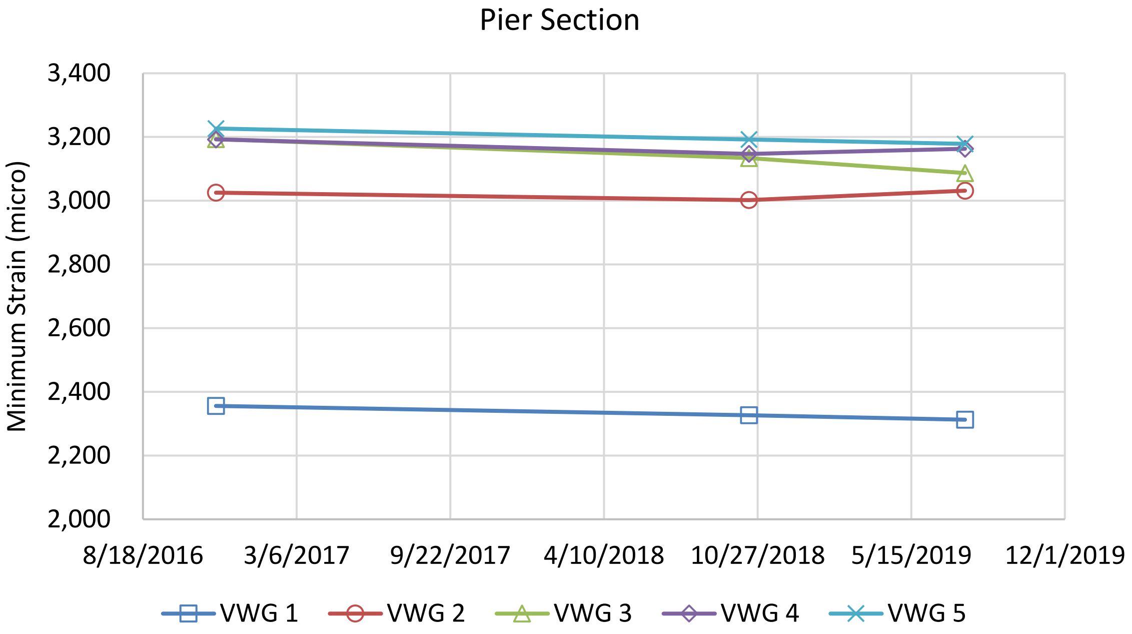

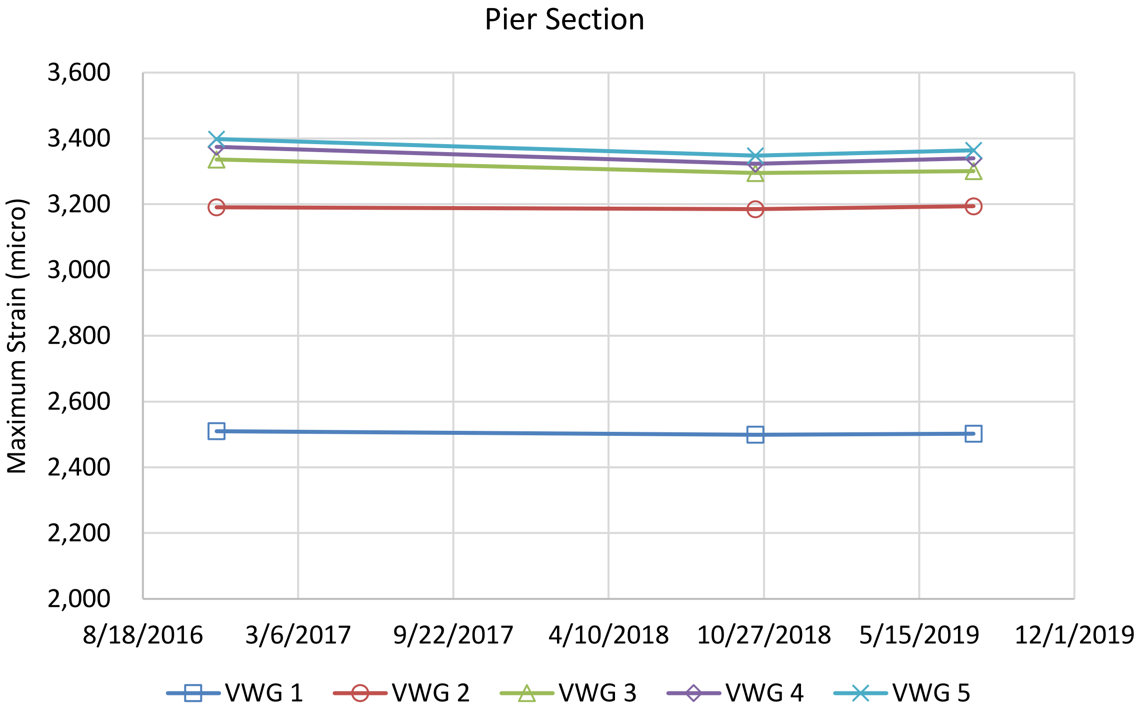

FIGURE 4.14 Changes in minimum and maximum strain readings at the pier section

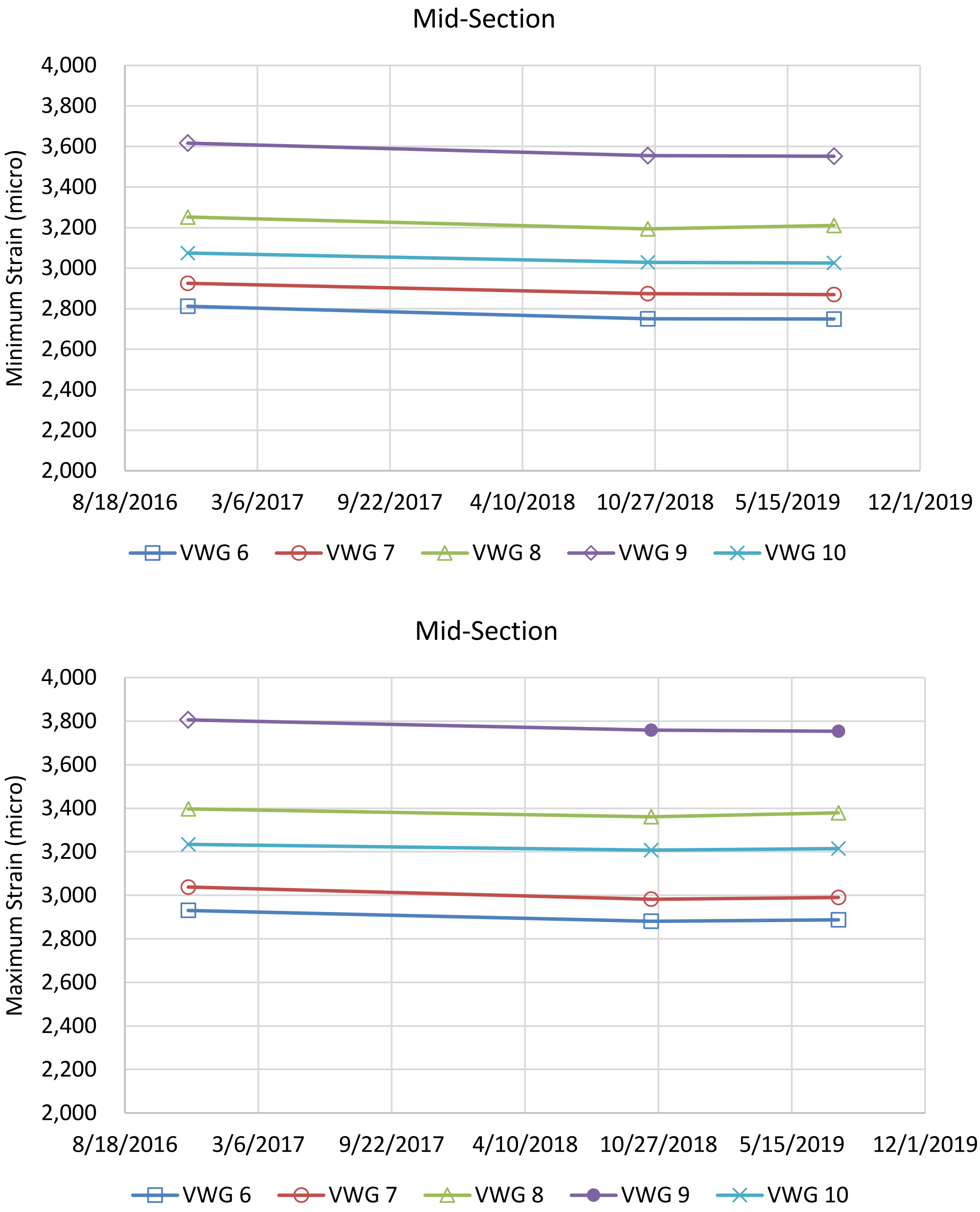

FIGURE 4.15 Changes in minimum and maximum strain readings at the mid-section

Table 4.2 Comparing strain readings collected at different times

Extreme Values	**Minimum**				**Maximum**			
Pier Section	**7/24/19**	**10/16/18**	**11/21/16**	**Diff.**	**7/24/19**	**10/16/18**	**11/21/16**	**Diff.**
VWG 1	2,313	2,327	2,356	43	2,502	2,499	2,510	7
VWG 2	3,031	3,002	3,025	(6)	3,194	3,185	3,190	(3)
VWG 3	3,087	3,134	3,193	106	3,300	3,295	3,336	36
VWG 4	3,163	3,147	3,193	30	3,339	3,323	3,374	35
VWG 5	3,178	3,192	3,227	48	3,363	3,348	3,398	35
Temperature (ºC)	-4	-4	-6		35	35	36	
Mid Section	**7/24/19**	**10/16/18**	**11/21/16**	**Diff.**	**7/24/19**	**10/16/18**	**11/21/16**	**Diff.**
VWG 6	2,749	2,750	2,812	63	2,888	2,881	2,930	43
VWG 7	2,869	2,874	2,925	56	2,990	2,982	3,038	48
VWG 8	3,210	3,194	3,252	42	3,379	3,361	3,397	18
VWG 9	3,552	3,556	3,616	65	3,753	3,759	3,806	52
VWG 10	3,025	3,029	3,074	49	3,214	3,207	3,234	20
Temperature (ºC)	-4	-4	-6		35	35	36	

5 CONCLUSIONS

The Kearney East Bypass bridge project is the first implementation of a new precast concrete deck system that has several unique features to enhance its constructability, structural efficiency, and durability. Multiple inspections, live load testing, and long-term monitoring were conducted to evaluate the performance of the new system and compare to the twin bridge constructed using the conventional CIP concrete deck. Also, FEA was conducted to model the structural behavior of the new system. Based on inspection, analysis results, and live load testing of that bridge and the comparison with CIP concrete deck bridge, the following conclusions were made:

1. The new precast concrete deck system was fully-composite with the supporting concrete girders similar to conventional CIP concrete deck. This was proven by comparing the measured strains and deflections with those obtained from the CIP concrete deck bridge. Also, monitoring the strain values over a three-year period indicated the adequacy of the shear connection under service loads.
2. Placing negative moment reinforcement in the haunch area over each girder line was sufficient for achieving live load continuity. This was proven by comparing the measured strains and deflections with those obtained from the CIP concrete deck bridge as well as the monitored strains at the pier section over three-year period.
3. Placing the deck post-tensioning strands in the haunch over each girder line was not only simpler in construction, but also structurally efficient as it results in pre-compression of the PC deck panels and the transverse joints, which was evident in the LVDT measurements.
4. The unreinforced transverse joints between adjacent precast concrete deck panels performed very well under live load with no displacements across the joint in either horizontal or vertical directions, which proves the effectiveness of the post-tensioning system.
5. Moment distribution factors of the new system were accurately predicted by FEA, which were significantly lower than those predicted by AASHTO LRFD provisions for type “k” bridges.
6. Changes in measured girder strains over a three-year period after the bridge is open to traffic indicated very small loss of prestressing. No significant changes in strain were observed during the monitoring period.

5. REFERENCES

1. American Association of State Highway and Transportation Officials (AASHTO). (2014). "AASHTO LRFD Bridge Design Specifications: Customary U.S. Units." 7th Edition, Washington, D.C.

2. Badie, S. S., and Tadros, M. K. (2008). "Full-Depth, Precast-Concrete Bridge Deck Panel Systems." National Cooperative Highway Research Program, NCHRP 12-65, Report 584, Transportation Research Board, Washington, D.C.

3. Chung, W.S. (2003). "A cracked concrete material model for the non-linear finite element analysis of slab-on-girder bridges." Doctoral dissertation, Perdue University, West Lafayette, IN.

4. Cook, R.D., Malkus, D.S., and Plesha, M.E. (1989). "Concepts and applications of finite element analysis." Third Edition, Wiley, New York, NY.

5. Hanna, K., Morcous, G., and Tadros, M. K. (2010). "Second Generation Precast Deck Panel (NUDECK) System." Technical Report, Nebraska Department of Roads (NDOR), NE, December.

6. Laurendeau, M., Barr, P., Higgs, A., Halling, M., Maguire, M., and Fausett, R. (2015). "Live-Load Response of a 65-Year-Old Pratt Truss Bridge." ASCE Journal of Performance of Constructed Facilities, 29(6).

7. Morcous, G., and Khayat, K. H. (2014) "Design and Performance of Self-Consolidating Concrete for Connecting Precast Concrete Deck Panels and Bridge I-Girders", MS&T Project No. DTRT-06-G-04, August, Rolla, MO.

8. Morcous, G., and Tadros, M. K. (2014). "Implementation of 2nd Generation of Precast Concrete Deck System NUDECK to the Kearney East Bypass Project." 2014 PCI Annual Convention and National Bridge Conference, Washington, D.C., September.

9. Morcous, G., Hatami, A., and Asaad, M. (2015) "Evaluating the Constructability of NUDECK Precast Concrete Deck Panels for Kearney Bypass Project", NDOR Technical Report M336, February, Lincoln, NE.

10. Morcous, G., Jaber, F., and Volz, J. (2017). "Implementation of A New Precast Concrete Deck System to the Kearney East Bypass Project." 2017 PCI Annual Convention and National Bridge Conference, Cleveland, OH, March.

11. Morcous, G., Tadros, M. K., Hatami, A. (2013) "Implementation of Precast Concrete Deck System NUDECK (2nd Generation)" NDOR Technical Report M323, December, Lincoln, NE.

12. Precast/Prestressed Concrete Institute PCI. (2011). “State-of-the-art Report on Full-Depth Precast Concrete Bridge Deck Panels.” Published by PCI, SOA -01-1911, Chicago, IL, First Edition.

13. Sanayei, M., and Onipede, O. B. R. (1992). “Selection of noisy measurement locations for error reduction in static parameter identification.” Am. Inst. Aeronaut. Astronaut. J., 30(9), 2299–2309.

14. Torres, V., and Maguire, M. (2015). “Load Testing and Analysis of a 48-year old Out-of-Service Double Tee Girder Bridge.” Report to Center for Advanced Infrastructure and Transportation. Report Number CAIT-UTC-NC1.

6. APPENDICES

APPENDIX A: Bridge Fabrication and Construction

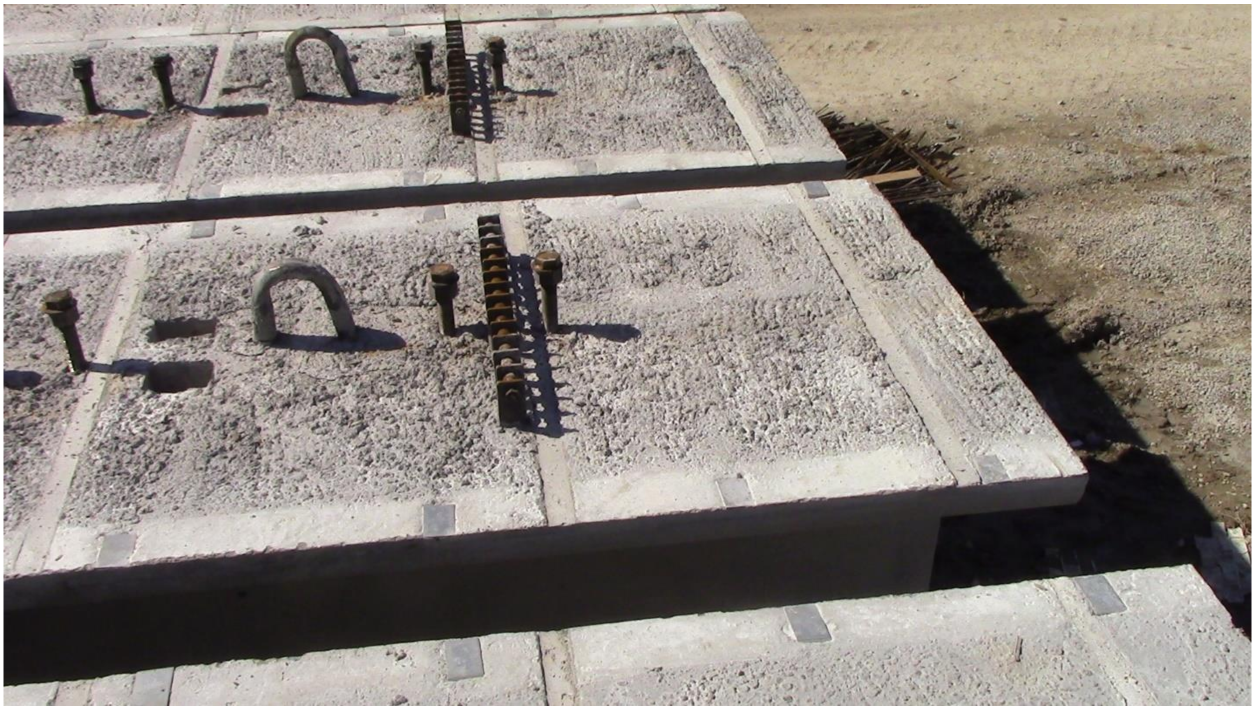

Summary of Compressive Strength Test Data for Precast/Prestressed Concrete Girders

Sample Date	Air Content	Water Cement Ratio	Required Release (psi)	Actual Release (psi)	Required Compressive Strength (psi)	Actual NDOR 28 Day (psi)	Actual Prestress Plant 28 Day (psi)	Actual Prestress Plant 56 Day (psi)
2/6/2015	2	0.31	7200	9035	10000	10413	10846	
1/29/2015	4	0.33	7200	7560	10000	9149	9598	11803
1/27/2015	3	0.32	7200	7720	10000	9653	10105	10527
1/24/2015	2.4	0.3	7200	9270	10000	10308	10834	
1/21/2015	3.8	0.31	7200	7525	10000	9577	10022	10495
4/14/2015	3.7	0.3	7200	7977	10300	11335	11986	
3/23/2015	2.5	0.32	7200	7675	10300	9725	10564	
3/13/2015	2.5	0.3	7200	10285	10300	12709	11516	
3/11/2015	3.7	0.3	7200	7595	10300	12090	12427	
3/9/2015	3.4	0.3	7200	7693	10300	11788	11210	
3/5/2015	3.3	0.3	7200	6985	10300	11739	11692	
3/3/2015	3.8	0.3	7200	7886	10300	10869	10446	
2/25/2015	3.5	0.3	7200	8161	10300	11567	11809	
2/23/2015	4	0.3	7200	8082	10300	9920	10774	
2/19/2015	3.5	0.3	7200	8337	10300	11853	11177	
2/16/2015	3.8	0.3	7200	9016	10300	10223	10881	
Average	**3.31**	**0.31**	**7,200**	**8,175**	**10,206**	**10,807**	**10,993**	**10,942**

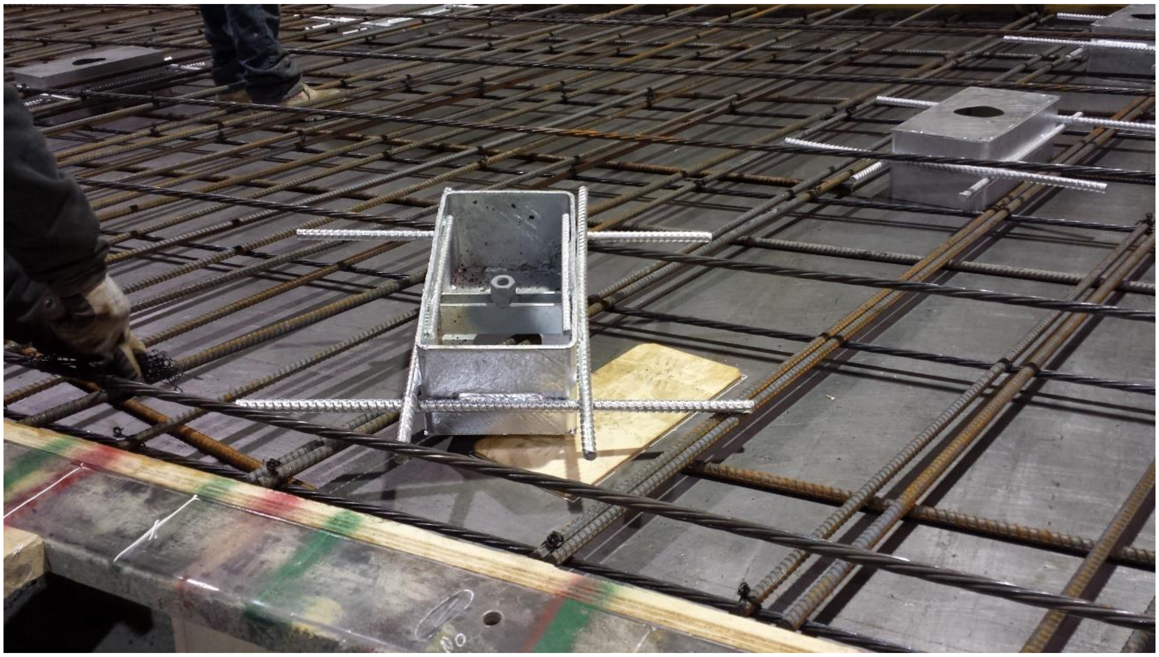

Summary of Compressive Strength Test Data for Precast/Prestressed Concrete Deck Panels

Sample Date	Air Content	Water Cement Ratio	Required Release (psi)	Actual Release (psi)	Required Compressive Strength (psi)	Actual NDOR 28 Day (psi)	Actual Prestress Plant 28 Day (psi)
3/9/2015	6.2	0.38	3500	3744	6000	8904	7739
3/5/2015	7.6	0.38	3500	3649	6000	7787	7440
3/3/2015	7	0.38	3500	3519	6000	6554	7241
2/28/2015	6.4	0.38	3500	4339	6000	6528	7836
2/26/2015	7.6	0.38	3500	3868	6000	7036	6664
2/23/2015	6.9	0.39	3500	4140	6000	6326	6578
2/19/2015	6.2	0.38	3500	3510	6000	5477	
2/16/2015	6.4	0.38	3500	3635	6000	8022	6821
Average	**6.79**	**0.38**	**3,500**	**3,801**	**6,000**	**7,079**	**7,188**

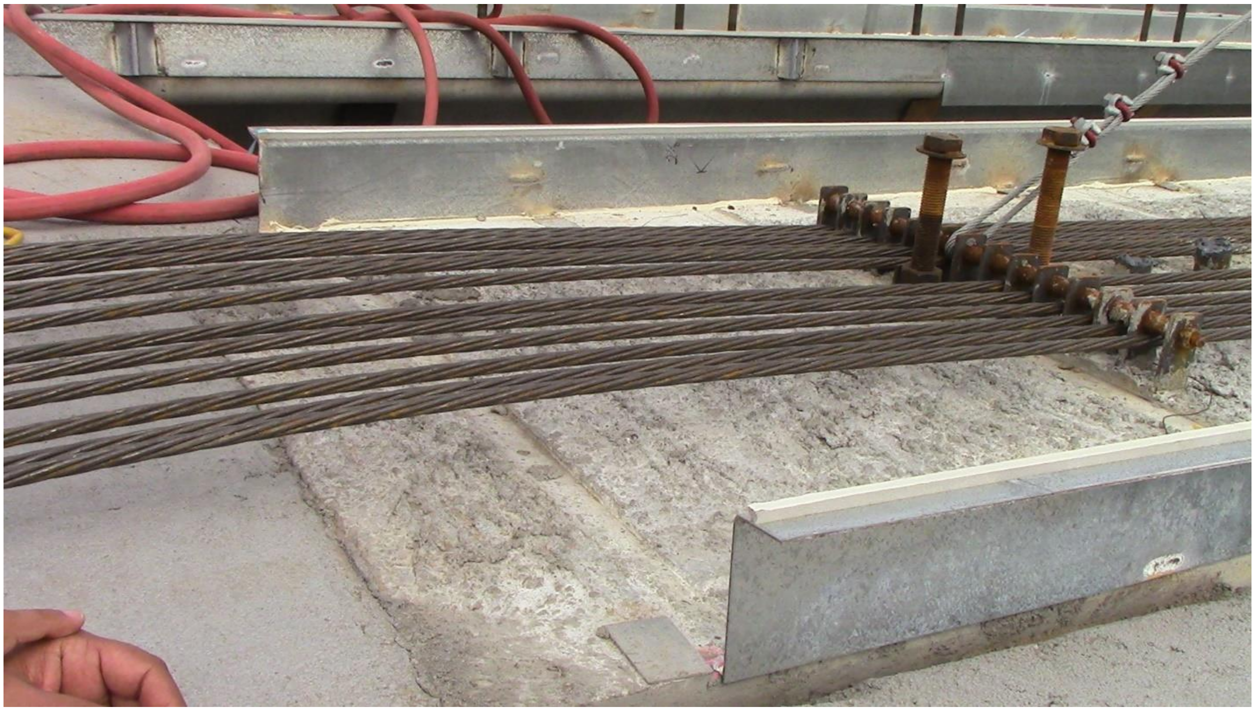

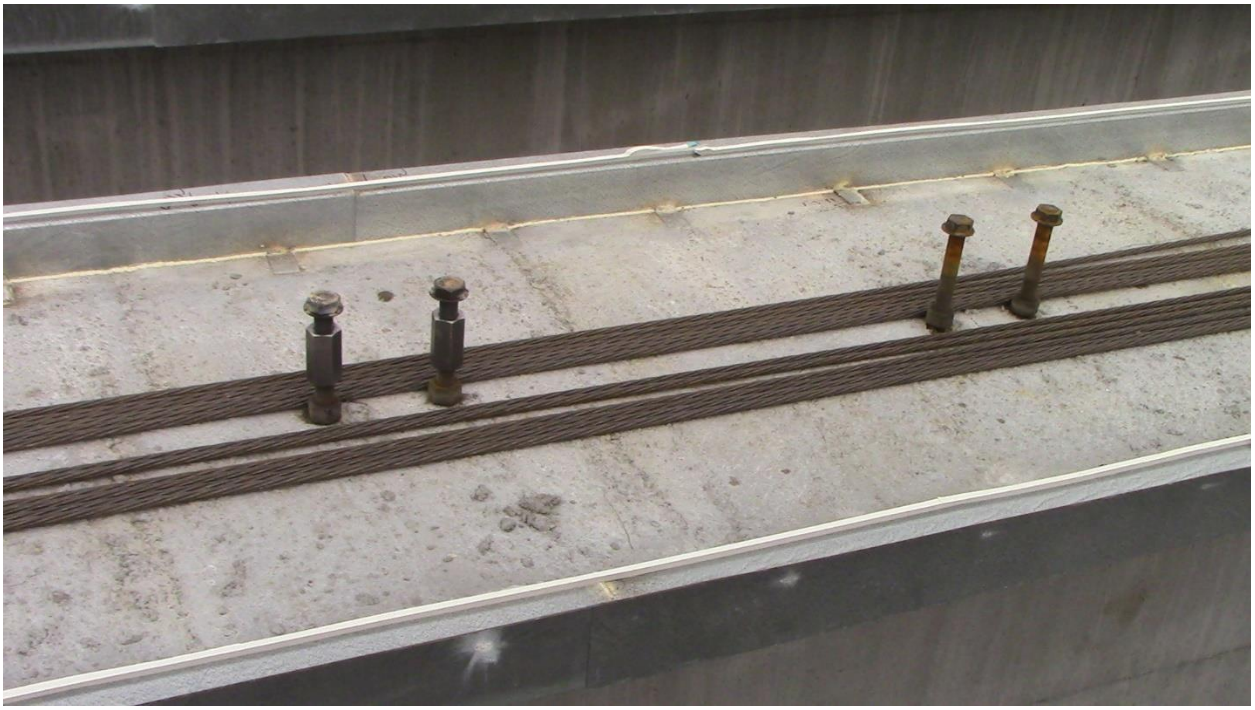

TILX 291646

Shim shot data used to calculate shear connector elevations and post-tensioning strand profiles for girders F, G, H, J, and K

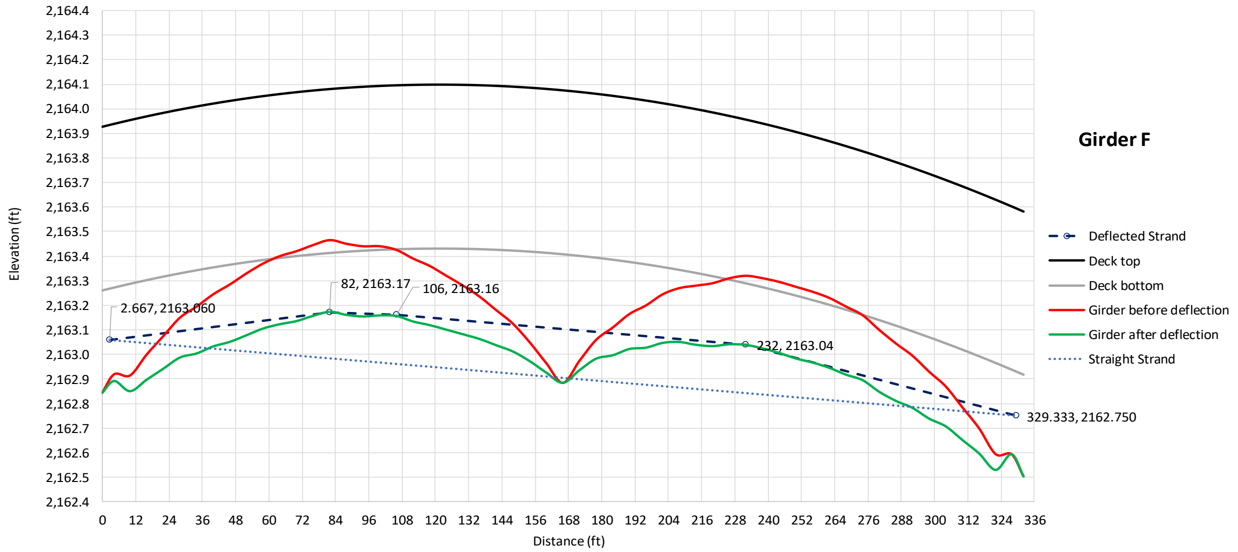

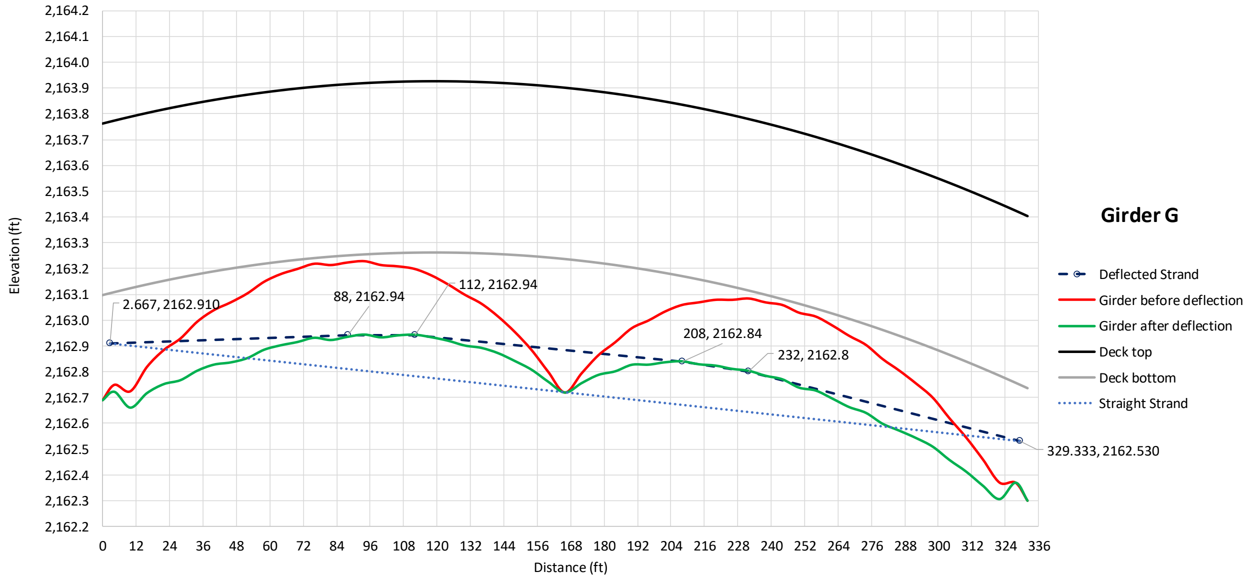

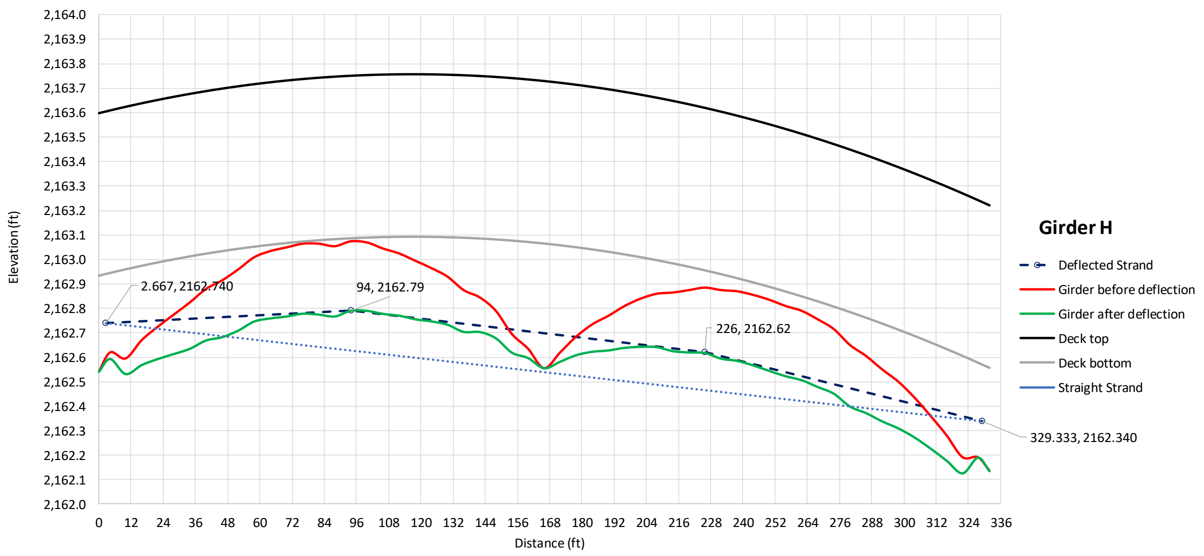
Girder H
Elevation (ft)
2,164.0
2,163.9
2,163.8
2,163.7
2,163.6
2,163.5
2,163.4
2,163.3
2,163.2
2,163.1
2,163.0
2,162.9
2,162.8
2,162.7
2,162.6
2,162.5
2,162.4
2,162.3
2,162.2
2,162.1
2,162.0
0 12 24 36 48 60 72 84 96 108 120 132 144 156 168 180 192 204 216 228 240 252 264 276 288 300 312 324 336
Distance (ft)
2.667, 2162.740
94, 2162.79
226, 2162.62
329.333, 2162.340
Deflected Strand
Girder before deflection
Girder after deflection
Deck top
Deck bottom
Straight Strand

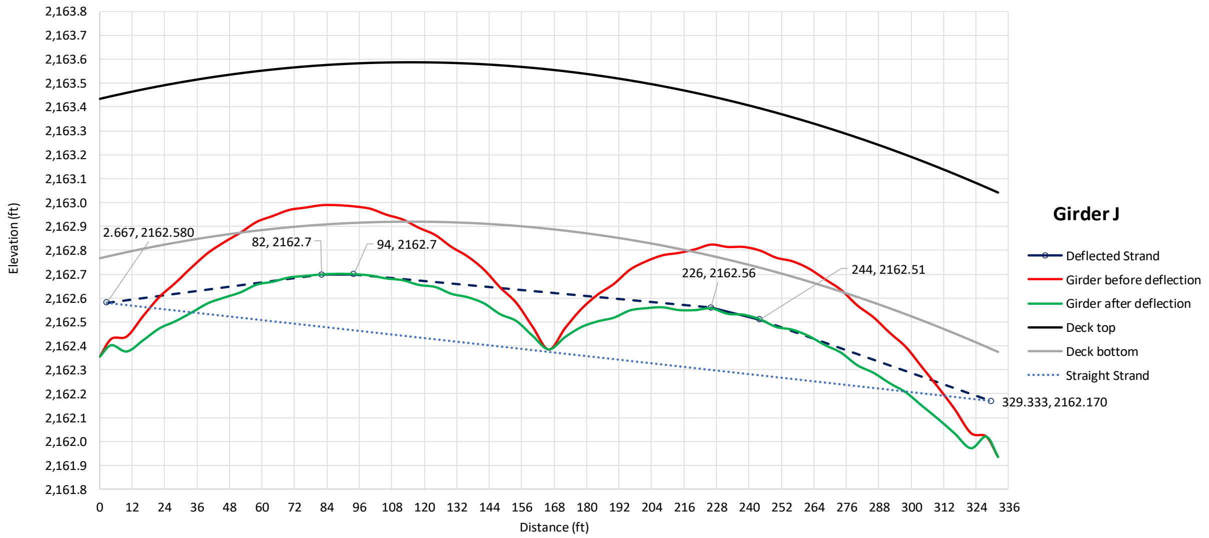
Girder J
Elevation (ft)
2,163.8
2,163.7
2,163.6
2,163.5
2,163.4
2,163.3
2,163.2
2,163.1
2,163.0
2,162.9
2,162.8
2,162.7
2,162.6
2,162.5
2,162.4
2,162.3
2,162.2
2,162.1
2,162.0
2,161.9
2,161.8
0 12 24 36 48 60 72 84 96 108 120 132 144 156 168 180 192 204 216 228 240 252 264 276 288 300 312 324 336
Distance (ft)
2.667, 2162.580
82, 2162.7
94, 2162.7
226, 2162.56
244, 2162.51
329.333, 2162.170
Deflected Strand
Girder before deflection
Girder after deflection
Deck top
Deck bottom
Straight Strand

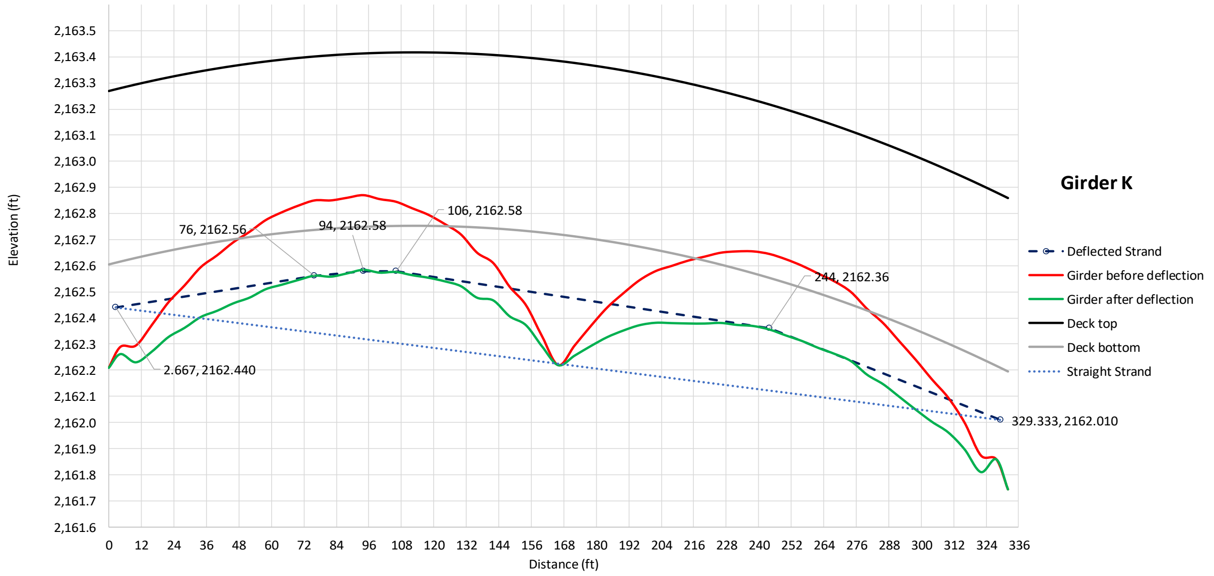
Girder K
Elevation (ft)
2,163.5
2,163.4
2,163.3
2,163.2
2,163.1
2,163.0
2,162.9
2,162.8
2,162.7
2,162.6
2,162.5
2,162.4
2,162.3
2,162.2
2,162.1
2,162.0
2,161.9
2,161.8
2,161.7
2,161.6
0 12 24 36 48 60 72 84 96 108 120 132 144 156 168 180 192 204 216 228 240 252 264 276 288 300 312 324 336
Distance (ft)
76, 2162.56
94, 2162.58
106, 2162.58
244, 2162.36
2.667, 2162.440
329.333, 2162.010
Deflected Strand
Girder before deflection
Girder after deflection
Deck top
Deck bottom
Straight Strand

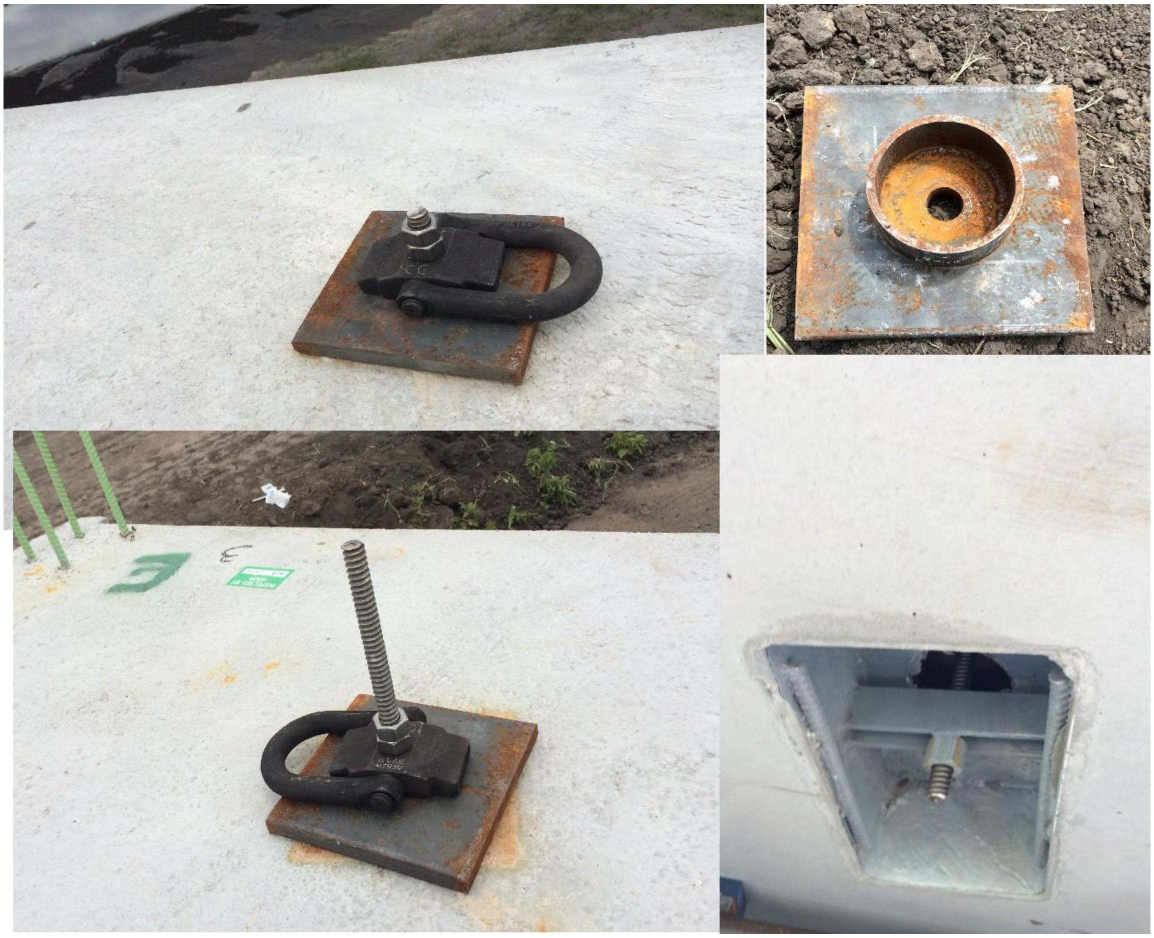

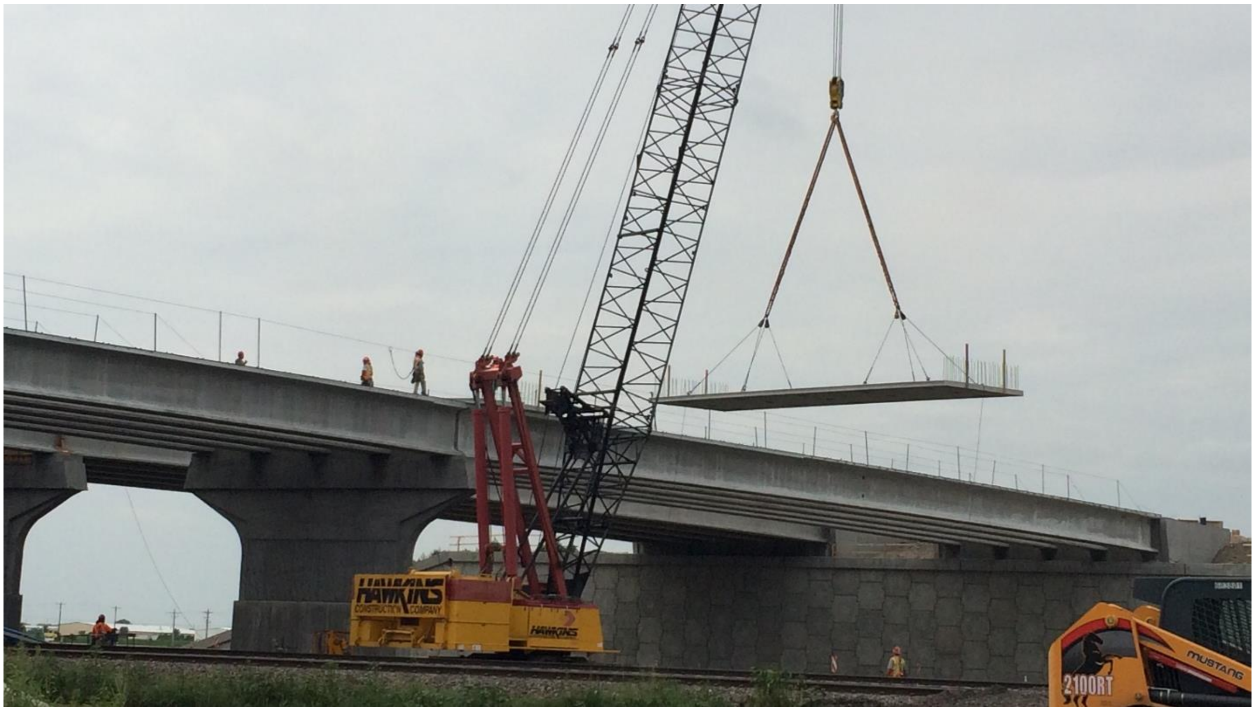
HAWKINS
CONSTRUCTION COMPANY
HAWKINS
2100RT
MUSTANG

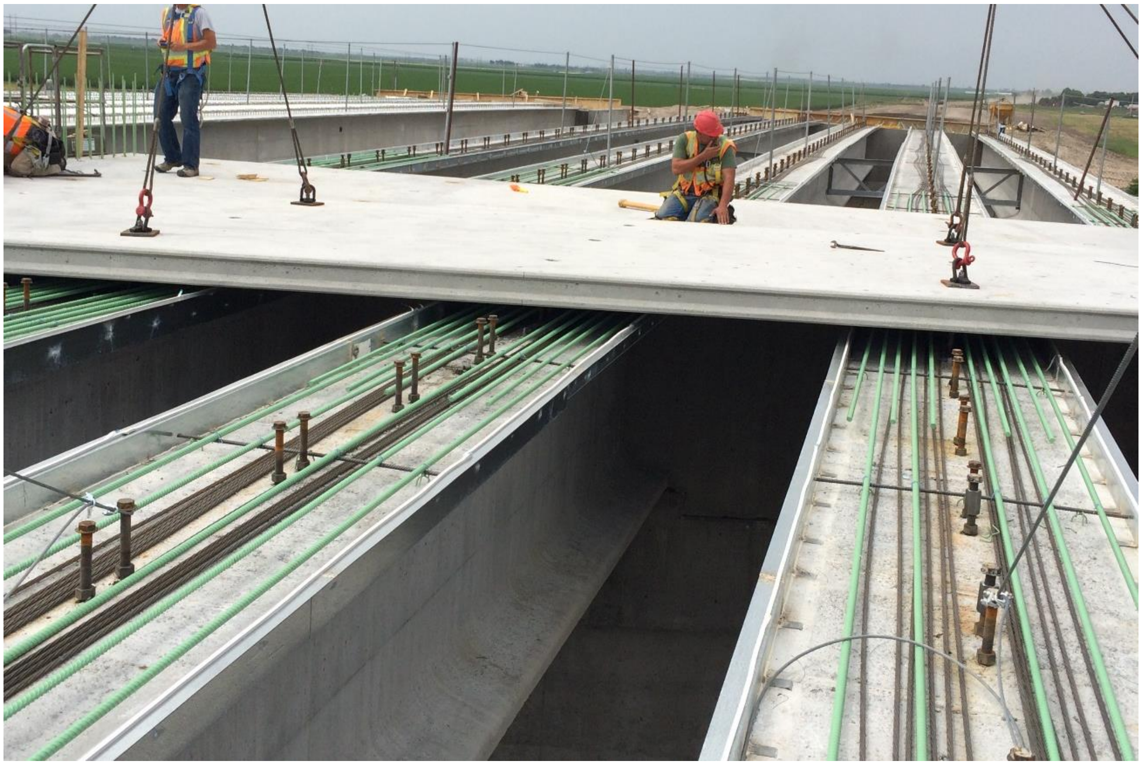

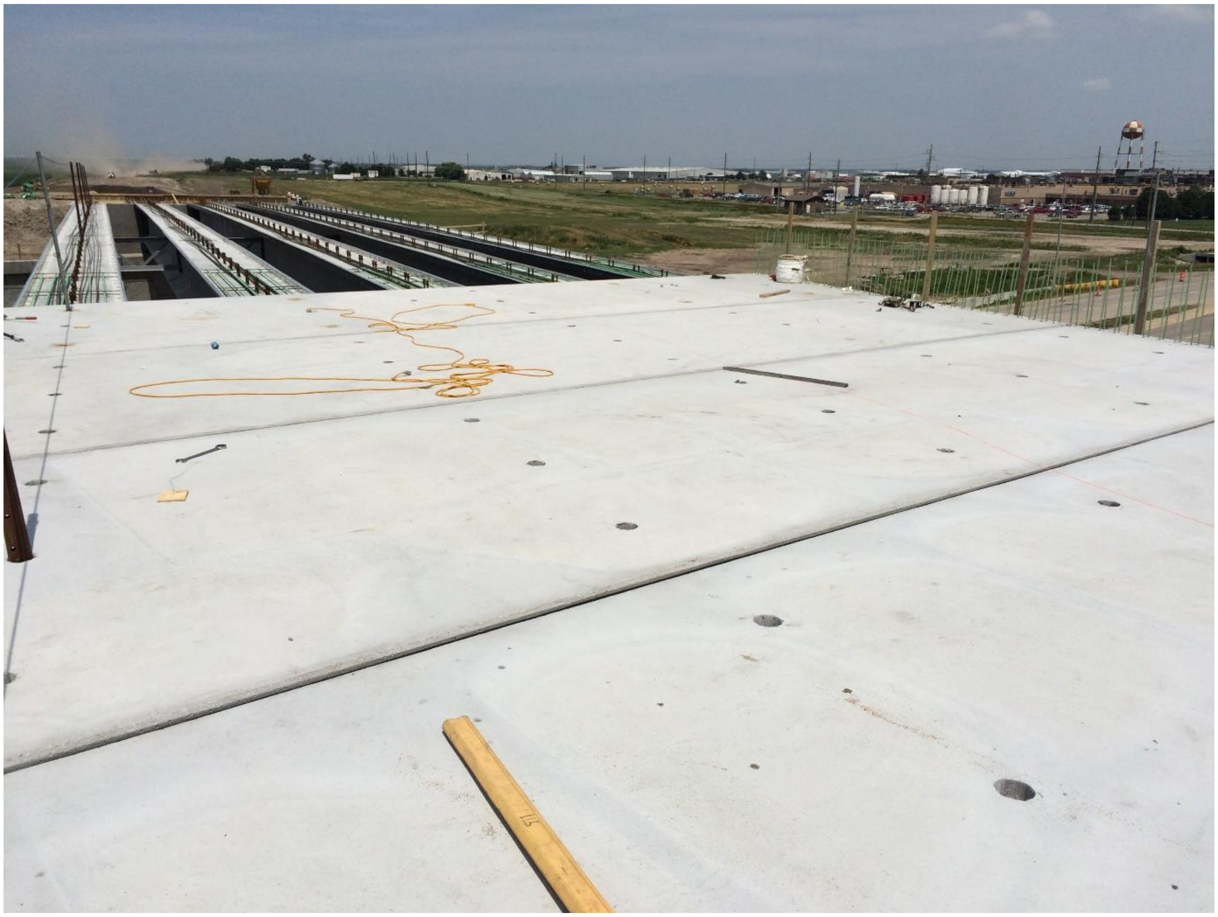

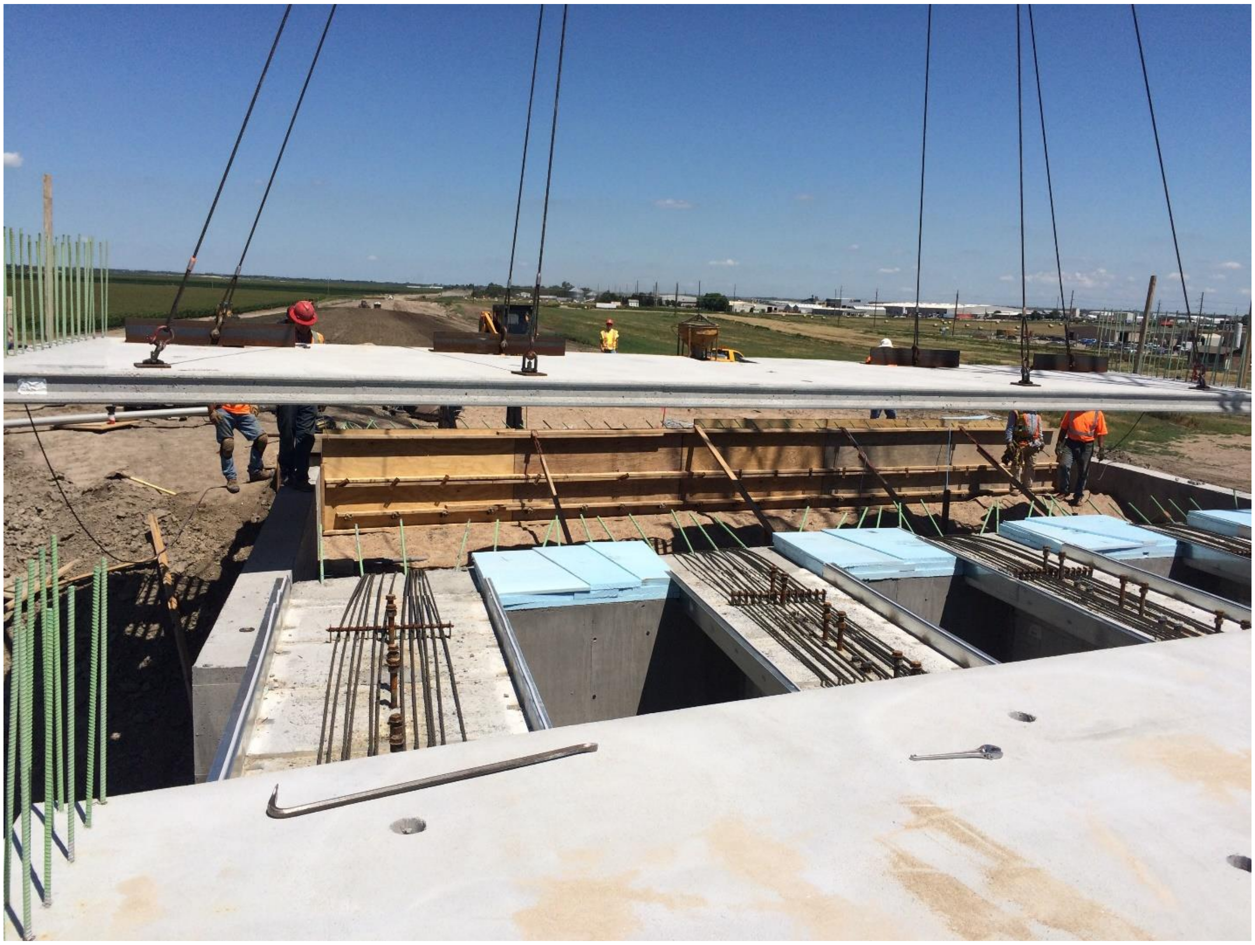

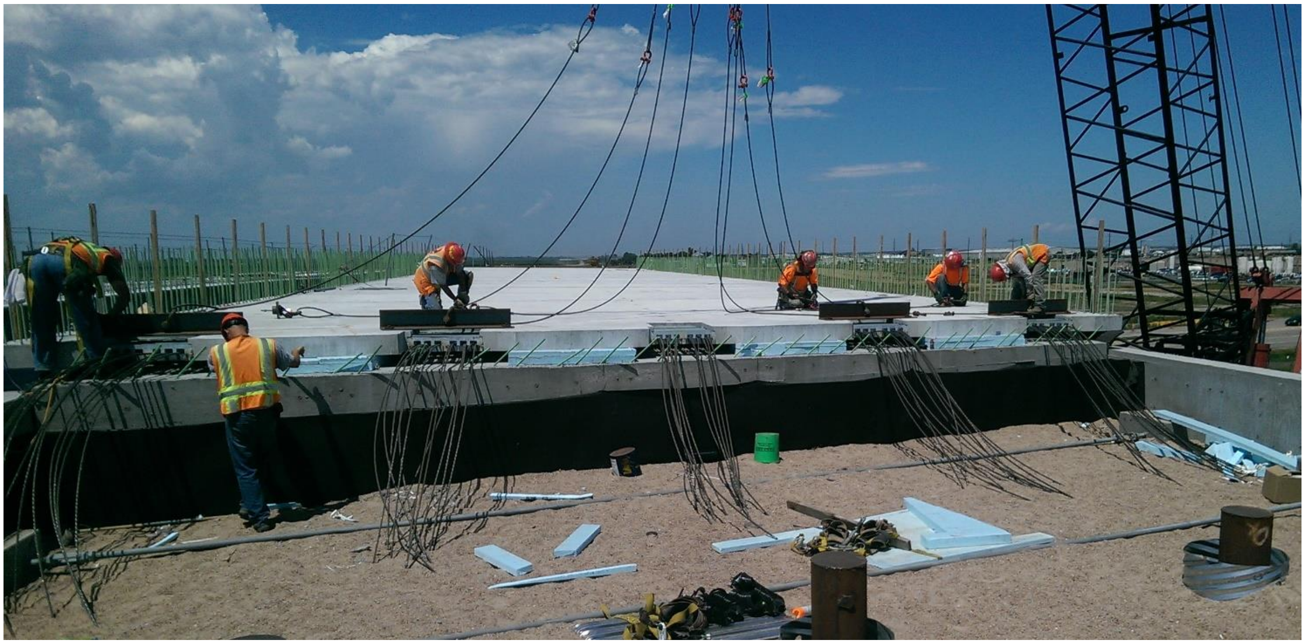

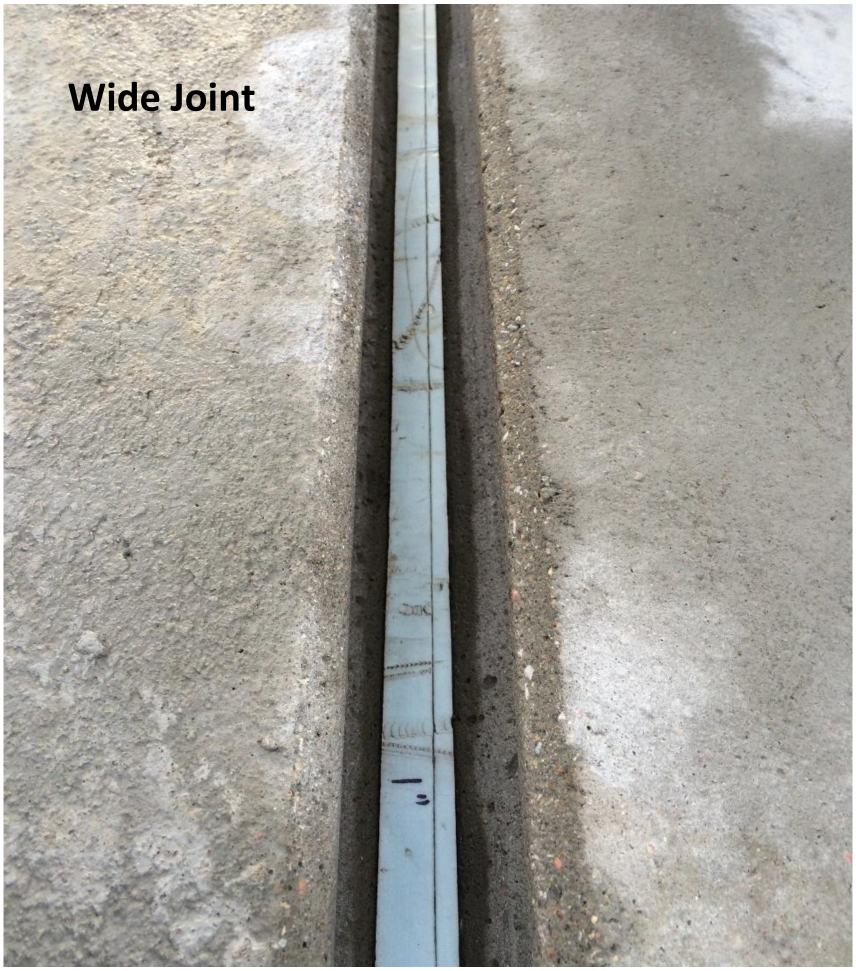
Wide Joint

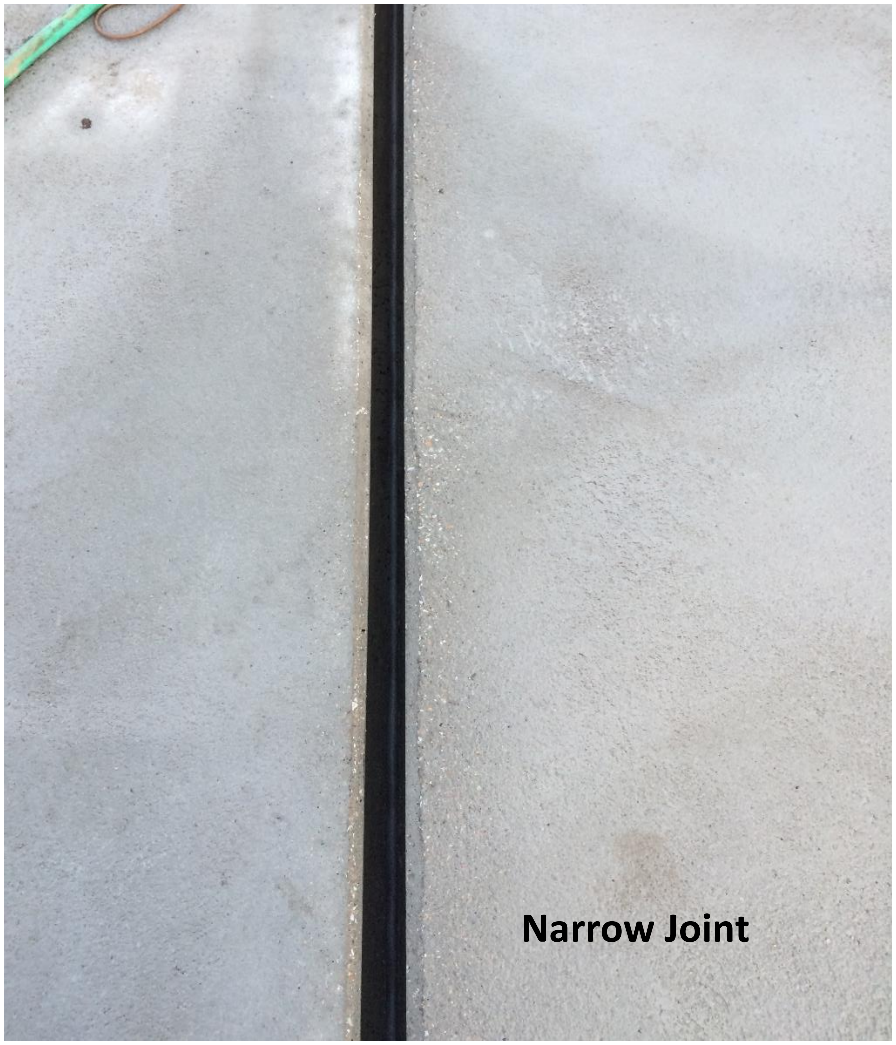
Narrow Joint

Transverse Joint Concrete	
Age (day)	**Compressive Strength (psi)**
5	4,470
7	4,678
28	5,360
Air Content (%)	10.5
Slump (in.)	6

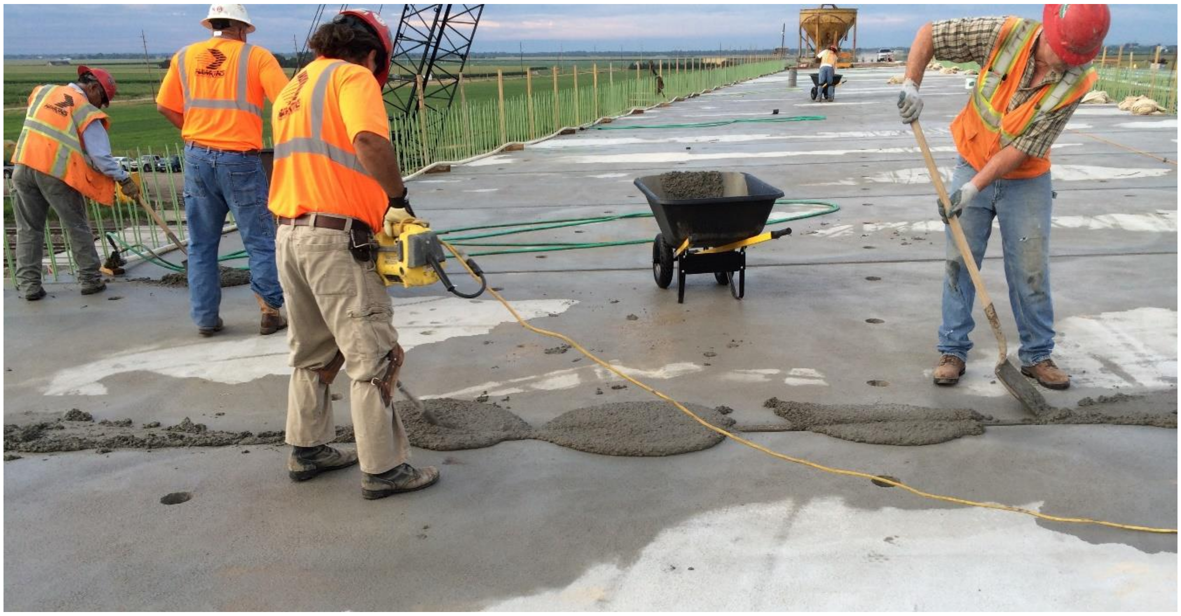

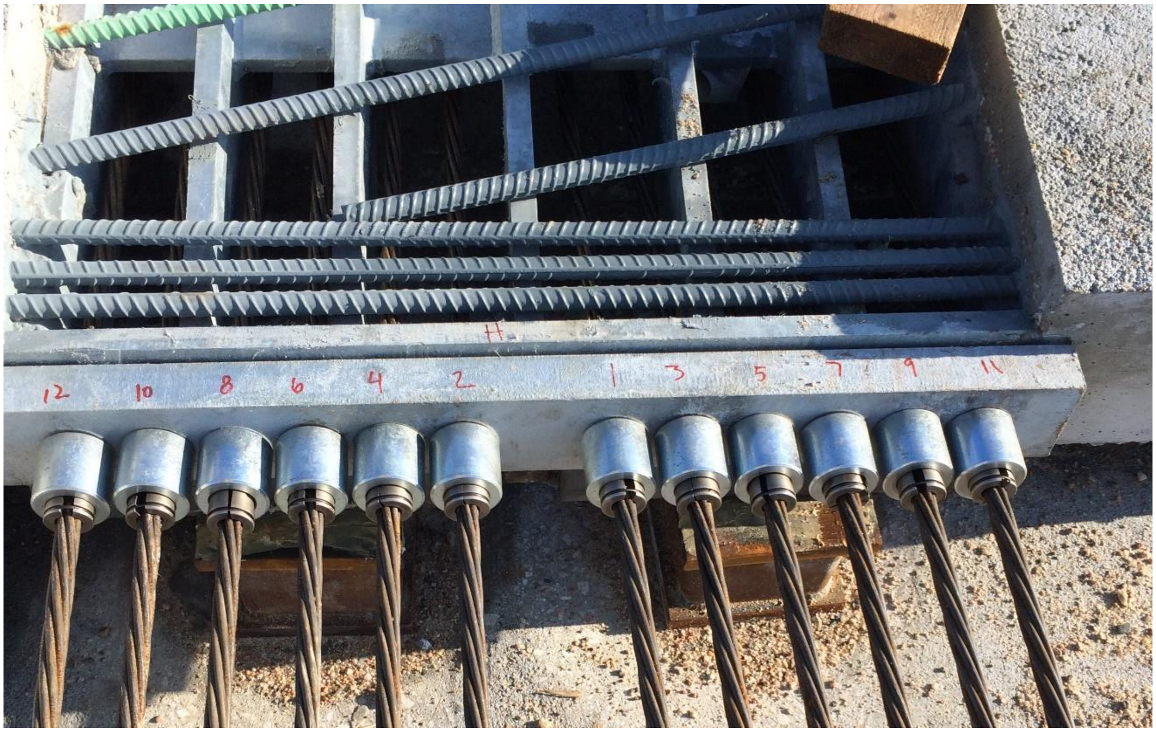
H
12
10
8
6
4
2
1
3
5
7
9
11

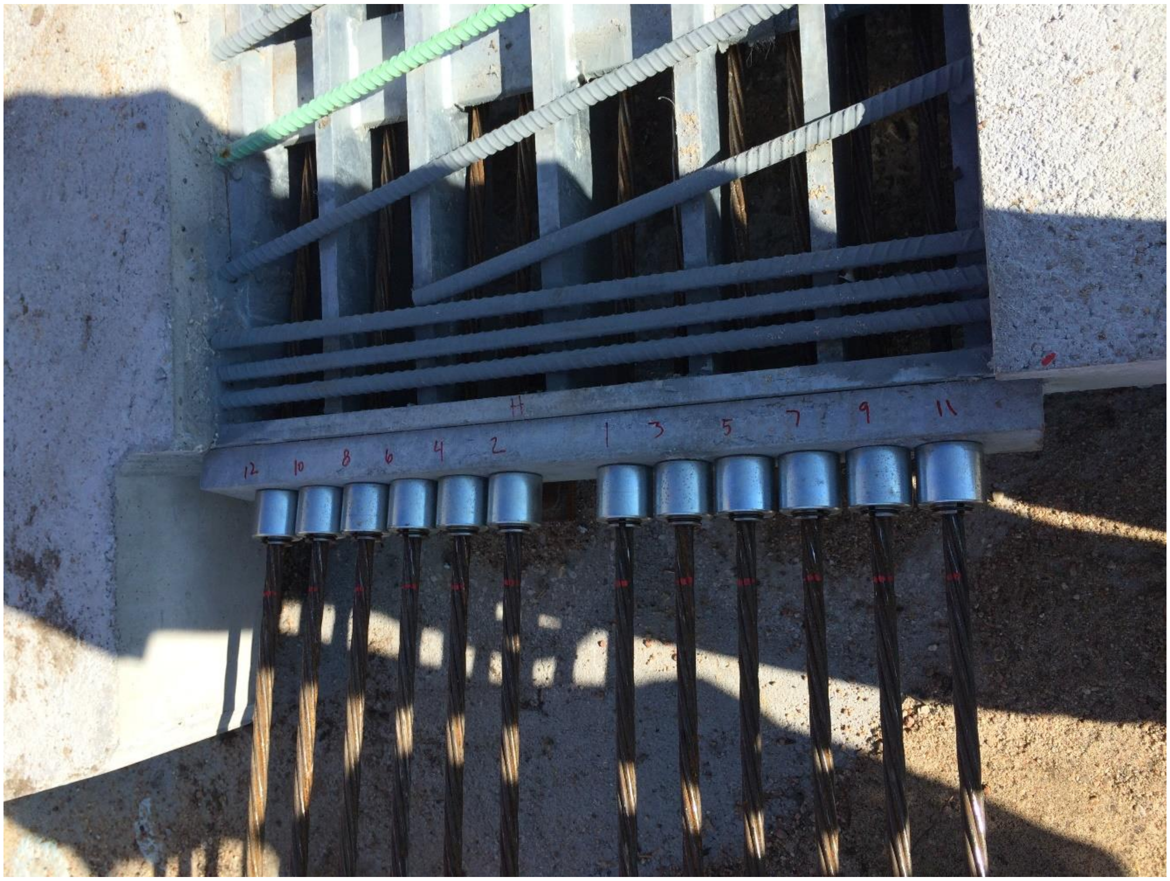
H
12
10
8
6
4
2
1
3
5
7
9
11

49
51
53
55
57
59

Girder H		Girder G		Girder J		Girder F		Girder K	
Strand #	**Elongation (in.)**	**Strand #**	**Elongation (in.)**	**Strand #**	**Elongation (in.)**	**Strand #**	**Elongation (in.)**	**Strand #**	**Elongation (in.)**
1	24.5	13	25.25	25	25.5	37	25.125	49	25.625
2	24.5	14	24.875	26	25.125	38	25.875	50	25
3	25.25	15	25.625	27	25	39	25.625	51	25.5
4	25.5	16	25.125	28	25	40	25.5	52	24.75
5	25	17	25.5	29	25	41	25.5	53	25.625
6	25.5	18	25.5	30	25	42	25.625	54	25.125
7	25.25	19	25.625	31	25.375	43	26	55	25.375
8	25	20	25.625	32	25.375	44	25.5	56	25
9	25	21	25.25	33	25.25	45	25.75	57	26.125
10	25.125	22	25.375	34	25.25	46	25.875	58	25
11	25.25	23	25.5	35	25.75	47	25.75	59	25.5
12	24.75	24	25.5	36	25.25	48	26.125	60	25.625
Min.	**24.5**	**Min.**	**24.875**	**Min.**	**25**	**Min.**	**25.125**	**Min.**	**24.75**
Max.	**25.5**	**Max.**	**25.625**	**Max.**	**25.75**	**Max.**	**26.125**	**Max.**	**26.125**
Average	**25.05**	**Average**	**25.40**	**Average**	**25.24**	**Average**	**25.69**	**Average**	**25.35**
Std. Dev.	**0.335**	**Std. Dev.**	**0.231**	**Std. Dev.**	**0.235**	**Std. Dev.**	**0.269**	**Std. Dev.**	**0.387**
COV	**1.3%**	**COV**	**0.9%**	**COV**	**0.9%**	**COV**	**1.0%**	**COV**	**1.5%**

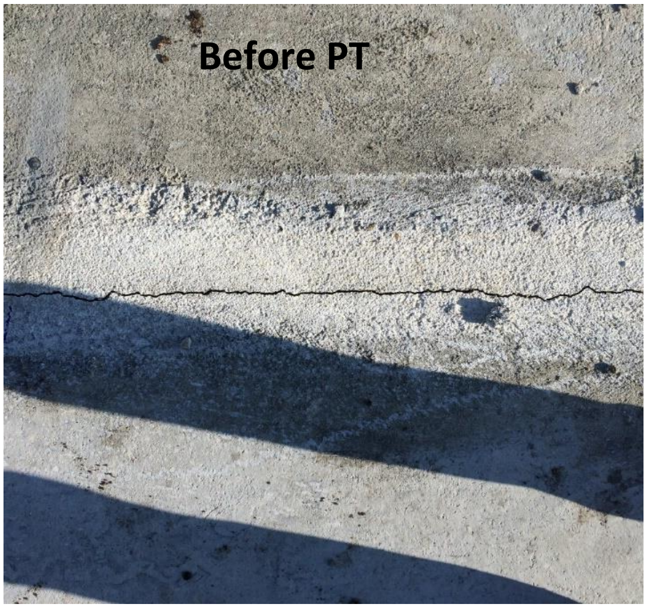

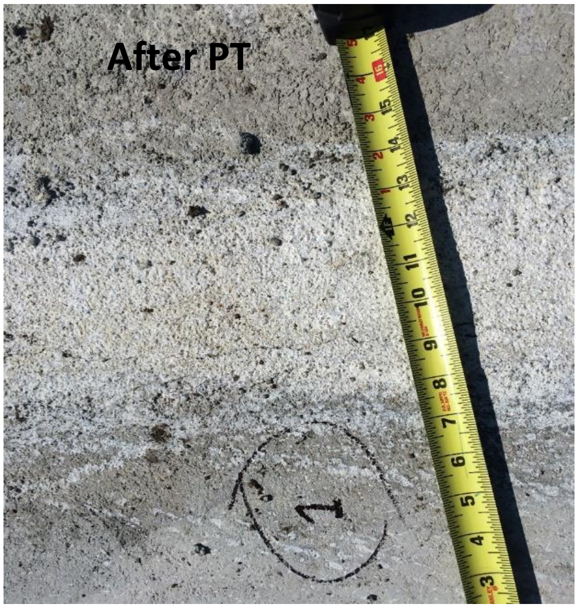

Location	DATE & Time	Parameter	Temp. (^{o}F)	Girder ID					
				F	G	H	J	K	Average
Span 1	8/5/2015 @ 9:00 am	Gauge Readingd before PT	66	15.74	16.66	16.52	13.80	25.84	
	8/7/2015 @ 7:00 am	Gauge Readings after PT	64	15.64	16.58	16.45	13.70	N/A	
		Deck Surface Strain		-8.E-05	-6.E-05	-6.E-05	-8.E-05	N/A	**(0.00007)**
		Deck Surface Stress (ksi)		-0.357	-0.285	-0.250	-0.357	N/A	**(0.31)**
Span 2	8/5/2015 @ 9:00 am	Reading before PT	66	23.75	19.39	20.32	22.37	24.70	
	8/7/2015 @ 7:00 am	Reading after PT	64	23.60	19.31	N/A	22.27	24.63	
		Deck Surface Strain		-1.E-04	-6.E-05	N/A	-8.E-05	-6.E-05	**(0.00008)**
		Deck Surface Stress (ksi)		-0.535	-0.285	N/A	-0.357	-0.250	**(0.36)**

Cast-in-Place SCC for Shear Pockets and Haunches

Age (day)	Girder Batch ID						Average
	H-3	H-3A	G-2	J-4	K-5	F-1	
4	8,120	7,240	7,480	6,790	7,380	7,860	**7,402**
7	8,360	7,250	7,690	7,170	7,510	7,870	**7,596**
28	9,200	9,050	9,170	8,430	8,420	9,030	**8,854**
Air Content (%)	2.6	3	4.2	4.6	4.6	4.6	**3.8**

SCC Batch #	1	2	3	4	5	6	7	8	9	10	Average
Quantity (cy)	6	6	6	6	6	6	6	6	6	6	6
Temperature	74	76	78	80	80	80	78	80	83	85	79.4
Slump Flow (in.)	27	31	29.5	31	28	29.5	29	28	30	28.5	29.15
	26	29	28.5	29	29	29	27	27	27	26.5	27.8
	26.5	30	29	30	28.5	29.25	28	27.5	28.5	27.5	28.475
T_{50} (sec.)	2	2	2	2	2	2	2	2	2	2	2
Penetration (in.)	0.5	1	0.625	0.875	0.875	1	0.75	0.5	0.875	0.5	0.75
VSI	0	1	0	1	0	1	0	0	1	0	0.4
J-Ring Flow (in.)				30.5							
				29.5							
				30							
Difference (in.)				0							

MENARDS
Dedicated to service and quality

APPENDIX B: Bridge Inspections

Structure Number: S010 05463L (CIP Deck)

Inspection Date: 6/22/2016

Several girder ends have fine cracks not in the direction of the shear cracks. They are too fine for epoxy injections. They should be monitored for growth. Bridge rails have vertical shrinkage cracks at 4 to 8 feet intervals. There is C.S. 2 cracking on paving slabs at both ends.

Deck rating = 9
Superstructure rating = 9
Substructure rating = 9

Second Inspection Date: 8/22/2017

There is C.S. 2 cracking on paving slabs at both ends.

Deck rating = 9
Superstructure rating = 9
Substructure rating = 9

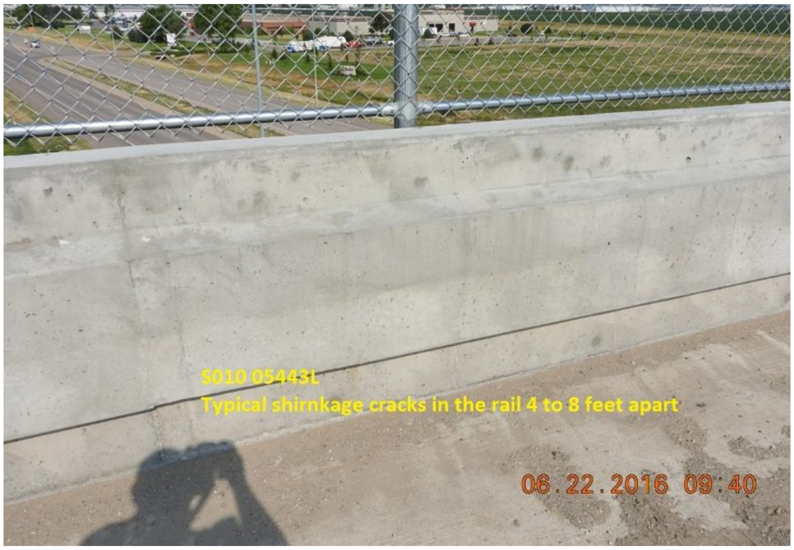
S010 05443L
Typical shirnkage cracks in the rail 4 to 8 feet apart
06.22.2016 09:40

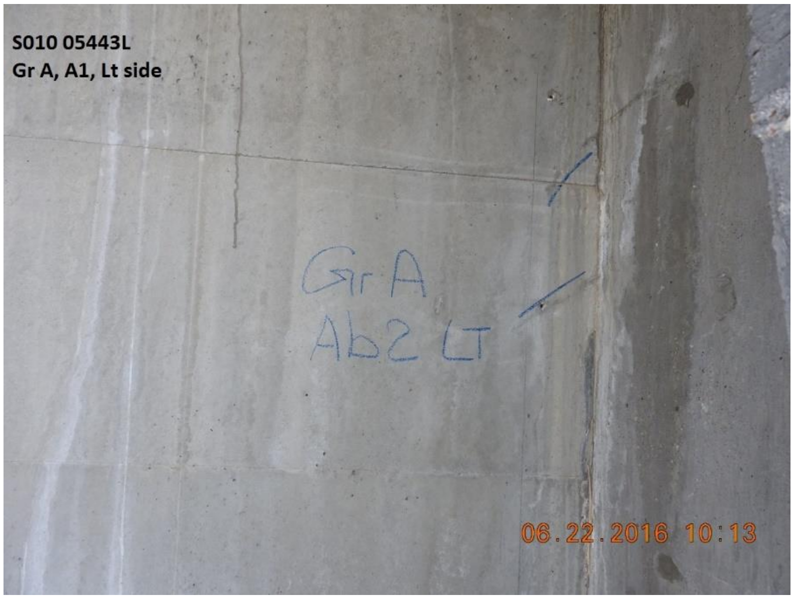
S010 05443L
Gr A, A1, Lt side
Gr A
Ab2 LT
06.22.2016 10:13

Structure Number: S010 05463R (Precast Deck)

Initial Inspection Date: 6/22/2016
Rails have vertical shrinkage cracks at 4 to 8 feet intervals. Every joint between the precast panels are cracked even after post tensioning. South paving section has 20 sq feet of crack and North paving section has 10 square feet of cracks. A few girders have diagonal cracks at the girder ends. These cracks are not in the direction of shear cracks. Cracks are too fine for epoxy injections. They should be monitored for growth.
Deck rating = 9
Superstructure rating = 9
Substructure rating = 9

Second Inspection Date: 8/22/2017
There is C.S. 2 cracking on paving slabs at both ends.
Deck rating = 8
Superstructure rating = 8
Substructure rating = 9

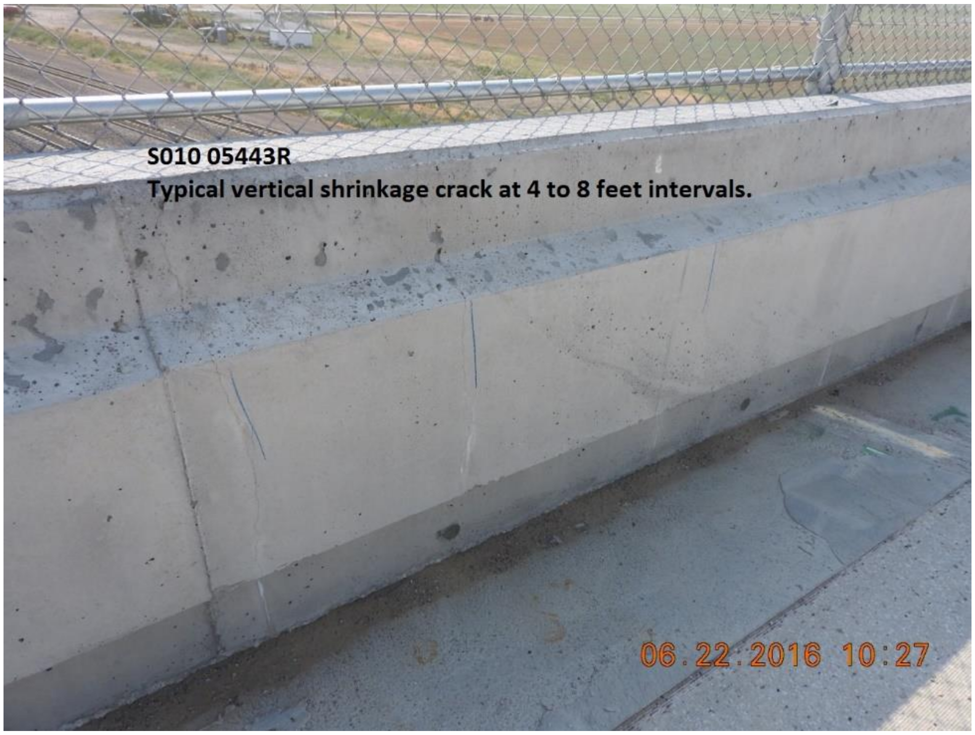
S010 05443R
Typical vertical shrinkage crack at 4 to 8 feet intervals.
06.22.2016 10:27

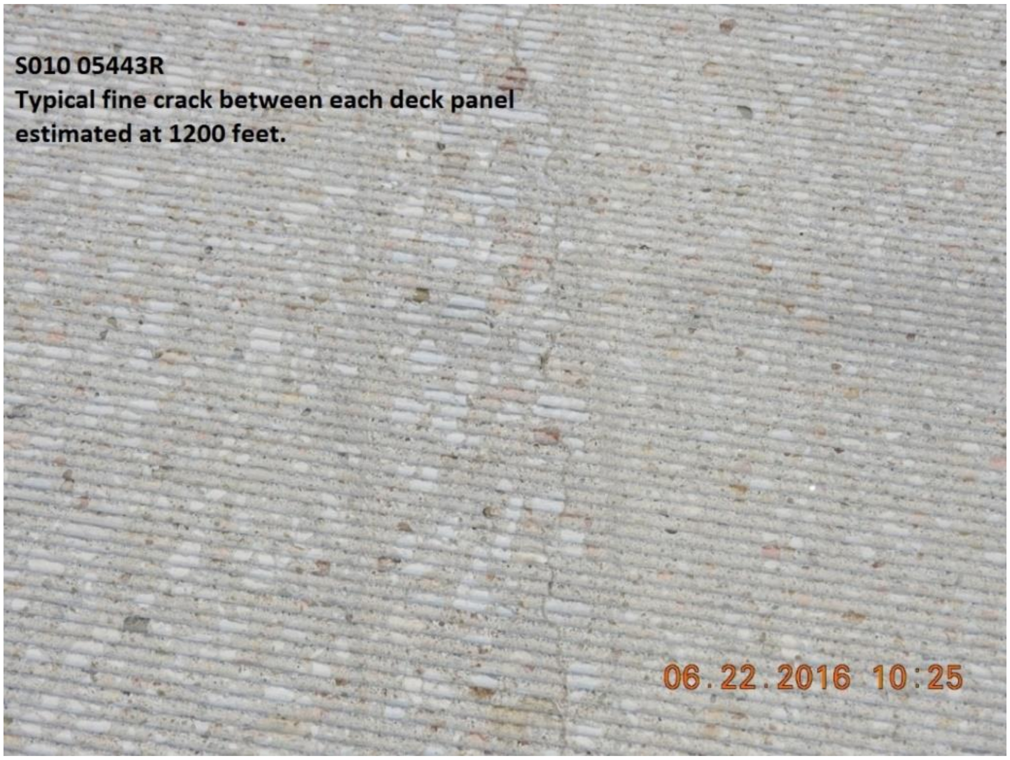

S010 05443R
Typical fine crack between each deck panel estimated at 1200 feet.
06.22.2016 10:25

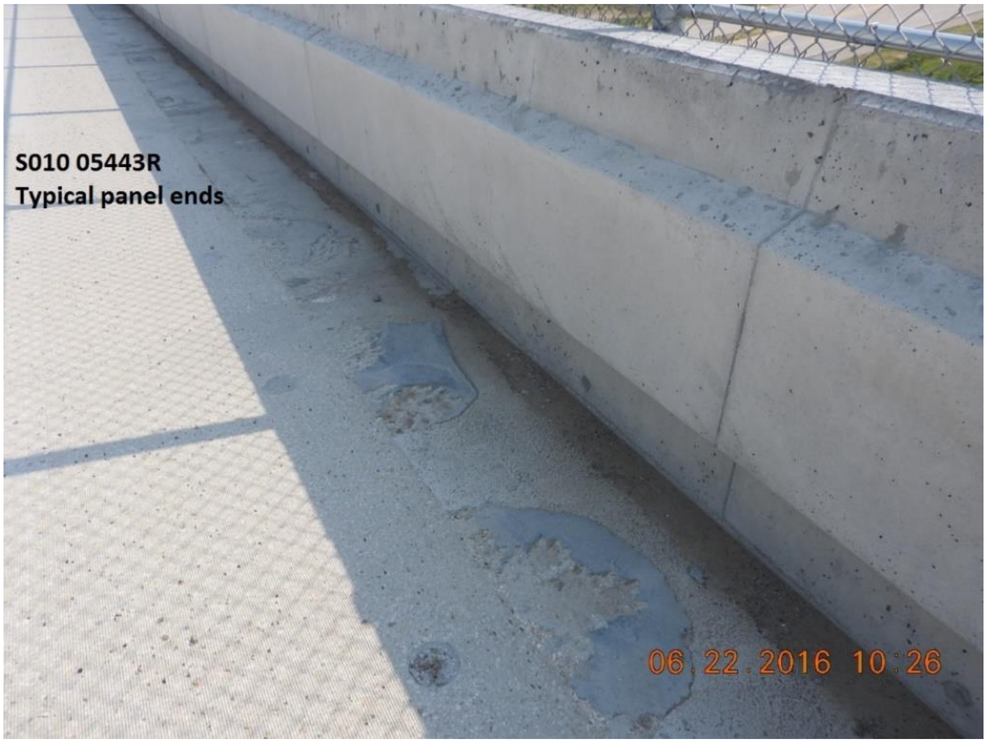

S010 05443R
Typical panel ends
06.22.2016 10:26

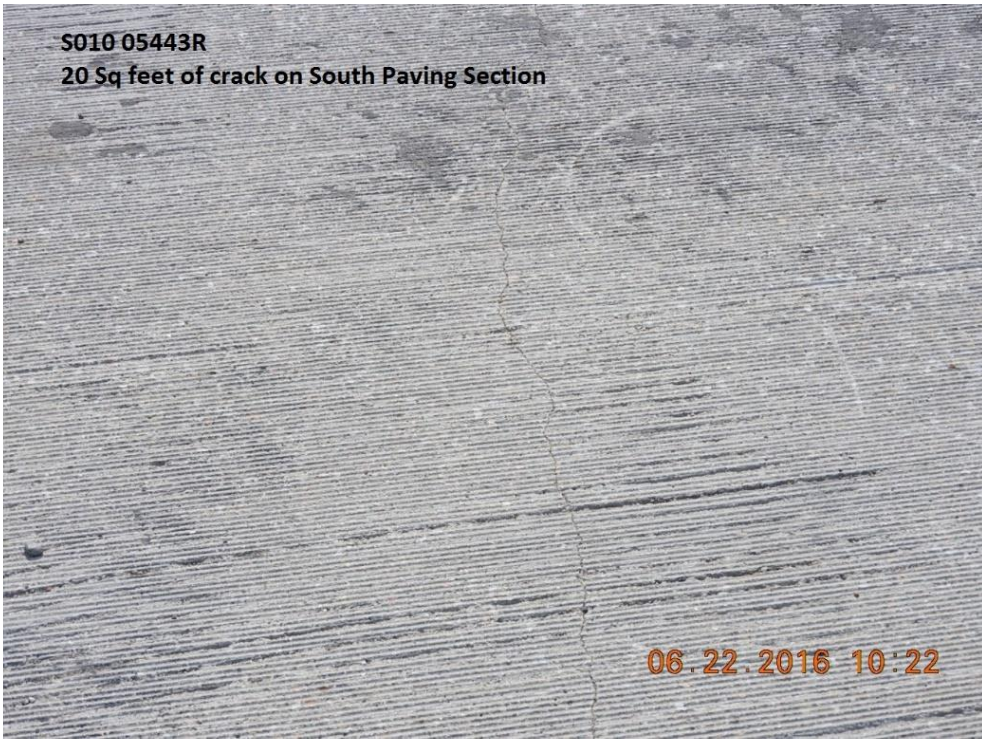

S010 05443R
20 Sq feet of crack on South Paving Section

06.22.2016 10:22

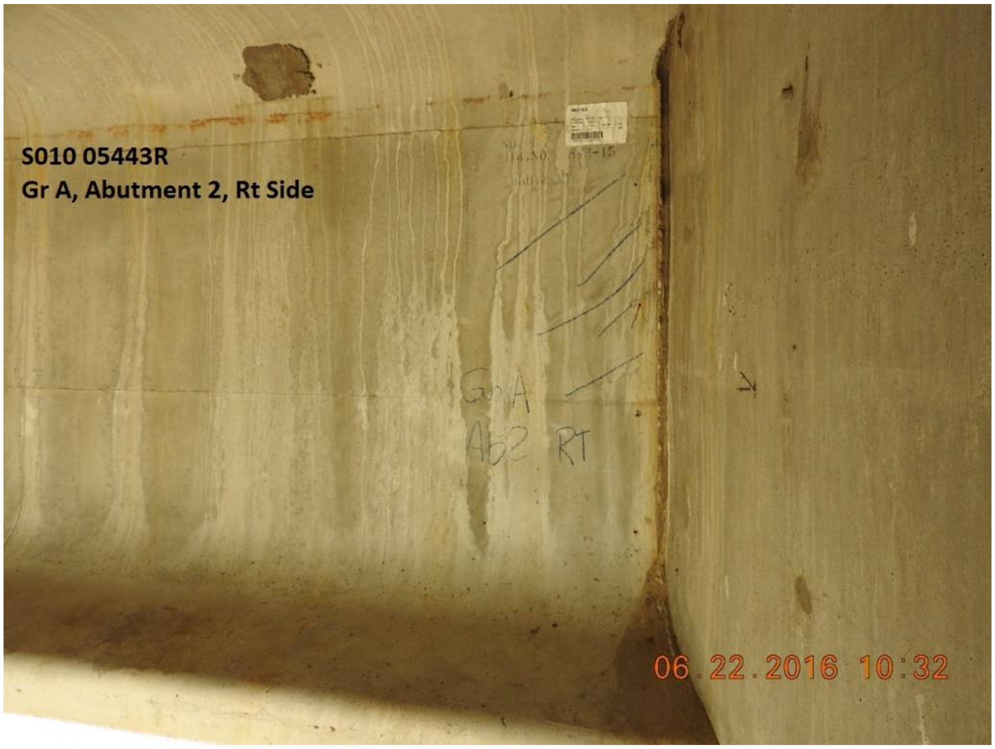

S010 05443R
Gr A, Abutment 2, Rt Side

06.22.2016 10:32

APPENDIX C: Prestress Loss Calculations

Elastic Shortening Losses

Girder Span	$L:=166\ \mathbf{ft}$
Girder Gross Area	$A_g:=858.7\ \mathbf{in}^2$
Girder C.G from bottom	$y_b:=32.06\ \mathbf{in}$
Girder Gross Inertia	$I_g:=612674\ \mathbf{in}^4$
Compressive strength at Release	$f_{ci}':=7.2\ \mathbf{ksi}$
Girder Aggregate Factor	$k_1:=1.0$
Girder MOE at Release	$E_{ci}:=33000\ \mathbf{ksi}\cdot k_1\cdot\left(\dfrac{145\ \mathbf{pcf}}{1000\ \mathbf{pcf}}\right)^{1.5}\cdot\left(\dfrac{f_{ci}'}{\mathbf{ksi}}\right)^{.5}=4889\ \mathbf{ksi}$
Girder Weight	$q_g:=A_g\cdot 150\ \mathbf{pcf}=0.894\ \dfrac{\mathbf{kip}}{\mathbf{ft}}$
Girder Weight Moment	$M_g:=q_g\ \dfrac{L^2}{8}=3081\ \mathbf{kip}\cdot\mathbf{ft}$
Strand Ultimate Srength	$f_{pu}:=270\ \mathbf{ksi}$
Prestressing Prior to Transfer	$f_{pi}:=75\%\cdot f_{pu}=202.5\ \mathbf{ksi}$
Strand MOE	$E_p:=28500\ \mathbf{ksi}$
Area of Prestressing Strands	$A_{ps}:=60\cdot 0.217\ \mathbf{in}^2=13.02\ \mathbf{in}^2$
Eccentricity of Strands	$e_{pg}:=27.14\ \mathbf{in}$
Elastic Shortening Loss	$\Delta f_{pES}:=\dfrac{A_{ps}\cdot f_{pi}\cdot\left(I_g+e_{pg}^{\ 2}\cdot A_g\right)-e_{pg}\cdot A_g\cdot M_g}{A_{ps}\cdot\left(I_g+e_{pg}^{\ 2}\cdot A_g\right)+A_g\cdot I_g\cdot\dfrac{E_{ci}}{E_p}}=22.7\ \mathbf{ksi}$
Elastic Shortening Loss	$ES:=\dfrac{\Delta f_{pES}}{f_{pi}}=11.231\%$
Concrete Stress at Prestress C.G.	$f_{cgp}:=\dfrac{E_{ci}}{E_p}\cdot\Delta f_{pES}=3.9\ \mathbf{ksi}$

Long-Term Losses (Approxmate Method)

Relative Humidity $H := 70\%$

Correction Factor of Relative Humidity $\gamma_h := 1.7 - H = 1$

Correction Factor of Concrete Strength $\gamma_{st} := \dfrac{5\ \mathbf{ksi}}{\left(1\ \mathbf{ksi} + f_{ci}'\right)} = 0.61$

Long-Term Prestress Loss $\Delta f_{pLT} := 10 \cdot \dfrac{f_{pi} \cdot A_{ps}}{A_g} \cdot \gamma_h \cdot \gamma_{st} + 12\ \mathbf{ksi} \cdot \gamma_h \cdot \gamma_{st} + 2.4\ \mathbf{ksi} = 28.4\ \mathbf{ksi}$

Long-Term Losses (Refined Method)

Between Release and Deck Placement Calculations

Volume-to-Surface Ratio $VS := 3\ \mathbf{in}$

Volume-to-Surface Factor $k_s := \max\left(1, 1.45 - 0.13 \cdot \dfrac{VS}{\mathbf{in}}\right) = 1.06$

Humidity Factor for Creep $k_{hc} := 1.56 - 0.8 \cdot H = 1$

Humidity Factor for Shrinkage $k_{hs} := 2 - 1.4 \cdot H = 1.02$

Compressive Strength Factor $k_f := \dfrac{5\ \mathbf{ksi}}{1\ \mathbf{ksi} + f_{ci}'} = 0.61$

Age at Prestress Release $t_i := 2\ \mathbf{day}$

Age at Deck Placement $t_d := 60\ \mathbf{day}$

Age at Final Load $t_f := 20000\ \mathbf{day}$

Time Development Factor $k_{td}(t) := \dfrac{t}{12\left(\dfrac{100\ \mathbf{ksi} - 4 \cdot f_{ci}'}{20\ \mathbf{ksi} + f_{ci}'}\right)\mathbf{day} + t}$

Shrinkage Strain $\varepsilon_{bid} := 0.48 \cdot 10^{-3} \cdot k_s \cdot k_{hs} \cdot k_f \cdot k_{td}\left(t_d - t_i\right) = 0.00021$

Creep Coefficient $\psi_b\left(t, t_o\right) := 1.9 \cdot k_s \cdot k_{hc} \cdot k_f \cdot k_{td}\left(t - t_o\right) \cdot \left(\dfrac{t_o}{\mathbf{day}}\right)^{-0.118}$

$\psi_{bid} := \psi_b\left(t_d, t_i\right) = 0.734$

Transformed Section Coefficient $K_{id} := \dfrac{1}{1 + \left(\dfrac{E_p}{E_{ci}}\right) \cdot \left(\dfrac{A_{ps}}{A_g}\right) \cdot \left(1 + \dfrac{A_g \cdot e_{pg}^{\ 2}}{I_g}\right) \cdot \left(1 + 0.7 \cdot \psi_b\left(t_f, t_i\right)\right)} = 0.757$

Shrinkage Prestress Loss
$$\Delta f_{pSR} := \varepsilon_{bid} \cdot E_p \cdot K_{id} = 4.43\ \mathbf{ksi}$$

Creep Prestress Loss
$$\Delta f_{pCR} := \frac{E_p}{E_{ci}}\, f_{cgp} \cdot \psi_{bid} \cdot K_{id} = 12.63\ \mathbf{ksi}$$

Relaxation Prestress Loss
$$\Delta f_{pR1} := 1.2\ \mathbf{ksi}$$

Total Prestress Loss between Release and Deck Placement
$$\Delta f_{pLT1} := \Delta f_{pSR} + \Delta f_{pCR} + \Delta f_{pR1} = 18.26\ \mathbf{ksi}$$

Change in Prestress Force
$$\Delta P_{id} := A_{ps} \cdot \Delta f_{pLT1} = 237.7\ \mathbf{kip}$$

Between Deck Placement and Final Calculations

Girder Compressive Strength
$$f_c' := 10\ \mathbf{ksi}$$

Girder MOE
$$E_c := 33000\ \mathbf{ksi} \cdot k_1 \cdot \left(\frac{145\ \mathbf{pcf}}{1000\ \mathbf{pcf}}\right)^{1.5} \cdot \sqrt{\frac{f_c'}{\mathbf{ksi}}} = 5762\ \mathbf{ksi}$$

Deck Compressive Strength
$$f_{cd}' := 6\ \mathbf{ksi}$$

Deck MOE
$$E_d := 33000\ \mathbf{ksi} \cdot k_1 \cdot \left(\frac{145\ \mathbf{pcf}}{1000\ \mathbf{pcf}}\right)^{1.5} \cdot \sqrt{\frac{f_{cd}'}{\mathbf{ksi}}} = 4463\ \mathbf{ksi}$$

Modulur Ratio
$$n := \frac{E_c}{E_d} = 1.291$$

Total Deck Thickness
$$h_s := 7.5\ \mathbf{in}$$

Deck Design Thickness
$$t_s := 7\ \mathbf{in}$$

Haunch Thickness
$$t_h := 2.5\ \mathbf{in}$$

Haunch Width
$$b_h := 48\ \mathbf{in}$$

Girder Spacing
$$S := 8.5\ \mathbf{ft}$$

Deck Weight per Girder
$$q_d := 150\ \mathbf{pcf} \cdot \left(h_s \cdot S + t_h \cdot b_h\right) = 0.922\ \frac{\mathbf{kip}}{\mathbf{ft}}$$

Deck Weight Moment
$$M_d := q_d \cdot \frac{L^2}{8} = 3175.4\ \mathbf{kip} \cdot \mathbf{ft}$$

Rail Weight per Girder
$$q_r := 0.4\ \frac{\mathbf{kip}}{\mathbf{ft}} \cdot \frac{2}{6} = 0.133\ \frac{\mathbf{kip}}{\mathbf{ft}}$$

Rail Weight Moment
$$M_r := q_r \cdot \frac{L^2}{8} = 459.267\ \mathbf{kip} \cdot \mathbf{ft}$$

Transformed Deck Width
$$b_e := \frac{S}{n} = 79\ \mathbf{in}$$

Gross Deck Area
$$A_d := S \cdot t_s + b_h \cdot t_h = 834\ \mathbf{in}^2$$

Composite Section Height	$h_c := 80.9\ \mathbf{in}$
Composite Section Area	$A_c := A_g + \frac{A_d}{n} = 1504.7\ \mathbf{in}^2$
Composite Section C.G.	$y_{bc} := \frac{A_g \cdot y_b + \frac{A_d}{n} \cdot \left(h_c - \frac{t_s}{2}\right)}{A_c} = 51.53\ \mathbf{in}$
Composite Section Inertia	$I_c := I_g + A_g \cdot \left(y_{bc} - y_b\right)^2 + \frac{b_e \cdot t_s^3}{12} + \frac{A_d}{n} \cdot \left(h_c - \frac{t_s}{2} - y_{bc}\right)^2 = 1372798\ \mathbf{in}^4$
Composite Section Eccentricity	$e_{pc} := e_{pg} + \left(y_{bc} - y_b\right) = 46.61\ \mathbf{in}$
Deck C.G. Eccentricity	$e_d := h_c - \frac{t_s}{2} - y_{bc} = 25.874\ \mathbf{in}$
Transformed Section Coefficient	$K_{df} := \frac{1}{1 + \left(\frac{E_p}{E_{ci}}\right) \cdot \left(\frac{A_{ps}}{A_c}\right) \cdot \left(1 + \frac{A_c \cdot e_{pc}^2}{I_c}\right) \cdot \left(1 + 0.7 \cdot \psi_b\left(t_f, t_i\right)\right)} = 0.766$
Total Shrinkage Strain	$\varepsilon_{bif} := 0.48 \cdot 10^{-3} \cdot k_s \cdot k_{hs} \cdot k_f \cdot k_{td}\left(t_f - t_i\right) = 0.00032$
Shrinkage Strain	$\varepsilon_{bdf} := \varepsilon_{bif} - \varepsilon_{bid} = 0.00011$
Shrinkage Prestress Loss	$\Delta f_{pSD} := \varepsilon_{bdf} \cdot E_p \cdot K_{df} = 2.42\ \mathbf{ksi}$
Total Creep Strain	$\psi_{bif} := \psi_b\left(t_f, t_i\right) = 1.13$
Creep Coefficient	$\psi_{bdf} := \psi_b\left(t_f, t_d\right) = 0.756$
Concrete Stress due to prestress loss, deck and rail weight	$\Delta f_{cd} := -\left(\frac{\Delta P_{id}}{A_g} + \frac{\Delta P_{id} \cdot e_{pg}^2}{I_g} + \frac{M_d \cdot e_{pg}}{I_g} + \frac{M_r \cdot e_{pc}}{I_c}\right) = -2.438\ \mathbf{ksi}$
Creep Prestress Loss	$\Delta f_{pCD} := \left(\frac{E_p}{E_{ci}} \cdot f_{cgp} \cdot \left(\psi_{bif} - \psi_{bid}\right) + \frac{E_p}{E_c} \cdot \Delta f_{cd} \cdot \psi_{bdf}\right) \cdot K_{df} = -0.091\ \mathbf{ksi}$
Relaxation Prestress Loss	$\Delta f_{pR2} := 1.2\ \mathbf{ksi}$
Total Prestress Loss between Deck Placement and Final Load	$\Delta f_{pLT2} := \Delta f_{pSD} + \Delta f_{pCD} + \Delta f_{pR2} = 3.53\ \mathbf{ksi}$
Total Long-Term Prestress Loss	$\Delta f_{pLT} := \Delta f_{pLT1} + \Delta f_{pLT2} = 21.78\ \mathbf{ksi}$
Total Long-Term Prestress Loss	$LT := \frac{\Delta f_{pLT}}{f_{pi}} = 10.8\%$